NAVAL
POSTGRADUATE
SCHOOL

MONTEREY, CALIFORNIA

THESIS

DESIGN AND CONSTRUCTION OF A THERMAL CONTACT RESISTANCE AND THERMAL CONDUCTIVITY MEASUREMENT SYSTEM

by

Christopher R. Deigel

September 2015

Thesis Advisor:	Sanjeev B. Sathe
Second Reader:	Garth V. Hobson

Approved for public release; distribution is unlimited

THIS PAGE INTENTIONALLY LEFT BLANK

REPORT DOCUMENTATION PAGE		*Form Approved OMB No. 0704–0188*

Public reporting burden for this collection of information is estimated to average 1 hour per response, including the time for reviewing instruction, searching existing data sources, gathering and maintaining the data needed, and completing and reviewing the collection of information. Send comments regarding this burden estimate or any other aspect of this collection of information, including suggestions for reducing this burden, to Washington headquarters Services, Directorate for Information Operations and Reports, 1215 Jefferson Davis Highway, Suite 1204, Arlington, VA 22202-4302, and to the Office of Management and Budget, Paperwork Reduction Project (0704-0188) Washington, DC 20503.

1. AGENCY USE ONLY *(Leave blank)*	2. REPORT DATE September 2015	3. REPORT TYPE AND DATES COVERED Master's thesis	
4. TITLE AND SUBTITLE DESIGN AND CONSTRUCTION OF A THERMAL CONTACT RESISTANCE AND THERMAL CONDUCTIVITY MEASUREMENT SYSTEM		5. FUNDING NUMBERS	
6. AUTHOR(S) Deigel, Christopher R.			
7. PERFORMING ORGANIZATION NAME(S) AND ADDRESS(ES) Naval Postgraduate School Monterey, CA 93943-5000		8. PERFORMING ORGANIZATION REPORT NUMBER	
9. SPONSORING /MONITORING AGENCY NAME(S) AND ADDRESS(ES) Officer of Naval Research		10. SPONSORING / MONITORING AGENCY REPORT NUMBER	

11. SUPPLEMENTARY NOTES The views expressed in this thesis are those of the author and do not reflect the official policy or position of the Department of Defense or the U.S. Government. IRB Protocol number _____N/A_____.

12a. DISTRIBUTION / AVAILABILITY STATEMENT Approved for public release; distribution is unlimited	12b. DISTRIBUTION CODE

13. ABSTRACT (maximum 200 words)

This study was aimed at the development of an accurate thermal contact resistance and thermal conductivity measurement system that was simple enough to be constructed and operated by multiple users. A method based on Fourier's Law of Conduction was developed. The purpose of this device is to analyze component interfaces and advanced material applications within Department of Defense's energy systems to improve fuel efficiency and performance.

Comprehensive details of the design, construction, and operation of the experimental device are presented. Challenges included maintaining one-dimensional conduction, uniformity of temperature distribution, control of heat loss, and sample to plate interface resistance control. Numerical heat transfer and uncertainty analyses with applied engineering judgement were extensively used to come up with an optimized design and construction method that guaranteed high accuracy and replicability.

Accurate measurements are demonstrated by analyzing Pyroceram 9606 and 99.8% Alumina reference samples. Results indicate capability to measure thermal conductivity from 0.1 to 40 W/m-K with respective accuracy within 3–6.5%. Ability to reduce result uncertainty within 10% is achieved. Replicability analysis indicates reproducible results within 6% for different users. Recommendations are provided for experimental research utilizing the proposed measurement system addressing current heat transfer issues facing the Department of Defense.

14. SUBJECT TERMS Thermal contact resistance, thermal conductivity, measurement system			15. NUMBER OF PAGES 179
			16. PRICE CODE
17. SECURITY CLASSIFICATION OF REPORT Unclassified	18. SECURITY CLASSIFICATION OF THIS PAGE Unclassified	19. SECURITY CLASSIFICATION OF ABSTRACT Unclassified	20. LIMITATION OF ABSTRACT UU

NSN 7540–01-280-5500

Standard Form 298 (Rev. 2–89) Prescribed by ANSI Std. 239–18

THIS PAGE INTENTIONALLY LEFT BLANK

DESIGN AND CONSTRUCTION OF A THERMAL CONTACT RESISTANCE AND THERMAL CONDUCTIVITY MEASUREMENT SYSTEM

Christopher R. Deigel
Lieutenant, United States Navy
B.S., University of Rochester, 2006

Submitted in partial fulfillment of the
requirements for the degree of

MECHANICAL ENGINEER

and

MASTER OF SCIENCE IN MECHANICAL ENGINEERING

from the

NAVAL POSTGRADUATE SCHOOL
September 2015

Approved by: Dr. Sanjeev B. Sathe
Thesis Advisor

Dr. Garth V. Hobson
Second Reader

Dr. Garth V. Hobson
Chair, Department of Mechanical and Aerospace Engineering

THIS PAGE INTENTIONALLY LEFT BLANK

ABSTRACT

This study was aimed at the development of an accurate thermal contact resistance and thermal conductivity measurement system that was simple enough to be constructed and operated by multiple users. A method based on Fourier's Law of Conduction was developed. The purpose of this device is to analyze component interfaces and advanced material applications within Department of Defense's energy systems to improve fuel efficiency and performance.

Comprehensive details of the design, construction, and operation of the experimental device are presented. Challenges included maintaining one-dimensional conduction, uniformity of temperature distribution, control of heat loss, and sample to plate interface resistance control. Numerical heat transfer and uncertainty analyses with applied engineering judgement were extensively used to come up with an optimized design and construction method that guaranteed high accuracy and replicability.

Accurate measurements are demonstrated by analyzing Pyroceram 9606 and 99.8% Alumina reference samples. Results indicate capability to measure thermal conductivity from 0.1 to 40 W/m-K with respective accuracy within 3–6.5%. Ability to reduce result uncertainty within 10% is achieved. Replicability analysis indicates reproducible results within 6% for different users. Recommendations are provided for experimental research utilizing the proposed measurement system addressing current heat transfer issues facing the Department of Defense.

THIS PAGE INTENTIONALLY LEFT BLANK

TABLE OF CONTENTS

LIST OF FIGURES

xii

THIS PAGE INTENTIONALLY LEFT BLANK

LIST OF TABLES

THIS PAGE INTENTIONALLY LEFT BLANK

LIST OF ACRONYMS AND ABBREVIATIONS

1-D	one-dimensional
3-D	three-dimensional
AC	air conditioning
CJC	Cold Junction Compensation
COTS	commercial off the shelf
CPV	concentrated photovoltaic
DOD	Department of Defense
DON	Department of the Navy
E2C	Expeditionary Energy Concepts
ExFOB	Experimental Forward Operating Base
HVOF	high velocity oxygen fuel
IR	infrared
NPS	Naval Postgraduate School
ONR	Office of Naval Research
RTD	resistance temperature detector
SECNAV	Secretary of the Navy
TIMs	thermal interface materials
USD (AT&L)	Under Secretary of Defense for Acquisition, Technology, and Logistics
USN	United States Navy
WHR	waste heat recovery
WHRS	Waste Heat Recovery Systems
SI Units	International System of Units

THIS PAGE INTENTIONALLY LEFT BLANK

NOMENCLATURE

Symbols	Description	Units
$\Delta(\Delta x)$	thickness uncertainty	[m]
$\Delta(dT_{avg})$	difference in average temperature uncertainty	[ºC]
ΔA	area uncertainty	[m²]
ΔI	electrical current uncertainty	[A]
$\Delta L1$	side one length uncertainty	[m]
$\Delta L2$	side two length uncertainty	[m]
ΔRo	circular sample insulation thickness	[m]
ΔT_{COLD}	cold temperature uncertainty	[ºC]
ΔT_{HOT}	hot temperature uncertainty	[ºC]
ΔV	electrical voltage uncertainty	[V]
Δx	thickness uncertainty	[m]
A	material A	
B	material B	
C	material C	
CH	coolant channel height	[m]
CID	coolant channel inner diameter	[m]
CNL	coolant channel nozzle length	[m]
CO	coolant channel offset	[m]
COD	coolant channel outer diameter	[m]
Cp or cp	specific heat (constant pressure)	[J/(kgK)]
dT	temperature difference	[ºC]

Symbols	Description	Units
dT_{avg}	average temperature difference	[ºC]
dx	x-direction thickness	[m]
h	heat transfer coefficient	[W/m²K]
H	height	[m]
I	electrical current	[A]
k	thermal conductivity	[W/m-K]
$k_{\Delta Tavg}$	thermal conductivity calculated using average difference in temperature across sample	[W/m-K]
k_A	material A's thermal conductivity	[W/m-K]
k_B	material B's thermal conductivity	[W/m-K]
k_C	material C's thermal conductivity	[W/m-K]
$k_{comparison\ experimentalist}$	thermal conductivity calculated by another individual	[W/m-K]
$k_{expected}$	thermal conductivity from literature	[W/m-K]
$k_{experimentalist\ 1}$	thermal conductivity calculated by author	[W/m-K]
$k_{insulation}$	insulation thermal conductivity	[W/m-K]
$k_{material}$	material thermal conductivity	[W/m-K]
$k_{measured}$	measured sample thermal conductivity	[W/m-K]
k_{sample}	sample thermal conductivity	[W/m-K]
L	length	[m]
$L1$	side one length	[m]
$L2$	side two length	[m]
L_A	material A's thickness	[m]

Symbols	Description	Units
L_B	material B's thickness	[m]
L_C	material C's thickness	[m]
Li	square sample side length	[m]
Lo	square sample insulation thickness	[m]
q	heat transfer	[W]
q_x	one-dimensional heat transfer	[W]
q''	heat flux	[W/m²]
$q_{contact}''$	heat flux across surfaces in direct contact	[W/m²]
q_{gap}''	heat flux across a gap/void	[W/m²]
q_x''	one-dimensional heat flux	[W/m²]
$q_{x\,tot}''$	total one-dimensional heat flux	[W/m²]
q'''	heat generation	[W/m³]
R	general function	
Ri	circular sample radius	[m]
$R_{material}''$	material thermal resistivity	[m-K/W]
$R_{t,c}''$	thermal contact resistance	[m²-K/W]
$R_{t,c\,TOT}''$	total thermal contact resistance	[m²-K/W]
t	time	[s]
T	thickness	[m]
T1 or T_1	side one temperature	[ºC]
T2 or T_2	side two temperature	[ºC]
T_3	side three temperature	[ºC]

Symbols	Description	Units
T_4	side four temperature	[°C]
$T_{AMBIENT}$	ambient room temperature	[°C]
T_{avg}	average temperature	[°C]
T_B	material B's temperature	[°C]
T_{BASE}	sample base temperature	[°C]
T_C	cold temperature	[°C]
T_{CENTER}	temperature at center of sample top surface	[°C]
T_{EDGE}	temperature at edge of sample top surface	[°C]
T_H	hot temperature	[°C]
TD	thermocouple channel depth	[m]
Temp	temperature	[°C]
TL	thermocouple channel length	[m]
TO1	thermocouple channel offset 1	[m]
TO2	thermocouple channel offset 2	[m]
TW	thermocouple channel width	[m]
U	x-direction velocity	[m/s]
V	y-direction velocity or electrical Voltage	[m/s] or [V]
W	z-direction velocity or width	[m/s] or [m]
w_k	thermal conductivity uncertainty	[W/m-K]
w_R	result uncertainty	
$w_{1,2,...,n}$	independent variable uncertainties	
$x_{1,2,...,n}$	independent variables	
ρ	density	[kg/m³]

ACKNOWLEDGMENTS

I would like to first thank God for giving me the strength, intellectual capability, and perseverance to complete this thesis.

Much recognition and appreciation are due to my loving wife, Caitlin, for supporting me over the last two and a half years as I completed my thesis and obtained my two engineering degrees. She continually provided unwavering support to me as she took care of both of us, while working and commuting multiple hours to and from UC Santa Cruz to obtain her degree in business management economics. It is apparent to me now the true meaning of the phase *"Behind every great man, there stands a great woman."* Caitlin, you are not only that great woman, you are also my best friend, and I could not be where I am today without you.

In his commencement address in 2005 at Stanford, Steve Jobs said that you cannot connect the dots of life moving forward, only when looking back. As I look back, I cannot acknowledge enough the positive influence that my thesis advisor, Dr. Sathe, has had on me throughout my time at NPS. He has acted as not only my thesis advisor, but also my mentor preparing me for my future. He has been a true inspiration and has unfailingly led me through both good and tough times while completing my coursework. None of this would have been possible albeit for a brief conversation we had in a parking lot when I was first starting school. Thank you for mentoring me throughout this entire process and showing me the power of visualization.

Lastly, I want to thank all my friends and colleagues who have been there for me throughout this process. You have all provided me support and guidance crucial to my successes. Specifically, I want to thank all the members of the Waste Heat Recovery and Concentrated Photovoltaic team. Additionally, I want to thank John Mobley in the school's machine design shop for taking time with me throughout the design and construction phases of my project. Finally, I want to thank my Mom, Dad, Allison, Jessica, and father-in-law, Tom, for always being there to listen and encourage me.

THIS PAGE INTENTIONALLY LEFT BLANK

I. INTRODUCTION

A. PROBLEM STATEMENT

With the recent budgetary issues associated with sequestration, the U.S. military has emphasized doing more with less. This has become quite apparent through the Department of Defense's (DOD's) struggle to continue to supply the warfighter around the world with supplies essential for mission success. One key issue is the overall dependency of our forces on fossil fuels. In many situations, our high dependency on fuel requires extensive logistical support and incurs additional unnecessary risks, such as loss of lives, as we strive to complete missions successfully [1]. To meet the goals of energy efficiency set forth by the DOD, this report lays down the ground work and establishes the infrastructure for all future experimental research in waste heat recovery (WHR) and concentrated photovoltaic (CPV) fields at the Naval Postgraduate School (NPS). The focus of this project is the overall design and construction of a thermal contact resistance and thermal conductivity measurement system that can be built and operated at any facility. The purpose of this device is to characterize new materials for their possible inclusion into WHR, CPV, and potential laser cooling systems. The range of thermal conductivity measurement ability makes the system ideal for characterizing materials such as heat exchanger gaskets, thermal interface materials (TIMs), thermal coatings, and other advanced proprietary materials currently under investigation by the DOD. By improving the way the DOD manages thermal contact resistance and thermal conductivity in complex energy systems, advancements can be made to improve energy efficiency, reducing the military's dependency on fossil fuels.

Over the past decade, many reports and strategies have been produced to guide the DOD in innovative ways to reduce our fuel dependency. One such report titled *More Fight - Less Fuel* was written in 2006 by a task force formed through the Defense Science Board under the direction of the Under Secretary of Defense for Acquisition, Technology and Logistics (USD [AT&L]). This document includes various findings and recommendations to minimize the DOD's dependence on fuel [1]. In response to an energy agenda established by the president of the United States, the Secretary of the Navy (SECNAV) has addressed five energy goals in his Energy Message to the Fleet (see Figure 1).

Figure 1.   Secretary of the Navy's 5 Energy Goals in his Energy Message to
the Fleet

1. Energy Efficient Acquisition	Evaluation of energy factors will be mandatory when awarding contracts for systems and buildings.
2. Sail the "Great Green Fleet"	DON will demonstrate a Green Strike Group in local operations by 2012 and sail it by 2016.
3. Reduce Non-Tactical Petroleum Use	By 2015, DON will reduce petroleum use in the commercial vehicle fleet by 50%.
4. Increase Alternative Energy Ashore	By 2020, DON will produce at least 50% of shore based energy requirements from alternative sources; 50% of DON installations will be net-zero.
5. Increase Alternative Energy Use DON-Wide	By 2020, 50% of total DON energy consumption will come from alternative sources.

From R. Mabus, *Department of the Navy's Energy Program for Security and Independence,* Darby, PA: DIANE, 2010.

These goals have been established as a means to reduce the nation's dependency on fossil fuels [2, 3]. As shown in Figure 1, focus is placed on methods to increase energy security both on shore and in the tactical arena. Through the adaptation of alternative energy sources, conservation of current fuel supplies, and an increase in energy efficiency of current and developing systems, the DOD can begin to reduce its fossil fuel dependency. By advancing research in these three areas, the U.S. military can ensure its continued ability to project power abroad.

In recognition of the guidance put out by the SECNAV, the Waste Heat Recovery Systems (WHRS) team was established in 2013 at NPS in Monterey, California. This team was assembled to investigate current and developing technologies that can be used to advance Navy and Marine Corps heat exchanger technology. The investigation in these new technologies aims to increase DOD's energy efficiency and reduce our reliance on fossil fuels through the adaptation of WHR devices. By successfully completing these objectives, the team will assist the Navy in accomplishing its Energy Goals and Strategy outlined in Figure 1. Upon initiation, a six year WHRS Program Roadmap was generated which outlines the proposed research milestones to include numerical modeling and experimental research (see Figure 2).

Figure 2.　U.S. Navy's WHRS Program Roadmap 2014–2020

WHRS Program Roadmap 2014-2020
Sathe, Millsaps NPS

US Navy & NPS Capability

Infrastructure
- Computational Heat Transfer Laboratory
- Ultra High Reliability (UHX) Heat Exchanger Laboratory
- Measurement Methods
    - IR
    - Thermal Contact Resistance
    - Thermo-Mechanical Fatigue

Thermal Properties New Material Research

Heat Exchanger Models
- Local & Global (System) Integration
- Thermal Stresses
- Temperature and Flow Distribution
- Transient Effects

Design/Maintenance
- Heat Exchanger Designs
- System Level Considerations (Bypass/Novel Methods)

Turbulence/Fluids/Thermal Models
- Ducts
- Vanes
- Filters
- Infrared Radiation
- Closure Methods
- Convergence
- Pulsatile Flow
- Swirling Flow
- Mass Transfer/Particle Deposition

- IR Signature Reduction
- Thermal Radiation in Scattering, Absorbing and Emitting Media
- Pressure Drop Mitigation
- Waste Heat Recovery (COTS) Technology Evaluation

2014　2015　2016　2017　2018　2019　2020

From S. Sathe and K. Millsaps, *WHRS Program Roadmap 2014–2020,* Monterey, NPS, 2014.

At the time that this report was generated, the group had already achieved the milestone of establishing an Ultra High Performance and Reliability Heat Exchanger Laboratory through funding from the Office of Naval Research (ONR). In addition, multiple completed numerical studies have evaluated WHR in exhaust ducts for the Navy's gas turbines and the Marine Corps' diesel generators. These previous studies have investigated ways to reduce infrared (IR) signature [5], reduce thermal stresses in WHR devices [6], and mitigate pressure drops in ducts with turning vanes [7]. Comprehensive goals are outlined in Figure 2. Using an incremental approach to solving the military's energy issues, studies such as this one can generate the information needed to meet the goals set forth by the SECNAV.

Contributing to the work already accomplished by the WHRS team, this particular project focuses on the overall design and construction of an experimental system to measure thermal contact resistance and thermal conductivity accurately. By accomplishing this work, this project lays the groundwork and establishes the infrastructure for all future experimental research in the WHR and CPV fields at NPS as outline in Figure 2. With the recent large investments of the DOD into improving WHR and energy efficiency, attention needs to be drawn toward fully understanding the affect that both measurements have on the implementation of devices such as commercial off the shelf (COTS) WHR, CPV, and laser cooling components. Furthermore, accurate thermal contact resistance and thermal conductivity measurements will make the system ideal for evaluating new materials that could improve efficiencies in these systems (see Figure 2). Many of the new proprietary materials being developed by the DOD could lead to significant improvements in energy efficiency through their incorporation in system components such as gaskets and TIMs. Through the development of future new technological design and on-site capability, this study advances the WHRS group forward to meet the overarching goals of the USD (AT&L) and the SECNAV in improving the energy efficiency of shore based and tactical units.

B. AIM

This project aims to establish the onsite and internal DOD capability to thermally characterize materials and thereby determine which types would be of benefit to the WHR, CPV, and laser-cooling systems (see Figure 2). This will include the design and construction of an experimental measurement system that can accurately measure thermal contact resistance and thermal conductivity consistently from 0.1 to 40 W/m-K within a 5% margin of error. Focus will be placed on a simplistic design and construction method for the proposed system that will allow it to be easily built at any Department of the Navy (DON) or DOD research facility enabling that particular site to conduct on-site material thermal property research. The accuracy of this device will be evaluated using Pyroceram 9606 and 99.8% Alumina reference samples.

The focus on a simple measurement system design and construction method is aimed at enabling the device to be used by any researcher or engineer while still providing accurate results. This is in contrast to more complex measurement systems currently in use at many prestigious research facilities and commercial establishments throughout North America. The complexities associated with these systems often preclude researchers without extensive training from operating or repairing them. The proposed design allows for the commissioning and operation of a measurement system that can be completed by any experimentalist regardless of background.

Using this system, thermal properties of advanced proprietary materials being generated at NPS, as well as throughout the DOD, can be determined through future studies. The properties of materials such as high velocity oxygen fuel (HVOF), cold spray coatings, composites, and other advanced materials can then be assessed for their applicability in complex energy systems to control temperature and heat distribution.

C.   SCOPE OF REPORT

The presented work covers research in analytical, numerical, and experimental domains employed in the construction of a system to measure thermal contact resistance and thermal conductivity from 0.1 to 40 W/m-K. The first portion of this report will focus on the efforts contributed to the design and construction of the measurement system, including the rationale for particular design choices. The second portion will cover the experimental design layout and analysis of results. In this section, accuracy and replicability of the experimental measurements will be analyzed. Uncertainty analysis will be conducted on the produced data using the Kline and McClintock Uncertainty Analysis. Finally, a section of this report is devoted to future recommendations for the employment of the system design to include thermal contact resistance and thermal conductivity measurements as a function of pressure and sample temperatures.

THIS PAGE INTENTIONALLY LEFT BLANK

II. BACKGROUND

As the DOD strives to reduce dependency on fossil fuels through increasing energy efficient use, it must start by revisiting the basic principles of thermal energy and heat transfer. All too often, the decision is made to proceed with a new technology without first considering the possible adverse consequences, such as temperature, heat, and thermal stress distributions, that result from material selection of subcomponents. In most of these cases, the result of this inability to fully comprehend how component material selection effects the thermal environment within energy systems results in overheating and unbalanced thermal stresses as discussed in Koh [6]. Overheating and unbalanced thermal stresses lead to significant mechanical issues, such as component reliability, a problem that beset the U.S. Navy's (USN's) exhaust WHR devices employed aboard the Ticonderoga class cruisers and Spruance class destroyers [8]. In other cases, such as providing cooling air to electronics, temperature probe material selection and construction can contribute to inaccurate measurements, which can lead to increased cycling of air conditioning (AC) units increasing energy consumption. This specific situation was apparent in a few of the COTS cooling technologies being displayed to the Marines during their annual Expeditionary Energy Concepts (E2C) demonstration (previously known as Experimental Forward Operating Base (ExFOB)) in 2014. Similarly to other demonstrations the DOD hosts, the goal of E2C is to provide a forum in which civilian industry can demonstrate their COTS technologies to government stakeholders for future consideration and testing [9]. Without fully understanding how particular material choices in components can effect everything from temperature measurements to heat and thermal stress distributions, the DOD runs a high risk of purchasing future COTS units that will not be maximized for energy efficiency and/or reliability.

For a thermal measurement apparatus to be beneficial to the energy goals established by the SECNAV, several key performance criteria must be met.

- First and foremost, it must be able to measure thermal properties that are of interest to the DOD's current state of research and technology. For the

7

purposes of this study, underscored by current issues facing the DON, the choice was made to focus on thermal conductivity and thermal contact resistance.

- Secondly, the apparatus should improve upon experimental designs proposed through previous completed work in order to guarantee high measurement accuracy while minimizing result uncertainties.

- Thirdly, the chosen design and construction method should allow the measurement system to be constructed at any DON/DOD facility and be used by any experimentalist regardless of background to produce accurate results.

By meeting these discussed criteria, the measurement system will be able to provide large value to the DOD and its energy program.

A. THERMAL CONDUCTIVITY AND THERMAL CONTACT RESISTANCE

Two factors that influence how accurately we manage the thermal environment in energy systems are thermal conductivity and thermal contact resistance. Both affect the way heat and thermal stresses are distributed throughout the system. An example of one of the implications that result from improperly managing thermal contact resistance and thermal conductivity is temperature measurement inaccuracies. A probe constructed of a poor thermally conductive material when inserted into a hot fluid will read a lower temperature than actual due to an established difference in temperature between the probe surface and actual thermocouple or resistance temperature detector (RTD) position. This difference in temperature is a direct result of the material selected. To further complicate the issue, if the surfaces between the probe housing and thermocouple/RTD are not in full contact, thermal contact resistance will contribute to an even larger difference between actual and measured temperature values. These measurement inaccuracies can lead to increased cycling of cooling systems or the failure to detect system malfunctions. Through accurate measurements of a component's thermal contact resistance and thermal conductivity, the most ideal component design and construction method can be chosen. The incorporation of these improved components, such as gaskets, probes and TIMs, into military systems can then contribute to the overall improvement of energy efficiency and reliability throughout the DOD.

1.   Thermal Conductivity

Conduction is one of three methods through which energy transfer takes place and can occur within a single body or between multiple bodies in contact with one another. This is accomplished when molecules in warmer regions transfer kinetic and vibrational energy to neighboring molecules in cooler regions via collisions and random motion [10]. The measure of the rate at which this energy transfer occurs in a given material is represented by the material's thermal conductivity (k). This material property, measured in the International System of Units (SI Units) as W/m-K, is one of the key components in Fourier's Law of Conduction (see Equation 1) [10].

$$q_x^{"} = -k\frac{dT}{dx} = -k\frac{(T_2 - T_1)}{L}$$

(1)

Equation 1 applies to a specific case of one-dimensional (1-D) heat transfer by conduction as displayed in Figure 3.

Figure 3.   One-dimensional conduction heat transfer
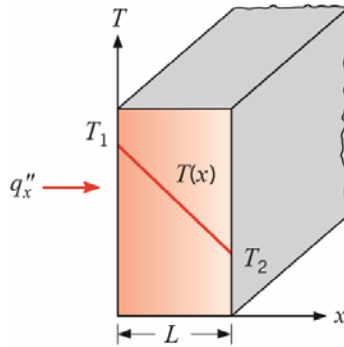
From T. L. Bergman and F. P. Incropera, *Introduction to Heat Transfer*, 6th ed. Hoboken, NJ: John Wiley & Sons, 2011.

In Figure 3, a linear, 1-D, heat flux ($q_x^{"}$ [W/m²]) is passed through a given material of length, L [m]. Based on the thermal conductivity of the material, a difference in temperature (dT), can be calculated. In materials with a high thermal conductivity, such

9

as metals, this difference in temperature is small. As a material's thermal conductivity decreases, the measured difference in temperature increases. This is one of the main reasons why metal is used extensively in the construction of temperature probes. The lower difference in temperature across the metal probe housing enables the thermocouple/RTD to accurately measure a fluid's temperature while still being protected. To calculate the total drop in temperature across n-multiple layered composite materials as shown in Figure 4, a summation of Fourier's Law of Conduction is used (see Equation 2).

Figure 4.   Temperature drop across multiple layered composite materials for a 1-D heat flux

From T. L. Bergman and F. P. Incropera, *Introduction to Heat Transfer*, 6th ed. Hoboken, NJ: John Wiley & Sons, 2011.

$$q_{x,tot}^{"} = \sum_{i=1}^{n} \left(-k \frac{dT}{dx} \right)_i \qquad (2)$$

As seen in Figure 4, with each additional layer of material the temperature drop increases across the overall composite. This drop is a function of each additional layer's thickness and thermal conductivity and does not address thermal contact resistance between the layers, which will be discussed in the following section. Equations 1 and 2

are suitable for basic analysis, however as the complexity of the thermal system increases, they are no longer suitable to predict temperature distributions.

For more complex thermal system environments, more variables must be taken into account to increase the accuracy in which temperature distributions are predicted. Equation 3 is an example of the general heat conduction equation based on a Cartesian coordinate system [10].

$$\frac{\partial}{\partial x}\left(k\frac{\partial T}{\partial x}\right)+\frac{\partial}{\partial y}\left(k\frac{\partial T}{\partial y}\right)+\frac{\partial}{\partial z}\left(k\frac{\partial T}{\partial z}\right)+q''' = \rho c_p\left(\frac{\partial T}{\partial t}+U\frac{\partial T}{\partial x}+V\frac{\partial T}{\partial y}+W\frac{\partial T}{\partial z}\right) \quad (3)$$

The left hand side of Equation 3 incorporates three-dimensional (3-D) heat transfer in a non-homogeneous material (variable thermal conductivity based on direction) with possible heat generation (q'' [W/m³]). The right hand side of this equation takes into account energy transfer due to fluid motion (U, V, W [m/s]) and unsteady conditions over time ($\frac{\partial T}{\partial t}$). Unlike Equation 1 and 2, the mathematics involved in this equation make it hard to predict temperature distributions in complex systems based on analytical rigor alone. For this reason, many complex conduction problems of real world scenarios rely on numerical software such as ANSYS. Material and composite thermal conductivity is a key parameter required in numerical analyses and can lead to gross inaccuracies if neglected or if the wrong value is used. These models contribute to the understanding of how heat transfer and thermal stresses are established throughout an energy system. Without the knowledge of a particular material's thermal conductivity, Equation 3 remains unsolvable regardless of the method used to analyze it.

The significant impact that material thermal conductivity has on the thermal environment within a system makes it an important property to measure accurately as the DOD proceeds to increase energy efficiency. Characterizing the thermal conductivity of materials such as composites and spray coatings can lead to improvements in component designs such as temperature probes, TIMs, and WHR device gaskets. The benefits of performing on-site measurements of the thermal conductivities of proprietary materials

11

currently under development by the DOD can lead to advances in many military applications without the added risk of having to send them to outside vendors for analysis. These applications range from relieving thermal stresses inherent in WHR applications to reducing IR signatures of ships and aircraft.

2.   Thermal Contact Resistance

In addition to thermal conductivity concerns within energy systems, thermal contact resistance also contributes to major issues in DOD applications. This becomes of primary concern in systems that exchange heat by means of conduction [12, 13]. When working with systems involving multiple layers through which heat transfer must occur, such as CPV and WHR devices, thermal contact resistance poses a significant challenge. This issue occurs through the formation of micro-voids at the interface between two objects when they are placed in contact with each other. These micro-voids are formed between surfaces of objects and impede energy transfer via conduction by effectively reducing the overall cross sectional area through which it can directly pass. Since these voids result from microscopic defects in each of the materials' surfaces, interfaces between otherwise visually smooth materials will still exhibit these micro-voids. When a heat flux is passed through the two materials, a difference in temperature can be measured across the interface due to the established thermal contact resistance (see Figure 5).

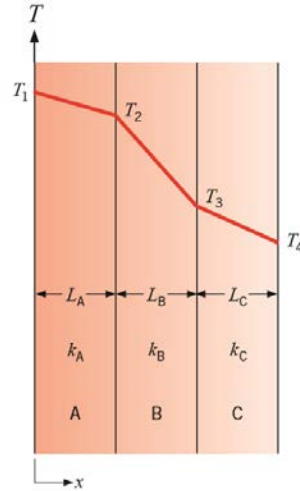Figure 5.   Temperature drop due to thermal contact resistance at the interface of materials
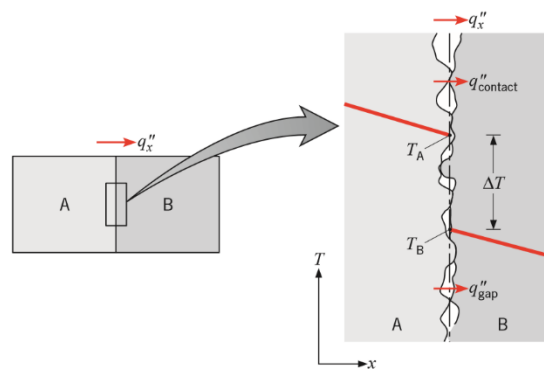
From T. L. Bergman and F. P. Incropera, *Introduction to Heat Transfer*, 6th ed. Hoboken, NJ: John Wiley & Sons, 2011.

In Figure 5, 1-D heat flux ($q_x^"$) is shown to occur between the areas of direct contact ($q_{contact}^"$) and across the micro-voids that are formed between materials A and B ($q_{gap}^"$). The energy transfer across the micro-voids is due to a combination of conduction and radiation, and often occurs at a less significant rate compared to the energy transferred directly through the contact surfaces [11]. Thermal contact resistance can be quantitatively calculated at an interface as a function of the difference in material surface temperatures across the interface established by a 1-D heat flux (see Equation 4) [11].

$$R_{t,c}^" = \frac{T_A - T_B}{q_x^"} \tag{4}$$

For complex systems that are composed of n-multiple interfaces, thermal contact resistances associated with each interface can be summed to calculate an overall effective thermal contact resistance inherent in the component depending on whether the interfaces are in parallel (see Equation 5) or series (see Equation 6).

$$R_{t,c\,TOT}^" = \sum_{i=1}^{n} \left(R_{t,c\,i}^" \right) \tag{5}$$

$$R_{t,c\,TOT}^" = \frac{1}{\sum_{i=1}^{n} \left(1 \middle/ R_{t,c\,i}^" \right)} \tag{6}$$

Similar to the effects of resistance in electrical applications, the means in which the thermal interface resistances are summated in a device can have substantial implications in the ability to transfer heat energy and minimize component temperatures. The difference in temperature between surfaces shown in Figure 5 is observed in CPV technology and WHR devices passing a constant heat flux to an otherwise constant temperature heat sink. As thermal contact resistance increases, a component must either increase in temperature for a constant heat energy transfer (e.g. CPV cell), or suffer from decreased energy transfer in situations with a constant temperature heat source (e.g. WHR devices). Therefore, complex multi-interface systems with high overall thermal contact resistance often suffer premature failure and exhibit excessively inefficient energy transfer capabilities. In order to increase the DOD's energy efficiency and

13

reliability of thermal systems, this impact must be taken into account including the various methods that can reduce the thermal contact resistance at a given interface.

Since thermal contact resistance is incurred by the establishment of micro-voids between two materials, there are three common methods through which it can be minimized. A first-step method used in commercial applications is to increase the flatness and smoothness of each material's surface through mechanical sanding, buffing, and/or polishing. In military applications, however, where normal operating environments (e.g., deserts and oceans) and routine maintenance can damage a component's surface, this method of creating precision-machined components is not viable. Furthermore, even if restricted to use in less caustic environments, the cost implications of manufacturing such items would significantly increase the cost of even the most routine item acquisition. A second method involves collapsing these voids by using pressure exerted on each of the two materials. Increasing the pressure between the materials' interfaces is a plausible method for reducing thermal contact resistance, but is limited when applied to fragile electronics and WHR devices where size and weight are of concern (e.g., higher pressures necessitate a more robust mechanical system design). Finally, an interstitial (filler) material with a thermal conductivity greater than air can be used to fill the voids between the two materials reducing the thermal contact resistance [11, 14]. In comparison to the first two methods, TIMs, such as soft metals and thermal greases, can be applied in a wide range of situations and are also cost effective. As discussed in Reddy [15], TIMs can also be combined in layers to achieve desired composite properties, further increasing the suitability of these materials in DOD applications.

Development of an infrastructure to characterize thermal conductivity and thermal contact resistance of advanced materials will be of great benefit to the DOD. Many of the materials currently undergoing development by the DOD are proprietary and therefore are unable to be sent out to many civilian laboratories for thermal characterization. Additionally, for samples that can be sent out, the process in many instances requires extensive time and high costs to complete. The commissioning of a simple measurement system that can accurately measure thermal contact resistance and thermal conductivity will allow a significant portion of these analyses to be performed at any DON/DOD

facility. Results from these material analyses can then be utilized during the development of new WHR devices, various energy system components, and evaluation of manufacturing processes to minimize thermal stresses and maximize energy transfer. To guarantee the accuracy and repeatability of these experimental results, current measurement techniques will be analyzed for strengths and weaknesses so that an optimized measurement system can be designed and constructed.

B.   INSIGHT GAINED FROM CURRENT MEASUREMENT TECHNIQUES

Since thermal conductivity and thermal contact resistance is key to engineering designs, over the past decades, numerous experimental systems have been developed and patented in the pursuit of accurately measuring thermal conductivity and thermal contact resistance. As a result, extensive literature review based exclusively on the experimental determination of thermal conductivity is available such as that discussed by Touloukian, Yovanovich, and Fletcher [16-21]. The many designs discussed are necessitated in order to measure thermal conductivity for various classes of materials over different ranges of temperatures [16]. These methods include both transient and steady state measurement analysis. Many of these methods discussed in literature, however, are conceptual and have not been physically implemented or assessed for measurement capability. Additionally, of the proposed measurement systems that have been physically assessed, many require specialized training to operate or introduce inaccuracies and uncertainties due to their inherent design which may make them unsuitable for use within many DOD facilities.

Compared to steady state analyses that use Fourier's Law of Conduction (see Equation 1), transient methods require a more complex calculation and equipment setups [22-24] and therefore have challenges concerning repeatability of analyses. This calculation requires the measurement of additional variables during analysis that can increase uncertainty in measurement results (Equation 7) [11, 25].

$$\frac{d}{dx}\left(k \frac{dT}{dx} \right) = \rho C_p \frac{dT}{dt} \tag{7}$$

Equation 7 indicates that to obtain accurate measurements of a material's thermal conductivity, the specific heat (C_p) and density (ρ) need to be measured. These values both vary due to temperature and are required to be measured during the analysis. These additional measurements lead to added complexities in the measurement device such as shown in the *Laser Flash Method* [26-29]. To ensure that the designed measurement device could be used in any DON/DOD facility by any researcher regardless of background, transient analysis was therefore rejected in favor of steady-state analysis techniques.

For steady state analysis, two common absolute methods, *Rod* and *Plate*, are proposed as ways to measure thermal conductivity using a longitudinal (1-D) heat flow (see Figure 6) [16].

Figure 6.   *Rod* and *Plate Method* experimental setups
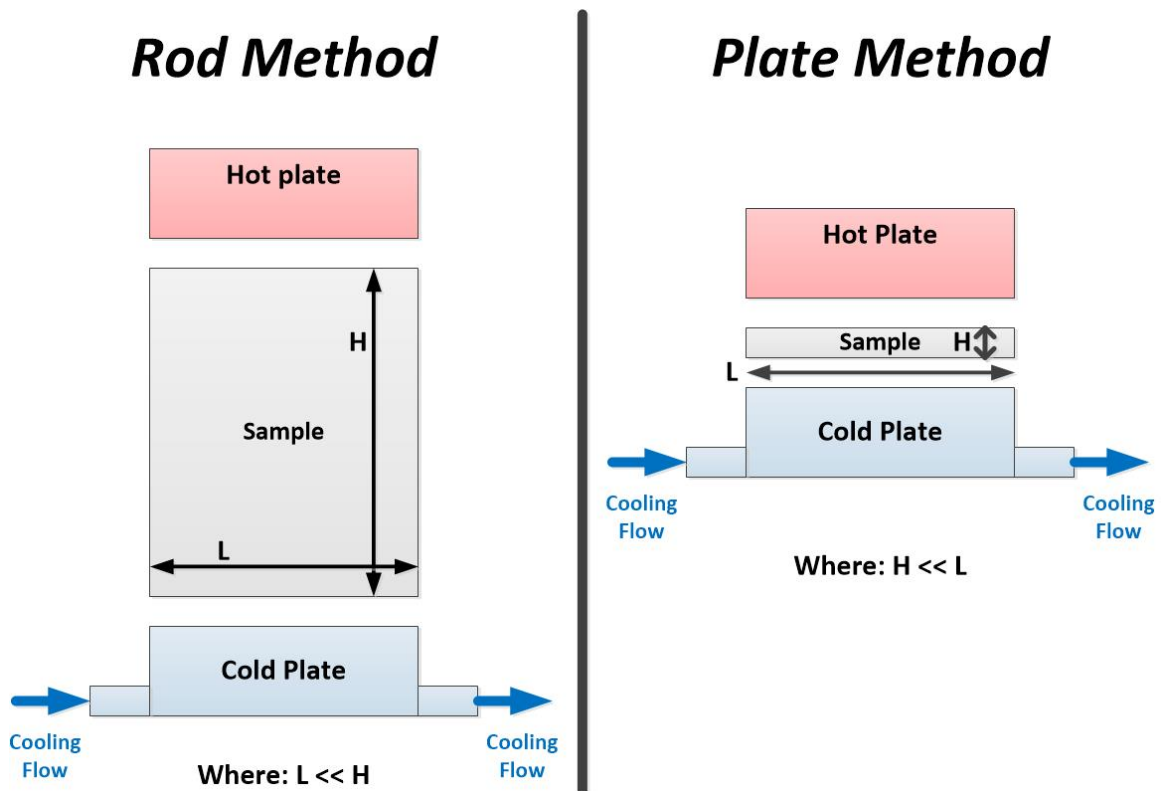
As shown in Figure 6 the primary difference between the *Rod* and *Plate* Methods is the thickness of the sample (H) compared to its side length (L). For either method, in

order to achieve accurate results, an appreciable temperature drop must be established across the sample material to calculate its thermal conductivity. This difference in temperature is then used to calculate a material thermal conductivity using the one-dimensional Fourier-Biot heat-conduction equation (see Equation 8) [16, 30].

$$k = \frac{-qdx}{AdT}$$
(8)

The one-dimensional Fourier-Biot heat-conduction equation can be understood as the rearrangement of Fourier's Law of Conduction (see Equation 1) using the definition for 1-D heat flux ($q_x^{"} = \frac{q_x}{A}$). In addition to requiring the measured drop in temperature across the sample material thickness, Equation 8 also requires the surface area (A [m²]) and the heat energy (q, [W]) that is being passed through the specimen. Due to less variables present within Equation 8 compared to Equation 7, fewer types of measurements need to be conducted during analysis reducing design and operation procedure complexities.

The first steady state method, known as the *Rod Method*, is suitable for good conductors under a wide range of temperatures; excluding very high temperatures [16]. In this method, a linear heat flux is created and passed through a material specimen of significant thickness. The required thickness of the specimen is determined based on the predicted material thermal conductivity. For accurate thermal conductivity measurements, an appreciable temperature difference across the sample is needed thereby requiring material samples expected of high thermal conductivity to have a greater thickness. To ensure that the heat flux through the sample is linear, either vacuum chambers or guard heaters are recommended [16]. These methods prevent heat loss along the sides of the sample to minimize measurement inaccuracies. The *Rod Method* has been successfully demonstrated to accurately measure thermal conductivity and contact resistance as shown by work performed by Teerstra and Culham [31–32]. The number of different required types of measurements within this method however leads to increased result uncertainty. For example, in order to measure the temperature drop along the length of the sample, multiple sequential measurement devices must be used each contributing to device measurement uncertainty. Furthermore, the increased complexity

(i.e., vacuum chambers and lateral heat guards) necessary in the design of this system prevents it from being able to be built at any DOD facility and operated by any experimentalist regardless of background.

In comparison to the *Rod Method*, the *Plate Method* is able to measure thermal conductivity of samples without the need for a vacuum chamber or peripheral guard heaters by reducing the total side area of the measured sample. By reducing a material sample's thickness, a majority of the heat flux passed through the sample will be linear. In situations where it is desired to further minimize heat loss through the reduced side areas, insulation can be applied. In contrast to the *Rod Method*, this method works well only for low-conductivity materials [16]. The *Plate Method* has been applied successfully in research such as for measurement of fiberglass insulation by Sathe et al. [33] and is comprehensively discussed in Pratt [34]. Many proposed successful designs, however, have associated weaknesses. While the system designed by Sathe works well to measure insulation thermal conductivity [33], it cannot specifically measure thermal contact resistance at the interfaces, normally not necessary for fiberglass insulation measurements. Other proposed systems require multiple samples to be used during analysis [16]. In order for these systems to provide accurate measurements while minimizing uncertainties, identical samples must be used. Duplicate samples are very hard to produce due to material variances and manufacturing tolerances.

Both of the previously discussed methods can be used to accurately determine contact resistance using a method of calculating material thermal resistance as discussed in Teertstra [31]. This method involves creating a layered sample in which all variables are known with the exception of the thermal contact resistance. Using the relationship between thermal resistivity and thermal conductivity (see Equation 9), a parallel resistivity network analysis similar to Equation 5 can be utilized to calculate the thermal contact resistance from the measured composite's effective thermal conductivity.

$$R^{"}_{material} = \frac{1}{k_{material}}$$
(9)

By applying this calculation method, a thermal conductivity measurement apparatus can serve to also accurately measure thermal contact resistance.

Understanding the benefits and disadvantages of current measurement techniques for thermal contact resistance and thermal conductivity can help guide the project's design, construction, and operation procedures. Furthermore, the devices discussed indicate that a majority of the systems in use, such as those using the transient or *Rod Methods*, are very complex and require special training to operate let alone construct within any particular facility. Therefore, it is imperative that a simplistic design be produced that can be constructed and utilized to measure these properties at any DOD facility. Even with a simplistic design however, as shown by some *Plate Method* systems currently in use, inaccuracies can occur without fully understanding heat transfer theory. These intricacies that go into designing an accurate and reliable measurement system need to be understood to produce a device that is of value to the DOD.

C. DIFFICULTIES IN ENSURING REPLICABLE ACCURATE MEASUREMENTS

Before moving directly to designing a thermal contact resistance and thermal conductivity measurement system, it is important to first emphasize how certain effects can impact the accuracy and replicability of measurement results calculated using Fourier's Law of Conduction (see Equation 1). By understanding these effects, certain design choices can be made to maximize measurement accuracies eventually resulting in a proposed design method for the project. The first adverse effect is the propensity of a generated heat flux to move through a material in a multi-dimensional manner. This is usually a result of heat losses from the device due to conduction, convection, and radiation, which can greatly reduce the amount of heat transferred through a sample material [11]. Second, based on the method of cooling and the effect of the surrounding environment, a temperature distribution within an object will tend to vary in multiple directions. Finally, unwanted thermal contact resistance can reside between the sample and device surfaces. This contact resistance can affect the difference in temperature across the sample causing the device to measure a lower than actual thermal conductivity. Based on the measurements required to calculate the thermal conductivity of a sample material using Fourier's Law of Conduction, any inconsistency in these factors can lead to inaccurate and highly variable measurement results.

To ensure accurate and replicable results, it is imperative that a 1-D heat flux be preserved throughout the thermal contact resistance and thermal conductivity measurement system. In a basic system composed of a sample, hot, and cold plate, heat flux (q") from the hot plate can travel in multiple directions (see Figure 7).

Figure 7.   Heat loss resulting from an uninsulated measurement device
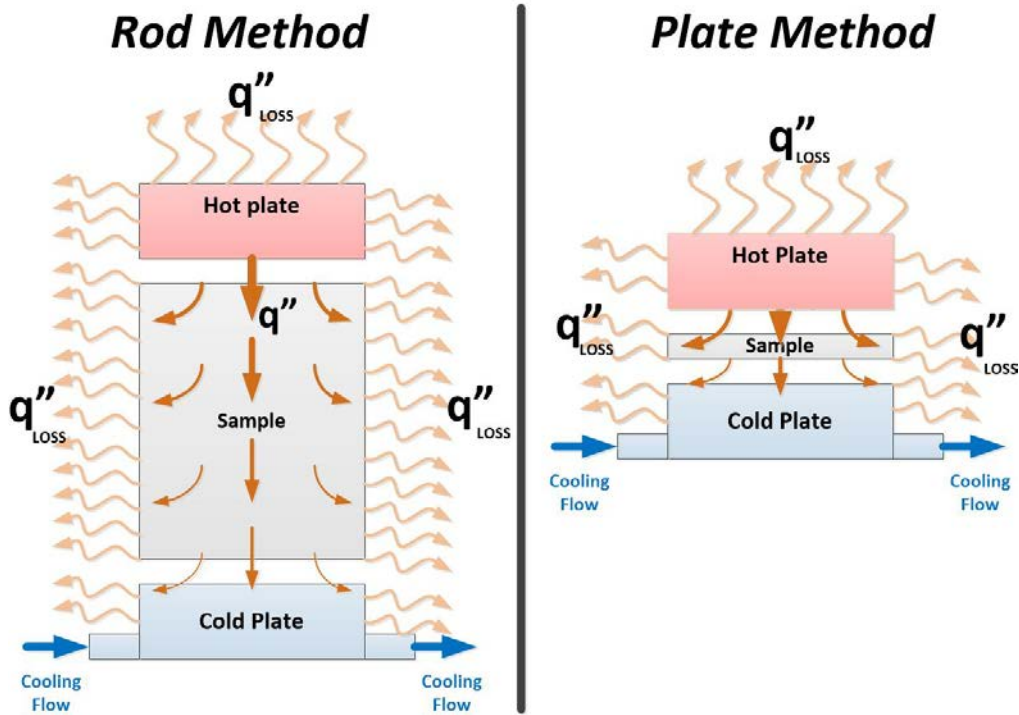
As shown in Figure 7, heat flux can leave the hot plate to the environment from the top as well as from all exposed sides of the device for either *Rod* or *Plate Methods*. This not only disrupts the 1-D heat flux going through the sample required to use Fourier's Law of Conduction, it also greatly reduces the amount of heat flux. Based on the surrounding environment, this decrease could be minimal or substantial leading to high variability within the heat transfer term (q) of Equation 1. To control this heat loss as well as maintain a 1-D heat transfer through the device multiple methods have been proposed [16]. Methods such as a vacuum chamber and guard heaters have been proven successful for the *Rod Method* [17, 18, 31, and 32] while insulation is suggested to be used for the *Plate Method* [16] (see Figure 8).

20

Figure 8.   Insulated measurement devices to reduce heat loss
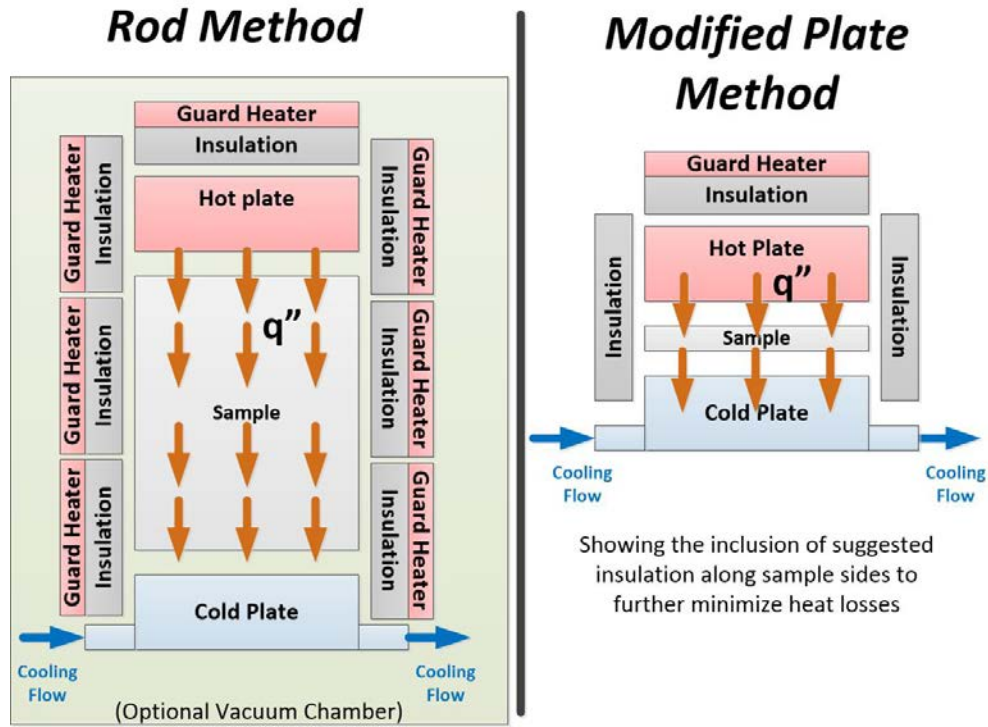
As shown in Figure 8, the use of an additional upper guard heater with insulation can further reduce heat loss and redirect any heat flux from the hot plate back toward the sample. The use of upper guard heaters is consistent with the *Rod Method* and leads to the increased complexity as shown in Figure 8, which can be detrimental to the ease of system use and replicability of results. Contrary to this, incorporation of upper guard heaters to the *Plate Method* is a modification to the basic design presented and does not pose a significant increase in complexity [16]. By comparing the two methods side by side, it is evident that this modified plate method is much simpler to design and construct making it a preferred choice for the purposes of this project. By reducing the heat loss and ensuring a 1-D heat flux through the sample, the modified plate method allows for accurate and replicable measurement results of thermal contact resistance and thermal conductivity to be calculated using Fourier's Law of Conduction while minimizing the complexity normally associated with the *Rod Method*.

The next step to guaranteeing accurate and replicable results are generated by the measurement system is to ensure that a uniform temperature distribution is established at

the sample-to-device interfaces. This is important since the difference in temperature across the sample for a non-uniform temperature distribution can vary greatly depending on where measurements are made. In order to reduce variability in these cases, a large number of measurements must be conducted at various locations to provide an accurate average differential temperature. In order to conduct fewer measurements, thereby simplifying the design, construction, and operation of the device, a uniform temperature distribution is required. This uniform temperature distribution however is affected by multiple different design decisions. The main contributing factor out of these is the method of heat removal from the device. Ideally, the device would have a side held at a constant uniform temperature to which the heat generated by the hot plate could be rejected. The ability to create this is limited, however, in applications where a working fluid is used (see Figure 9).

Figure 9.   Measurement device temperature distribution due to parallel coolant flow
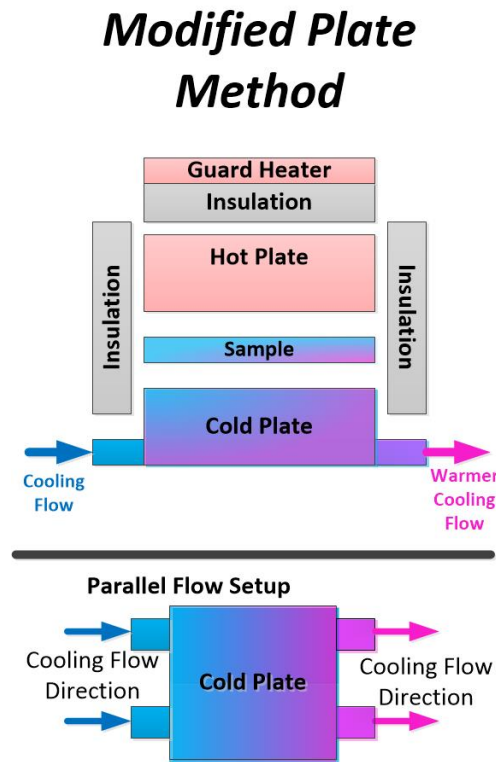
In Figure 9, the cooling channels of the modified plate method are shown with parallel flow going through them. As heat is rejected to these channels the fluid temperature rises causing a temperature gradient to form through the rest of the measurement device. By switching one of the flow directions, this gradient is minimized and a larger portion of the device is at a uniform temperature distribution (see Figure 10).

Figure 10.   Measurement device temperature distribution due to counter coolant flow
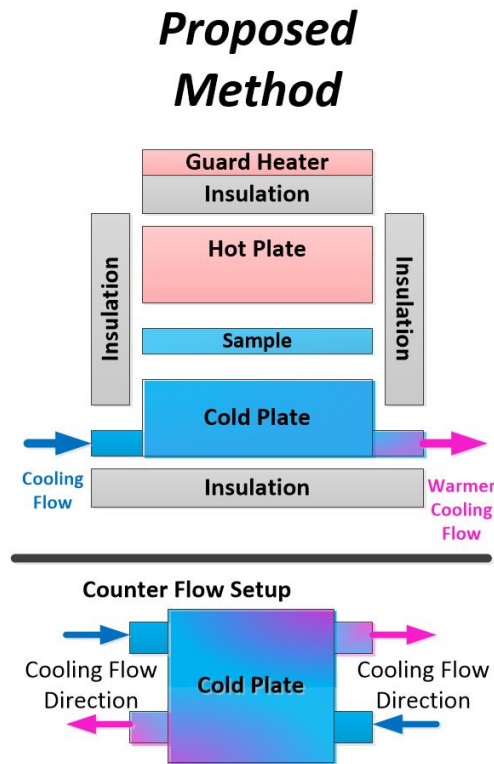
In addition to using counter flow shown in Figure 10, added channels or increased channel inner diameter can also lead to a more complete distribution. To further improve the uniform temperature distribution at this point and reduce variability, insulation can be provided around the device to minimize any temperature gradient established along the sides due to interaction with the environment. Increasing the accuracy, while reducing the variability of differential temperature measurements, will improve the capability of a measurement system to provide accurate and replicable results. This added set of design

modifications to ensure temperature uniformity establishes the proposed method for the measurement device presented in this report.

Finally, the last consideration that needs to be made when designing and constructing a thermal contact resistance and thermal conductivity measurement system is the thermal contact resistance that is inherent in the design itself. Due to the thinness of the sample, thermal interface resistance is a lot more critical in designs based on the P*late Method* compared to the *Rod Method*. Specifically of concern is the contact resistance established between the sample and the hot and cold plates (see Figure 11).

Figure 11.   Measurement device thermal contact resistance location
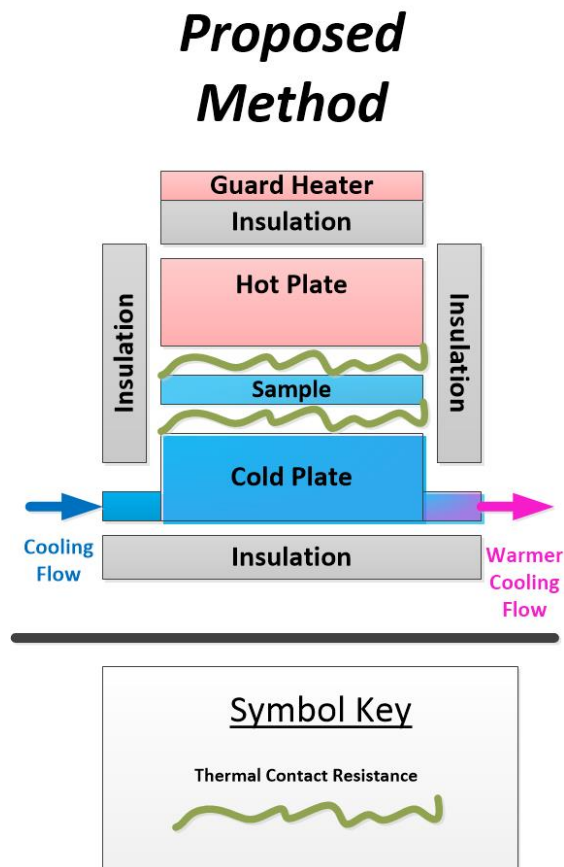
As shown in Figure 11, this contact resistance forms when the device and sample are placed in contact with one another. This layer of contact resistance is highly variable and can be influenced by the smoothness of the sample, oil/chemical residue on the

surfaces, or plausible condensation that can form on the cold plate during operation. The variability of this contact resistance can greatly affect the replicability of the measurement results in addition to accuracy. To resolve this issue, thermal grease can be applied to the interface between the cold, hot, and sample plates (see Figure 12).

Figure 12.   Thermal grease application location on measurement device
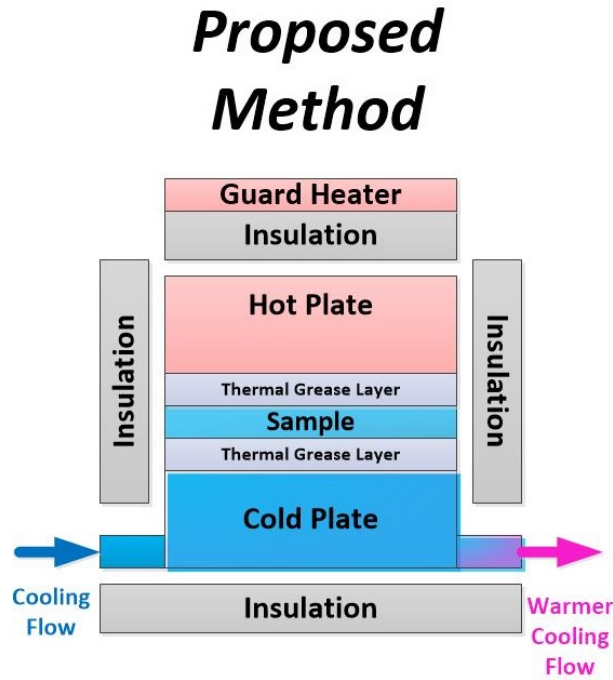
This layer of grease acts to reduce the thermal contact resistance and ensures less variable conditions between measurements due to the previously mentioned factors. By using a thermal grease layer, which can be controlled through application, more accurate and replicable results can be produced using the proposed measurement system and Fourier's Law of Conduction.

By analyzing and understanding the main factors that can prohibit the accurate and replicable measurements of thermal contact resistance and thermal conductivity using Fourier's Law of Conduction, design choices can be made to reduce their effect. 1-D heat flux can be maintained, while minimizing heat losses, through the use of guard heaters, a vacuum chamber, and/or insulation. Uniform temperature distribution at the sample

interface can be assured by affecting the flow direction though coolant channels as well as the size and number of the channels themselves. Finally, adverse effects on measurement accuracy and replicability due to unwanted thermal contact resistance between the sample and the system can be reduced through the use of thermal greases. Understanding the impact that these design choices have on desired accuracies and measurement replicabilities offers the ability to propose a sound measurement device design. This proposed design will be referenced throughout the design and construction phase of this project.

D.   DETERMINING RESULT UNCERTAINTY

For the purposes of improving energy efficiencies within DOD applications, the thermal measurement apparatus must accurately measure thermal contact resistance and thermal conductivity. Additionally, the accuracy of this device must occur throughout multiple analyses done by various users. Since the measurements will be taken using only one device, the results obtained will be classified as from a single-sample experiment regardless of the number of runs conducted [35, 36]. Unlike a multi-sample experiment, where multiple measurement techniques and devices are employed, a single-sample experiment will have some measure of error present that cannot be removed through statistical analysis of the results [35]. Therefore, to ensure the thermal measurement apparatus produces the most replicable and accurate measurements possible, analysis of experimental uncertainties must be completed.

In order to fully understand where experimental uncertainties are introduced in the apparatus, the Kline and McClintock Uncertainty Analysis will be used (see Equation 10) [35, 36].

$$w_R = \left[\left(\frac{\partial R}{\partial x_1} w_1 \right)^2 + \left(\frac{\partial R}{\partial x_2} w_2 \right)^2 + \ldots + \left(\frac{\partial R}{\partial x_n} w_n \right)^2 \right]^{\frac{1}{2}} \tag{10}$$

where,

$$R = R\left(x_1,\ x_2,\ \ldots,\ x_n \right)$$

w_R – Uncertainty in the overall result

$w_1,\ w_2,\ \ldots, w_n$ – Uncertainties in the independent variables

26

Using the Kline and McClintock Uncertainty Analysis, the impact of uncertainties in variables (denoted: x_i) on overall calculated uncertainty can be recognized. Unlike error analysis on a common-sense basis, where errors may be combined in the most detrimental way, Equation 10 takes into account that all measurements will not occur in the worst case possible 100% of the time [35, 36]. This process allows for the identification of measurements that have the greatest impact on overall uncertainty. Using this information, decisions can be made during the design, construction, and operation process phases to minimize these uncertainties. This will in turn greatly improve the reliability in the measured thermal contact resistance and thermal conductivity results.

E. SUMMARY

The development of a thermal measurement apparatus that can reliably produce accurate thermal contact resistance and thermal conductivity data will be of great use to the DOD in establishing energy efficient systems. As discussed, many under development materials are proprietary and therefore cannot be sent to many civilian laboratories for thermal property characterization. This project aims at establishing a device that can be built in any DON/DOD facility and used by any researcher regardless of background. By discarding transient analysis techniques due to inherent complexities, steady-state thermal analysis indicates the most plausible way in designing a simplistic yet accurate measurement device. Two apparatus designs, the *Rod* and *Plate Methods,* currently in use by the civilian research sector are plausible methods of accomplishing this task. Further analysis into the complexities of each method indicates that a proposed method derived from the *Plate Method* will be better at satisfying the aims of this project. The finalized choice and reasoning of which method to utilize, as well as overall device design, construction, and operation, is covered in the next section of this report.

THIS PAGE INTENTIONALLY LEFT BLANK

III. EQUIPMENT DESIGN, CONSTRUCTION, AND OPERATION

Utilizing the covered literature research, the design, construction, and operation of the thermal contact resistance and thermal conductivity measurement apparatus can be addressed. At this point it is crucial to examine all plausible design methods to ensure accurate and replicable results. Analytical and numerical results generated in the design phase provide insight into subcomponent characteristics of the apparatus prior to being machined and assembled. In the construction phase of the project, COTS units are combined with machined components. These units were specifically chosen based on particular performance characteristics to maximize measurement accuracy and replicability. Finally, operating procedures for the overall system and subcomponents are discussed to ensure safety and reliability of the system during use.

A. DESIGN

In the design phase of the project, the aim was focused on producing a thermal contact resistance and thermal conductivity measurement system that could generate accurate results while having the capability to be constructed and replicated at any DOD facility and could be used by any researcher/engineer. Keeping this in mind, certain decisions were made regarding the particular measurement method to be used, dimensions of the apparatus, and material selected for machining the subcomponents. In all cases, driving factors included establishing temperature uniformity at the sample location, establishing a 1-D heat flux, minimizing unwanted heat loss to the surrounding environment via convection and radiation, and reducing production costs. From these decisions, components were designed using SolidWorks computer software. Using these models, parts were then machined to be incorporated in the construction of the overall system.

1. Method

For the purposes of measuring materials such as gaskets, TIMs, and thermal coatings the decision was made to develop the capability to measure thermal conductivity of materials ranging from 0.1-40 W/m-K. This range provides the ability to measure thermal conductivities of materials such as nonmetallic solids, oxides, and steels

commonly used in WHR, CPV, and laser cooling applications (see Figure 13)[11, 37]. Sample material thermal conductivity would be calculated using Fourier's Law of Conduction (see Equation 1) which minimizes the number of variables that would need to be measured compared to transient analysis (see Equation 7). By reducing the number of variables that would need to be measured, the uncertainty in the results can be minimized, and the simplicity of construction and repeatability can be improved.

Figure 13.   Ranges of material thermal conductivities at normal pressure and temperature
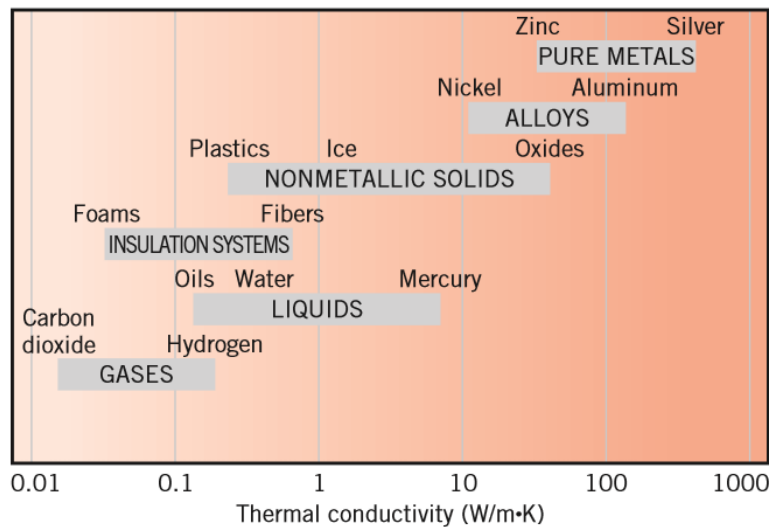
From T. L. Bergman and F. P. Incropera, *Introduction to Heat Transfer*, 6th ed. Hoboken, NJ: John Wiley & Sons, 2011.

In addition to the material sampling capability, the decision to measure this band of thermal conductivity was made based on the following:

- In order to accurately measure thermal conductivity between 0.1-40W/m-K the *Plate Method* as described by Touloukian [16] could be utilized. Using this method, a one dimensional heat flux can be established without added complexities such as a vacuum chamber or lateral guard heaters as recommend with the *Rod Method* [16]. As discussed previously, this 1-D heat flux is crucial to accurately determining sample thermal conductivity using Fourier's Law of Conduction (see Equation 1) and the Fourier-Biot heat-conduction equation (see Equation 8)

- Developing an apparatus based off the *Plate Method* first provides a frame work of best practices that can be used during the development of a system utilizing the *Rod Method* for the WHRS team.

Based on the reasoning presented, a proposed design (see Figure 12) derived from the *Plate Method* was chosen to measure thermal contact resistance and thermal conductivity in order to support the WHRS team efforts specified in the proposed WHRS Program Roadmap (see Figure 2). By being based off the *Plate Method*, the proposed design is able to generate extremely useful data based off new age materials and composites being generated throughout the DOD such as HVOF and cold spray coatings. This data can be used by the WHRS team in the development of WHR system components to minimize thermal stresses, improve temperature measurement accuracies of probes in inlet and exhaust ducts, and reduce IR signatures of ships.

2.   Sample Dimensions

After determining to use a proposed design derived from the *Plate Method* for measurement analysis, one of the first initial steps performed to ensure uniform temperature distribution and 1-D heat flux was to assess which apparatus design dimensions provided the best performance. In order to assess this for a real scenario, these analyses had to be performed without assuming adiabatic (no heat transfer) material boundaries. Using SolidWorks software, apparatus models of square and circular cross-sections were generated including a sample portion and surrounding insulation layer (see Figures 14 and 15).

Figure 14.   Square sample cross-section model with insulation
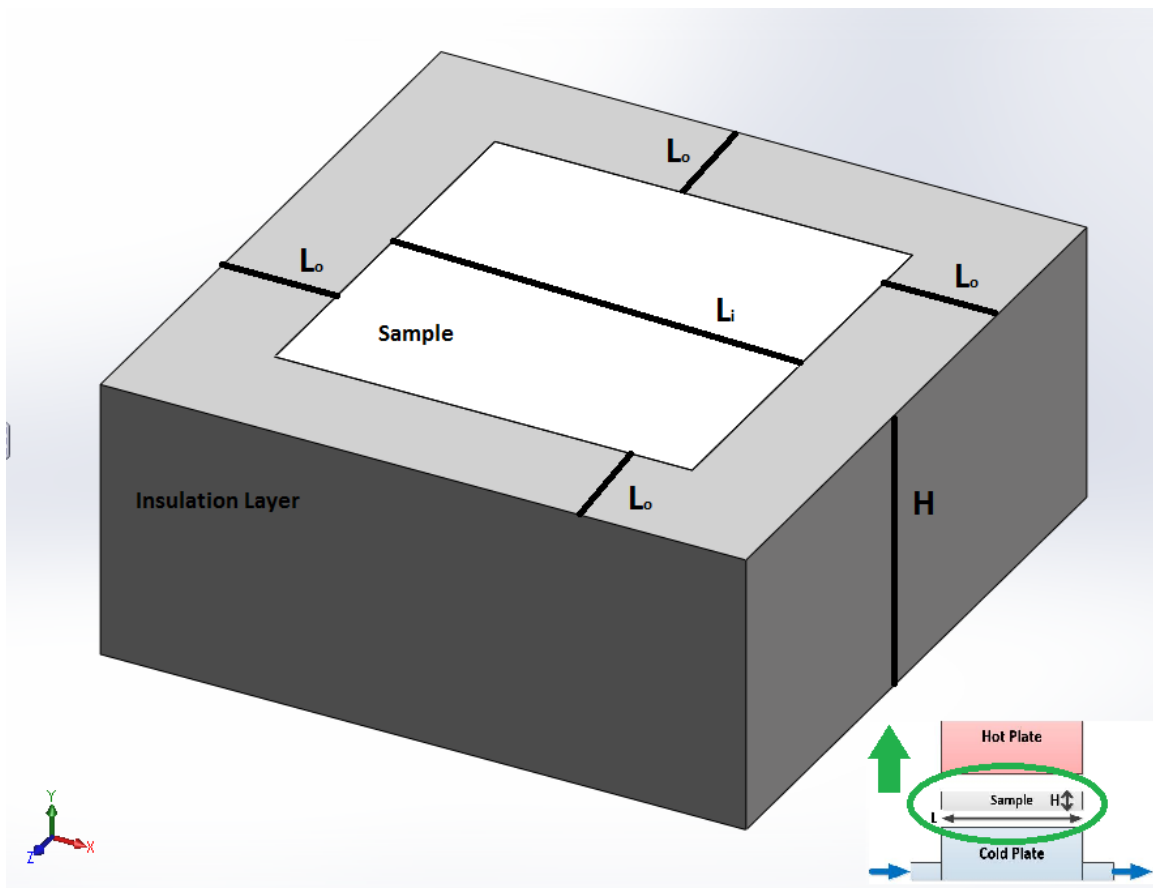
Figure 15.   Circular sample cross-section model with insulation
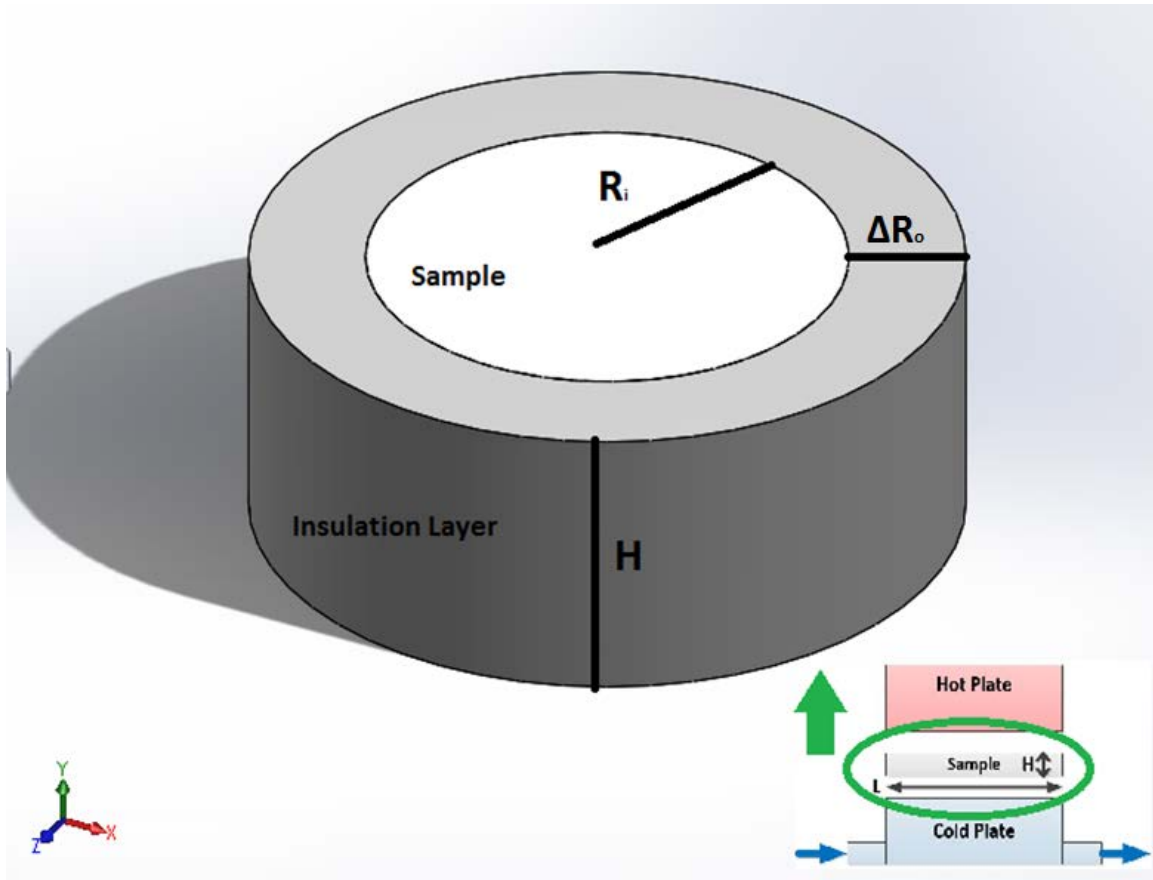
Dimensional values for each model (Square: Side Length – Li; Circular: Radius – Ri) were specifically chosen to create the same sample cross-section area, overall sample height (H), and same insulation thickness (Square: L_o; Circular: ΔR_o) along the side of each sample surface (see Table 1).

Table 1.   Dimensional Model Design Parameter Values

Model Dimensions						
Sample Cross-Section Type	R_i	ΔR_o	H	L_i	L_o	Cross-Section Area
	[m]	[m]	[m]	[m]	[m]	[m²]
Square	-	-	0.03	0.04502	0.0123	0.00202680
Circular	0.0254	0.0123	0.03	-	-	0.00202683

Next, ANSYS numerical analysis was performed using these models to measure their ability to maintain temperature uniformity and linear heat flux. For each model, a fine mesh grid and boundary conditions were generated (see Figures 16–19).

Figure 16.   Square sample cross-section model mesh
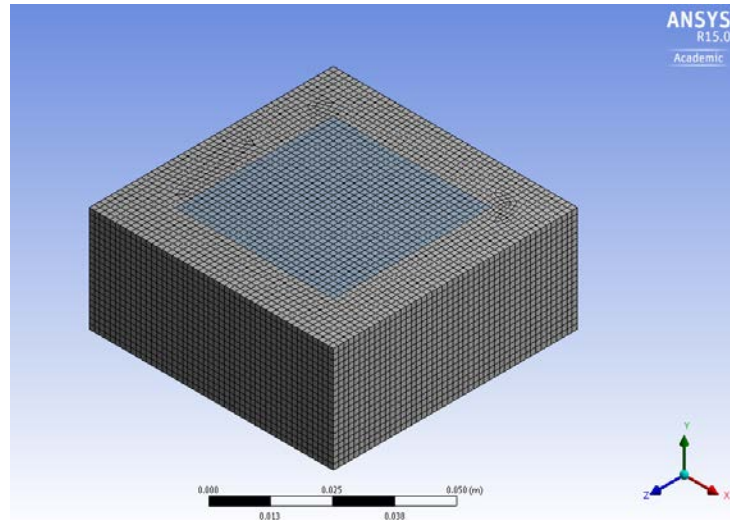
Figure 17.   Circular sample cross-section model mesh
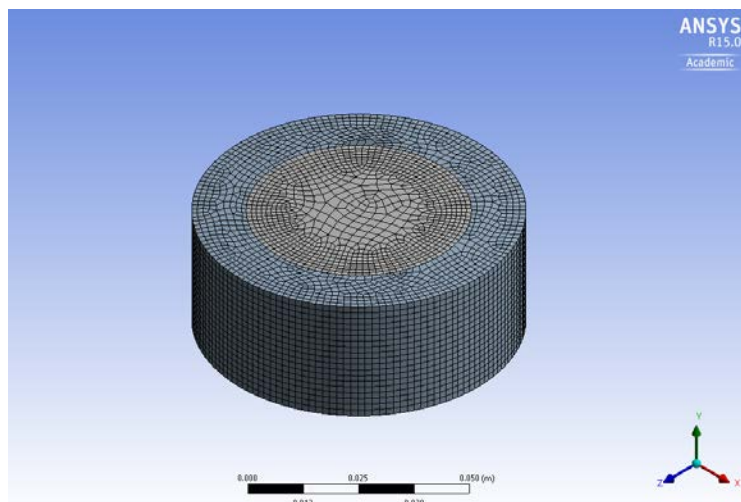
Figure 18.   Square sample cross-section model boundary conditions
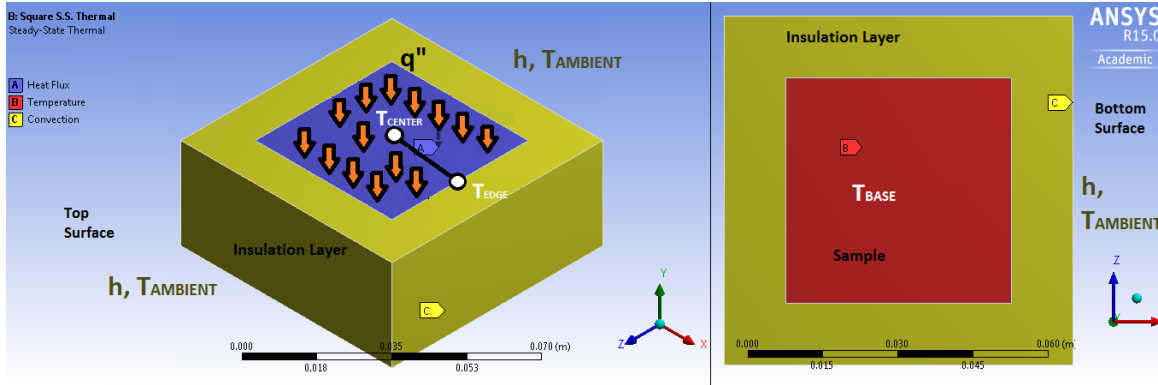
In figure, uniform heat flux boundary condition (orange and black arrows) applied to purple surface. Convection boundary conditions at yellow surfaces (h, $T_{AMBIENT}$). Isothermal boundary condition applied at red surface (T_{BASE})

Figure 19.   Circular sample cross-section model boundary conditions
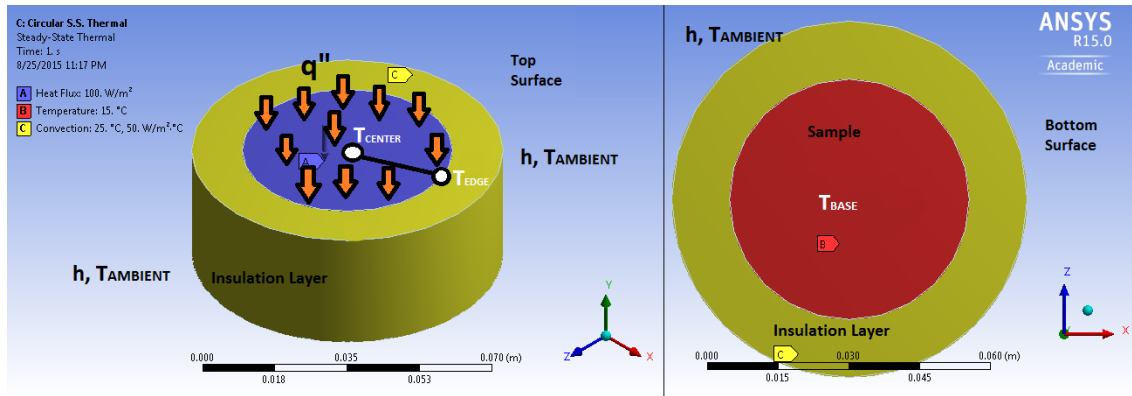
In figure, uniform heat flux boundary condition (orange and black arrows) applied to purple surface. Convection boundary conditions at yellow surfaces (h, $T_{AMBIENT}$). Isothermal boundary condition applied at red surface (T_{BASE})

Figures 16 and 17 show the layout of the fine mesh used in the numerical analysis. For the purposes of this investigation, a program controlled triangle surface mesh was used. Figures 18 and 19 show the boundary condition layout used for the model geometries, which was varied for different convection heat transfer coefficients (h) for a given heat flux through the sample (see Table 2).

Table 2.   Square versus circular ANSYS model design parameters

Sample Cross-Section Type	ANSYS Model Parameters					
	$T_{AMBIENT}$	T_{BASE}	h	k_{sample}	$k_{insulation}$	q"
	[˚C]	[˚C]	W/m²-K	W/m-K	W/m-K	W/m²
Square	25	15	10	400	4.5	100750
Square	25	15	50	400	4.5	100750
Square	25	15	100	400	4.5	100750
Circular	25	15	10	400	4.5	100750
Circular	25	15	50	400	4.5	100750
Circular	25	15	100	400	4.5	100750

A range of 10–100 W/m²-K was used for h to cover a significant range of typical values (2.0 – 250 W/m²-K) for air undergoing either free or forced convection processes [11]. Ambient temperature ($T_{AMBIENT}$) was selected for expected normal room temperature, while sample base temperature (T_{BASE}) was set at normal chiller operating temperatures expected to be used throughout this study. Thermal conductivities for both the sample (k_{sample}) and insulation ($k_{insulation}$) were based off representative values of materials expected to be used for a majority of the apparatus design such as metal for the hot and cold plates. It is important to note at this time that the $k_{insulation}$ used for these models was much greater (almost by a factor of 5) than the actual materials expected to be used in the device. This was purposely done to introduce conservatism into the design and ensure any imperfections in the mounted design insulation did not risk affecting the desired 1-D heat transfer and uniform temperature distribution. Finally, q" was set at 100,750 W/m² which correlates to 65 W/in², an available heater output produced by manufacturers. Additional analysis was also performed using a q" of 232,500.5 W/m², which corresponds to 150 W/in², the maximum expected heat flux to be used during device operation (see Appendix A).

Using the parameters in Table 2 and Appendix A, ANSYS temperature and directional heat flux results were generated for each of the different model cross-section types (see Figures 20–23).

Figure 20.   Square sample cross-section model temperature distribution
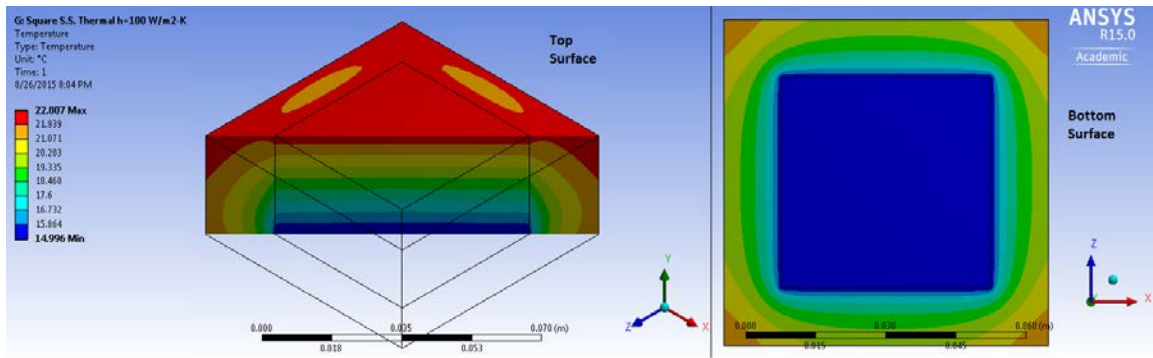
Figure 21.   Square sample cross-section model directional heat flux
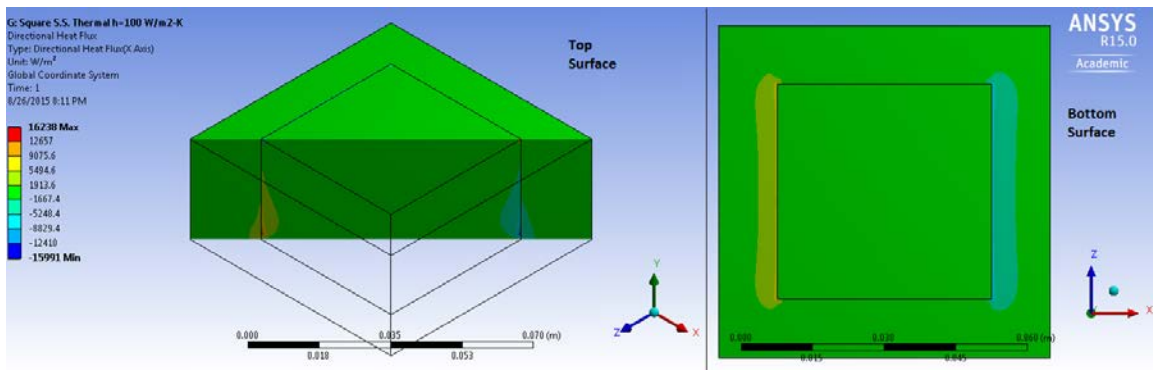
Figure 22.   Circular sample cross-section model temperature distribution
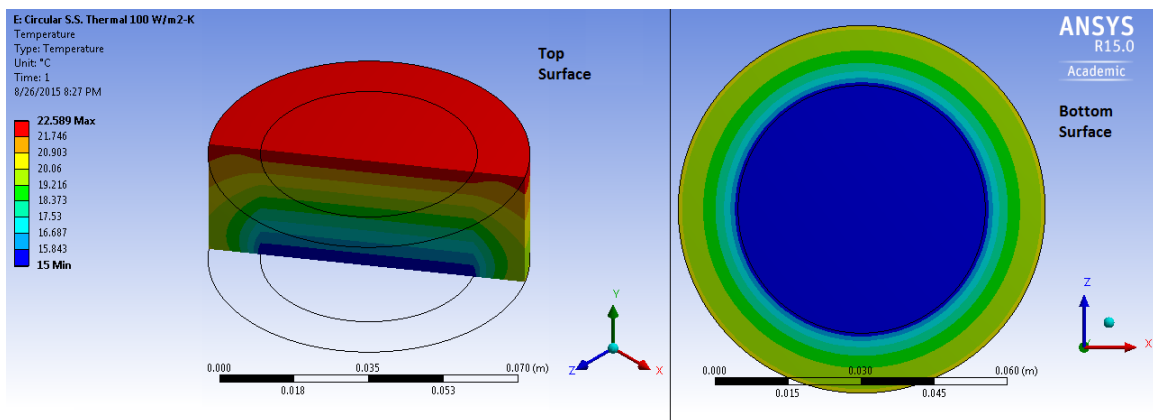
Figure 23.   Circular sample cross-section model directional heat flux
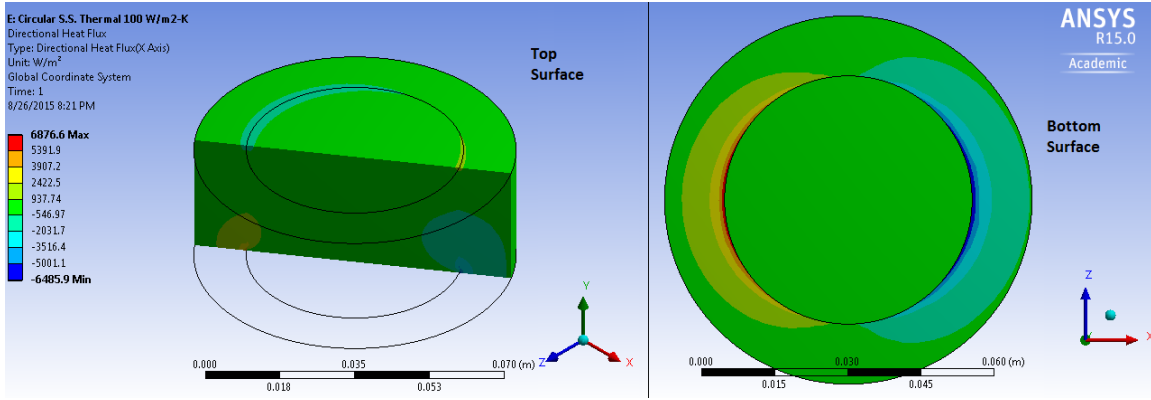
Figures 20–23 display outcomes from selected runs using a heat flux of 100,750 W/m² and 100 W/m²-K for h. These results indicate that for the same design parameters and heat transfer conditions, there is no significant difference in the temperature and directional heat flux distribution for either cross-sectional shape. Both models indicate a linear temperature distribution and 1-D heat transfer throughout the sample. To analytically verify a linear temperature distribution along the sample's top surface (X-Z plane), a departure from temperature uniformity was calculated for each run (see Equation 11).

$$\text{Departure from Temperature Uniformity } (\%) = \frac{T_{CENTER} - T_{EDGE}}{T_{CENTER} - T_{BASE}}(100\%) \qquad (11)$$

Equation 11 compares the departure from temperature uniformity of the top surface of the sample to the difference in temperature across the sample thickness. For each run this value was less than 0.1% indicating that the temperature distribution at the top surface of each run was uniform and did not vary depending on cross section type. It is important to indicate that the models reveal that the most linear temperature distributions and 1-D heat fluxes occur near the center of each model. For this reason, when determining where the temperature measurement devices should be attached, emphasis will be placed on locating them closer to the center of the apparatus. This reasoning agrees with recommendations mentioned in Touloukian [16].

Since the numerical results indicate that there is no difference between cross-section types for maintaining a linear temperature distribution and 1-D heat flux, either design is viable for the purposes of measuring thermal contact resistance and thermal conductivity. Keeping this in mind, the decision was made to proceed with a square cross-sectional apparatus to minimize the cost and generated waste when creating samples for analysis. Many of the samples that will be measured by this apparatus are created in rectangular sheets such as composites and HVOF and cold spray coatings. Using square samples maximizes the number of samples that can be obtained from a test specimen donor. This will allow for the efficient use of manufactured samples reducing the cost for testing and evaluation to the DOD.

In order to further reduce the overall cost of generating samples, a 0.000645m² (1 in²) cross-sectional area was chosen for each sample size. This area not only reduces the sample size required, but will reduce the power requirements to generate a heat flux large enough to establish a sufficient difference in temperature across the sample. To ensure a 1-D heat flux, while minimizing unwanted heat loss, the *Plate Method* approach requires that the cross-sectional surface area of the sample be much greater than the surface area of each of the sides [16]. For this study, the ratio of 10:1 for sample side length (L_i) to sample height (H) was selected (see Table 3).

Table 3.   Sample size design parameters and maximum machining tolerances

Sample Design Parameters				
Dimension	Size		Tolerance	
	[in]	[m]	[in]	[m]
L_i	1	0.0254	± 0.001	± 2.54E-5
H	0.1	0.00254	± 0.001	± 2.54E-5

Table 3 indicates that for the sample area size chosen the maximum sample thickness that is predicted to produce accurate measurements under the *Plate Method* approach is 0.00254m (0.1 in). Using this information, samples for analysis can be properly prepared for analysis to provide the most accurate and reliable thermal contact resistance and thermal conductivity results.

Determining the sample material dimensions also provides the overall device cross section measurements. In order to ensure 1-D heat flux through the sample, it is necessary that the device's cross section dimensions be identical to those of the sample being measured. Using the device cross section measurements as a starting point, the rest of the measurement system can be designed to ensure uniform temperature distribution and 1-D heat flux while minimizing overall heat loss.

3.   Hot and Cold Plate Material Selection

With the dimensions of the measurement system established in the proceeding section, the focus of the design now moved to determining which material should be used for the machining of the device sub-components making up the hot and cold plate sections (see Figure 24).

Figure 24.   Proposed method diagram showing hot and cold plate sections
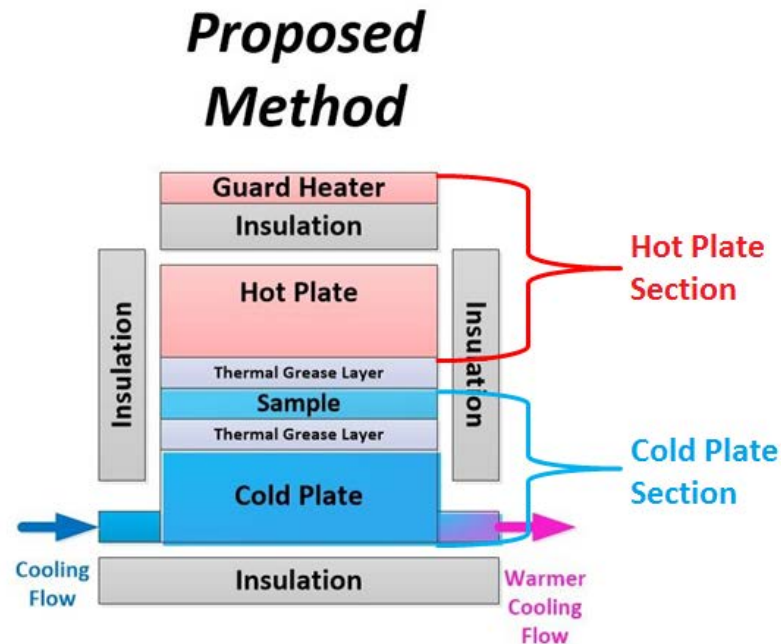
In order to maximize temperature uniformity at the sample interfaces while minimizing heat loss through the device insulation, the material used would need to have a relatively high thermal conductivity compared to the sample and insulation.

Additionally, to accurately produce the sub-component measurements indicated above, the material chosen should be easy to machine. For these reasons, aluminum, copper, and silver were proposed as viable material options based on their thermal conductivities (see Table 4).

Table 4.   Thermal conductivity and raw material cost for aluminum, copper, and silver

Raw Material Cost Analysis			
Material	**k**	**Cost***		**Cost*/k**
	W/m*K	US$/kg	US$/lb	(US$*(m*K))/(W*kg)
Aluminum	205.0	1.5278	0.693	0.007
Copper	385.0	7.0547	3.200	0.018
Silver	406.0	468	212.280	1.153
* Costs valid as of 28 August 2015			

After InvestmentMine, "Commodity and Metal Prices," 2015. [Online]. Available: http://www.infomine.com/investment/metal-prices/. [Accessed 28 August 2015].

Table 4 includes the thermal conductivities as well as raw material costs for aluminum, copper, and silver. As shown in the table, the cost/kg of silver far exceeds the other two material choices. In fact, on a unit mass (1 kg) basis, the cost per unit thermal conductivity for silver is approximately 1.15US$/k, while for the other two materials it is less than 0.02US$/k. This indicates diminishing returns for the small additional thermal conductivity gained by using silver over copper. Based on this rationale, the use of silver for the device sub-components was discarded.

For the remaining two material choices, copper and aluminum, the effects of using each material in a measurement system was reviewed. In particular, research was performed into the plausible ways in which either material could prevent accurate measurements over the operational life-time of the system. This research indicated that both materials have the propensity to form oxide layers when exposed to the environment [39]. Specifically, aluminum is known to form aluminum oxide, which has a thermal conductivity that is highly temperature dependent (see Figure 25).

Figure 25.   Various materials' thermal conductivity as a function of
temperature
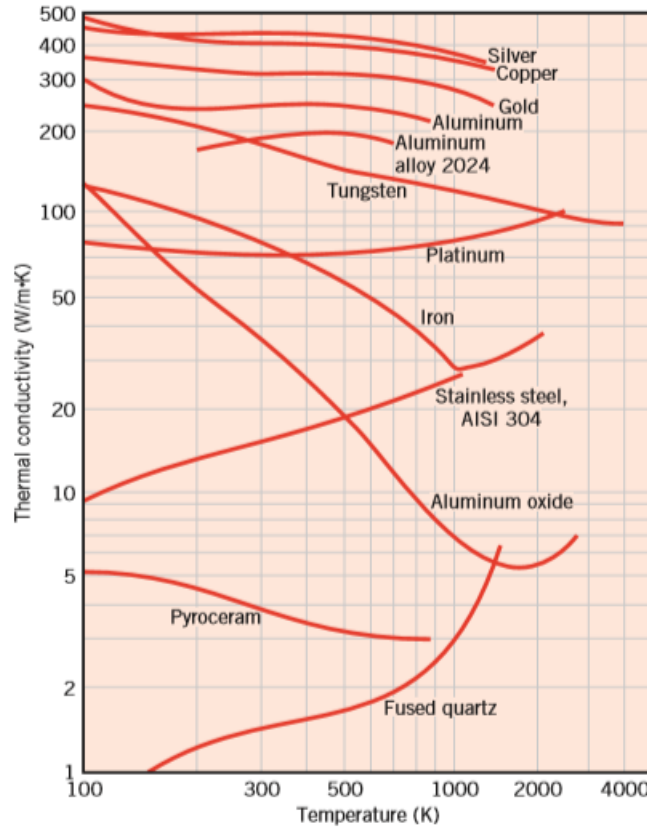
From T. L. Bergman and F. P. Incropera, *Introduction to Heat Transfer*,
6th ed. Hoboken, NJ: John Wiley & Sons, 2011.

As shown in Figure 25, aluminum oxide's thermal conductivity is highly variable in the temperature range in which the system will be conducting measurements; 298.15-373.15K (25 - 100°C). Formation of this oxide layer on the device surfaces on either side of the sample could introduce significant error in measuring a sample material's thermal conductivity. First, it would be extremely difficult to measure the temperature at the specific location in which the oxide layer existed. At best, an average temperature would need to be used, which would introduce added complexities and uncertainties into the measurement results. Secondly, the presence of an oxide layer greatly increases the presence of thermal contact resistance due to pitting in the device's material surface [40]. Both of these factors could have significant adverse effects on the accuracy of the

42

measurement system over its time in service. For this reason, copper was selected as the base material from which the device sub-components would be produced.

For the purposes of this project C110 copper was chosen for the material from which the sub-components would be machined. This particular copper alloy was chosen due to its high thermal conductivity compared to most other copper alloys [39]. The properties of this specific type of copper are included in Table 5.

Table 5. C110 copper material properties

C110 Copper Material Properties				
Name	Electrolytic tough pitch copper			
Alloy Number	C11000			
Nominal Composition [%]	99.90 Cu, 0.04 O			
Themal Conductivity (k)	0.934	[cal-cm/(s-cm-°C)]	390.786	[W/m-K]

Note: Alloy number C11000 is commonly referred to as C110 copper. After L. S. Marks, E. A. Avallone and T. Baumeister, *Marks' Standard Handbook for Mechanical Engineers*. 11th ed. New York, NY: McGraw-Hill, 1996.

The thermal conductivity value for C110 shown in Table 5 will be used during calculations to determine a measured sample's thermal conductivity. To ensure a high level of accuracy for the measurements, it is important that this value be used since the thermal conductivity of copper alloys can vary from less than 30 W/m-K for copper nickel to 390.8 for oxygen free C102 copper [39].

4.   Components

In order to ensure that the designed thermal contact resistance and thermal conductivity measurement system produced accurate results, the device components had to be produced with three key goals in mind. The first goal was to establish and maintain a 1-D heat flux throughout the device to ensure accurate measurements could be completed using Fourier's Law of Conduction (see Equation 1). The second goal was to ensure that a uniform temperature distribution was established at the interface between the sample and the hot and cold plates. The third goal focused on minimizing heat losses

throughout the device so that accurate measurements could be calculated using the input voltage and current into the main heater from the selected power unit. Using sound engineering judgement, component designs for the thermocouple plate, cold plate, and hot plate sections were created.

a. *Thermocouple Plate*

As one of the critical design components in the overall measurement system, much thought went into ensuring that the thermocouple plate was able to meet a few key criteria. In general the thermocouple plates served two purposes; retaining the thermocouples that would measure either cold or hot temperatures and functioning as the interface between the rest of the device and the sample. For these reasons, it was important to make sure that the thermocouple plate preserved the 1-D heat flux being established throughout the device and ensured a uniform temperature distribution at the sample interface.

One of the challenges of preserving the 1-D heat flux generated in the rest of the device resided in the method of installing the thermocouples. To ensure adequate temperature measurement coverage of the device, a 6 thermocouple layout was chosen (see Figure 26).

Figure 26.   Thermocouple plate SolidWorks model
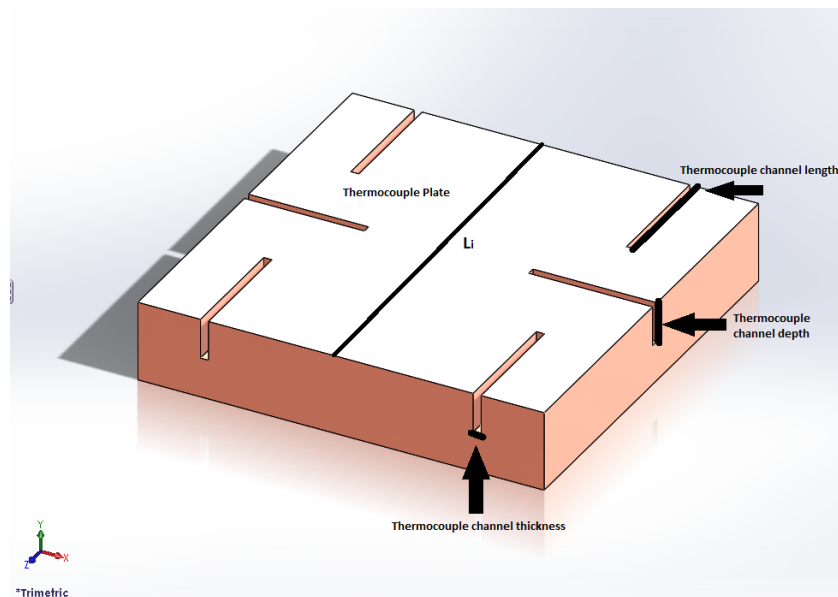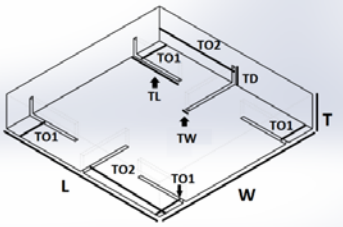
The thermocouple arrangement shown in Figure 26 ensures that temperature measurements are taken closer to the center of the device to obtain more uniform temperature readings as recommended by Touloukian [16] and indicated by ANSYS results produced in the previous section (see Figure 20). In order to ensure adequate attachment of the thermocouples, channels were designed to be machined into the plate. Channels were chosen over drilled holes since it would be easier to visually ensure that thermocouple beads made complete contact with the plate. Failure of the thermocouples to make full contact with the plate would lead to increased measurement errors and result inaccuracies. To minimize the affect these channels had on the 1-D heat flux, their thickness was limited to the width of the selected insulated thermocouple wire: 1.27 mm. By minimizing the thickness of these channels, sound engineering judgement was used in an attempt to preserve the 1-D heat flux established by the rest of the device.

Using the thermocouple plate to serve as the boundary between the sample and the rest of the device was done to minimize the measurement complexities and uncertainties associated with a multi-layered composite system. With each additional layer between the sample and the thermocouples, exact device thermal contact resistances and thermal conductivities had to be known to calculate a sample's thermal conductivity accurately. Any errors or uncertainties would directly affect the capability to use the device to measure thermal contact resistance and thermal conductivity as designed. Having the thermocouple plate serve this additional purpose meant that the plate thickness and channel depth had to be selected carefully. Ideally, the thermocouple beads would be situated as close to the device-to-sample interfaces as possible. This would ensure that the distance between temperature measurements was much smaller than the sample length as required by the *Plate Method* approach [16]. Placing the thermocouples at this location, however, required the channel depth to be almost as deep as the thickness of the plate itself. With this design, any issues incurred during machining or while establishing a notch for the thermocouple bead to reside in could cause an imperfection of the sample side of the plate. An imperfection in this surface would lead to the sample not fully contacting the thermocouple plate, disrupting heat transfer between the two surfaces. Furthermore, any temperature distribution irregularities caused by the

thermocouple acting as a thin fin [11] would affect the temperature uniformity at the sample surface. Therefore, the decision was made to make the depth of the thermocouple half the thickness of the plate. This would act to ensure no damage occurred to the sample side of the thermocouple plate during device construction and sufficient thickness for a uniform temperature distribution to be maintained.

Based on the reasoning presented, dimensions for the thermocouple plates were set to ensure 1-D heat flux and temperature uniformity at the surface boundary (see Table 6).

Table 6.   Thermocouple plate material and dimensions

Thermocouple Plate Material and Dimensions					
Measurement	Symbol	Diagram	Material	Value	Units
Width	W			0.0254	m
Length	L			0.0254	m
Thickness	T			0.00508	m
Thermocouple channel width	TW		Copper C110	0.00127	m
Thermocouple channel length	TL			0.00762	m
Thermocouple channel depth	TD			0.00254	m
Thermocouple channel offset 1*	TO1			0.004064	m
Thermocouple channel offset 2*	TO2			0.0127	m
* Thermocouple channel offset measured to center of the channel from edge of plate					

Using these dimensions, thermocouple plates were machined out of the selected C110 copper to be used in device construction (see Figure 27).

Figure 27.   Machined thermocouple plate
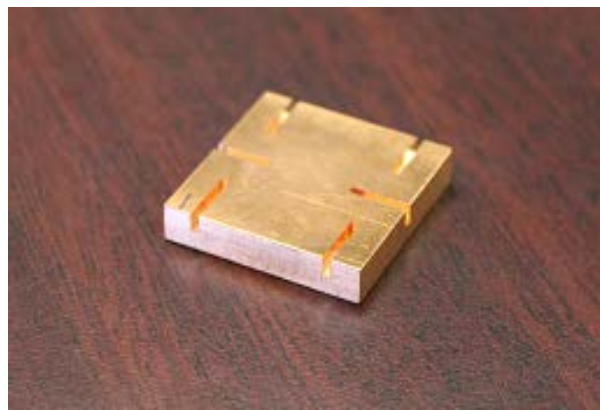
With the design of the thermocouple plates complete, attention would be focused on the cold plate section of the measurement system that would be crucial in establishing a uniform temperature distribution throughout the device.

b. Cold Plate Section

The second most crucial component in the thermal contact resistance and thermal conductivity measurement system was the cold plate section. The purpose of the cold plate design was to establish a heat sink for the device that setup a uniform temperature distribution at the sample measurement location. Additionally, for the purposes of future studies looking into the effects of pressure on contact resistance within components, the cold plate had to be designed robust enough to allow for large amounts of pressure to be placed upon it. Finally, through findings discovered using a prototype model (see *Prototype* section), a lower and upper cold plate was integrated into the design (see Figure 28).

Figure 28.   Cold plate section SolidWorks model
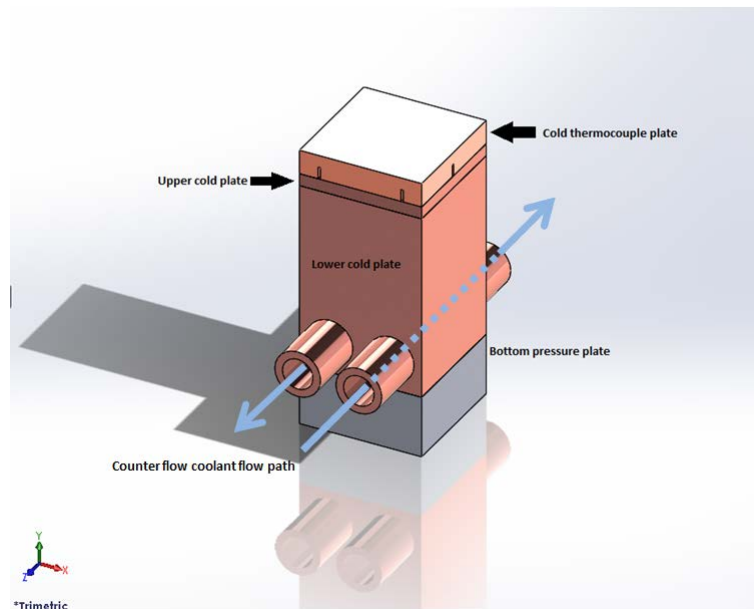
Blue arrows in figure indicate straight coolant channels with counter flow method applied to maximize uniformity of established temperature distribution

47

Figure 28 shows the cold plate section comprising of the bottom pressure plate, lower cold plate, upper cold plate, and cold thermocouple plate. The overall setup of this section served to create a uniform temperature distribution at the sample while providing a secure device base to incorporate future pressure measurements.
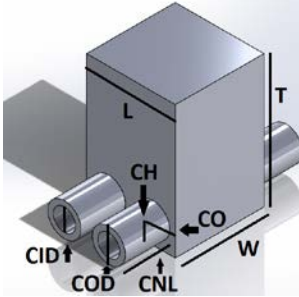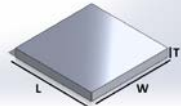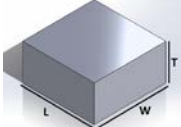
One of the key goals of designing the cold plate section was ensuring a uniform temperature distribution at the sample. For this reason, straight coolant channels were incorporated in the lower portion of the lower cold plate. These channels were designed to be machined into the plate using a solid piece of copper. The choice to use two channels enabled a counter flow technique to be used through the plate while minimizing the complexity of the cooling system hook up. The inner diameter of these channels was maximized to increase the surface area in which heat transfer occurred through the channel walls. A tradeoff on channel diameter had to be made however to allow for the fitment of the ends of the coolant system piping over each of the channel nozzles. Finally, the thickness of the lower cold plate was increased to allow room for the establishment of a uniform temperature distribution by the sample location.

To minimize the impact of the surrounding environment on the cold plate temperature distribution, incorporation of insulation surrounding the entire cold plate section was designed. Most of the insulation would involve the use of 3 layers of balsa wood around the sides of the lower cold plate. Balsa wood was chosen for this application due to its very low thermal conductivity (0.055 W/m-K) [11] and ease of application and modification compared to other common insulating materials. A thick foam material would then be used to insulate the remainder of the cold plate section to include the upper cold plate and thermocouple plate. The thickness of this layer of foam would be sufficient to also cover the sample and hot thermocouple plate portions of the fully assembled device. Foam was chosen over balsa wood since the layer would have to be able to flex around the installed thermocouple wires while being easy to install and remove during normal sample change out. Foam or balsa wood, however would not be ideal materials to use to insulate the base of the cold plate section. Either of these materials would compress over time due to the weight of the system leading to a reduction in their capability to insulate the device. For this reason, and to support future

studies in pressure effects, Pyrex was selected as the material from which the bottom pressure plate would be comprised. Pyrex has a low thermal conductivity (1.4 W/m-K) [11] and is incompressible providing a solid base from which the rest of the measurement device could be built [41].

Developing the cold plate section as discussed would assist in developing the uniform temperature distribution desired at the sample location. The reasoning outlined above led to the selection of dimensions for the overall section (see Table 7).

Table 7.   Cold plate section subcomponent material and dimensions

Cold Plate Section Subcomponent Material and Dimensions						
Subcomponent	Measurement	Symbol	Diagram	Material	Value	Units
Lower cold plate	Width	W		Copper C110	0.0254	m
	Length	L			0.0254	m
	Thickness	T			0.0381	m
	Coolant channel inner diameter	CID			0.00653	m
	Coolant channel outer diameter	COD			0.009578	m
	Coolant channel nozzle length	CNL			0.0127	m
	Coolant channel height	CH			0.00653	m
	Coolant channel offset*	CO			0.00653	m
Upper cold plate	Width	W		Copper C110	0.0254	m
	Length	L			0.0254	m
	Thickness	T			0.00254	m
Bottom pressure plate	Width	W		Pyrex	0.0254	m
	Length	L			0.0254	m
	Thickness	T			0.0254	m
* Coolant channel height and offset measured to center of the channel from edge of plate						

Using this design, sub-section parts were machined from C110 copper and Pyrex materials to be used in the final measurement device assembly (see Figure 29).

Figure 29.   Final machined and assembled cold plate section following
prototype enhancements (see section B3)
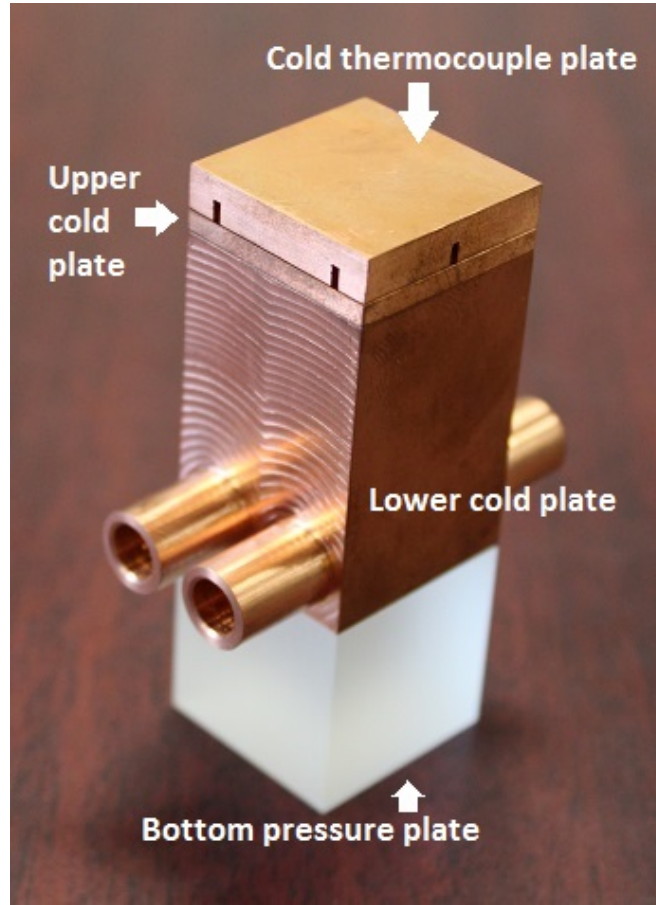
c.   *Hot Plate Section*

The final portion of the measurement system that needed to be designed was the hot plate section. The purpose of this section was to provide a uniform heat flux that would travel through the remainder of the device. For this reason, specialty heaters had to be selected based on their capability to produce a uniform heat flux during operation. Furthermore, to ensure that heat loss was minimized, the section needed to be insulated using different methods to ensure the energy produced by the heater was directed toward the sample. These design considerations were necessary to include in the hot plate section to ensure accurate measurements of thermal contact resistance and thermal conductivity measurement system using Fourier's Law of Conduction (see Equation 1).

The hot plate section was designed to consist of the hot thermocouple plate, hot plate, main and guard heaters, guard heater insulation, and top pressure plate (see Figure 30).

Figure 30.   Hot plate section SolidWorks model
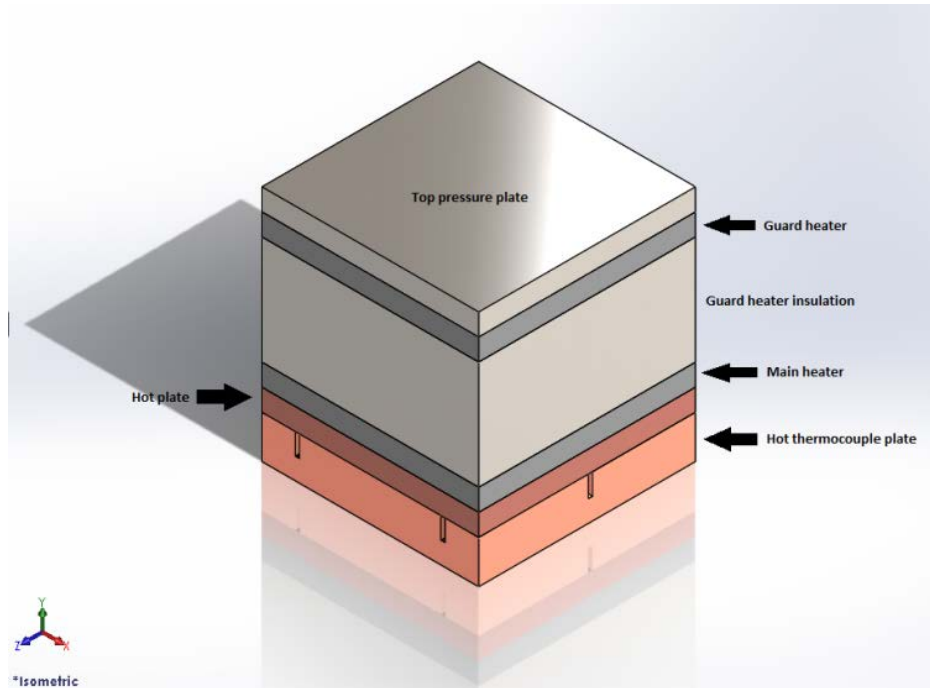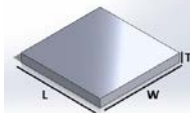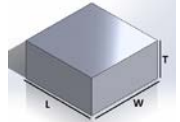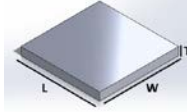
Figure 30 shows the layout of all the subcomponents comprised within the hot plate section of the measurement system. To ensure a uniform heat flux, WATLOW ULTRAMIC heaters were chosen for the design to be used as both the main and guard heaters (see Appendix A). These heaters are capable of putting out up to 150W of energy uniformly. This was important to the overall device since high thermally conductive materials would require higher output powers to create a large enough differential temperature across the sample to reduce result uncertainty. Since a uniform heat flux was already being produced by the heater itself, a thinner hot plate could be utilized between the heater and thermocouple plate. This is in contrast to the lower cold plate where a much larger plate thickness was required since the cooling channels did not sufficiently produce a uniform temperature distribution.

To ensure the uniform heat flux produced by the main heater was directed in a 1-D manner toward the sample, an upper guard heater assembly and side insulation had to

51

be incorporated into the design of the hot plate section. The guard heater was used to ensure that the heat flux from the main heater did not travel upwards away from the sample. To reduce the amount of energy traveling in this direction, a thick layer of Pyrex was placed between the two heaters. The combination of this thick insulation layer and operating the guard heater to minimize the temperature difference between the two heaters would force the upward heat transfer to zero (see Equation 1). To protect the guard heater from any pressures placed on the device, a top pressure plate was used to ensure equal distribution of pressure force. This upper pressure plate was machined out of Pyrex and would be much easier and less costly to replace than one of the purchased heaters. To address any heat loss from the sides of the hot plate section, three layers of balsa wood was used. This balsa wood insulation would line the hot plate section starting at the hot plate up to just below the upper surface of the top pressure plate. The remaining hot thermocouple plate sides would be covered by the foam layer discussed in previous portion concerning the cold plate section.

From the design discussion presented on the hot plate section, subcomponent parameters were created to be used in machining each of the parts (see Table 8).

Table 8.   Hot plate section subcomponent material and dimensions

Hot Plate Section Subcomponent Material and Dimensions						
Subcomponent	Measurement	Symbol	Diagram	Material	Value	Units
Top pressure plate	Width	W		Pyrex	0.0254	m
	Length	L			0.0254	m
	Thickness	T			0.00254	m
Guard heater insulation	Width	W		Pyrex	0.0254	m
	Length	L			0.0254	m
	Thickness	T			0.0127	m
Hot plate	Width	W		Copper C110	0.0254	m
	Length	L			0.0254	m
	Thickness	T			0.00254	m
* Coolant channel offset measured to center of the channel from edge of plate						

These subcomponents would then be used in the construction phase of this project to form the hot plate section (see Figure 31).

Figure 31.   Final machined and assembled hot plate section
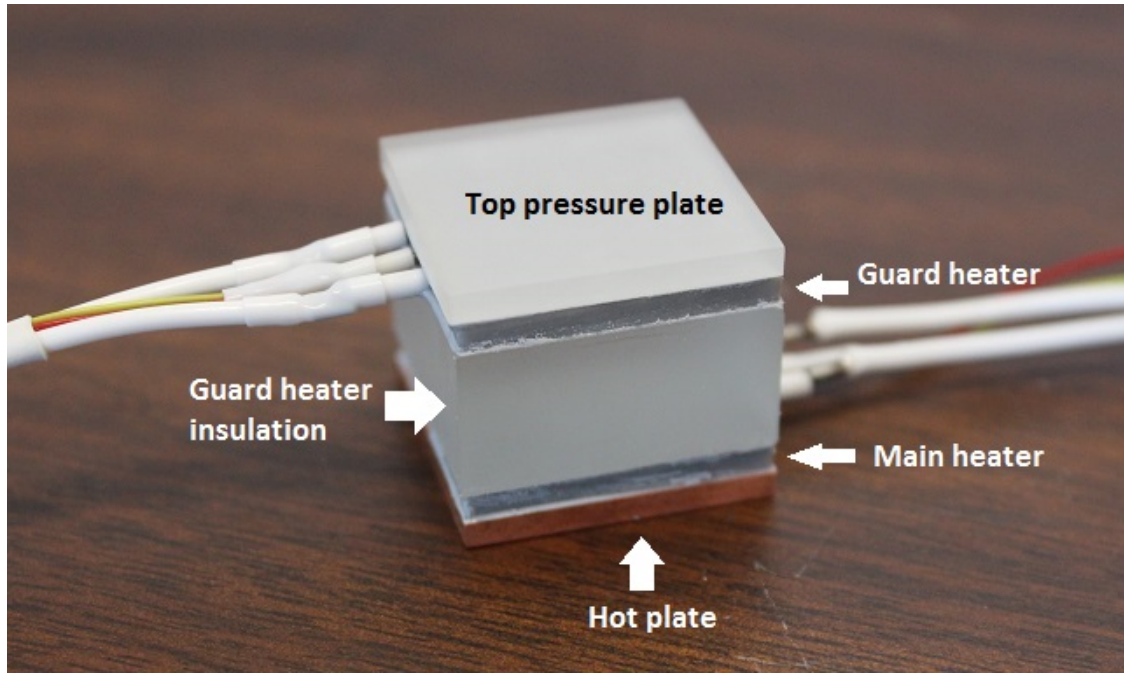
Hot plate section shown without hot thermocouple plate.

5.   Design Summation

From the design methodology discussed for the device dimensions, material selection, and component design, a measurement system can be built that can meet expectations set forth for measuring thermal contact resistance and thermal conductivity. The choice to use a square device cross sectional area was aimed at reducing the cost and waste incurred to manufacture material samples. C110 copper was chosen as a suitable base material for the device due to its high thermal conductivity and low cost compared to alternative materials. From these first two design decisions, the thermocouple plate, cold plate and hot plate sections were developed and machined. The thought processes behind the design of these subcomponents will lead to an overall assembly that can produce accurate measurements (see Figure 32).

Figure 32.   Complete measurement device SolidWorks model
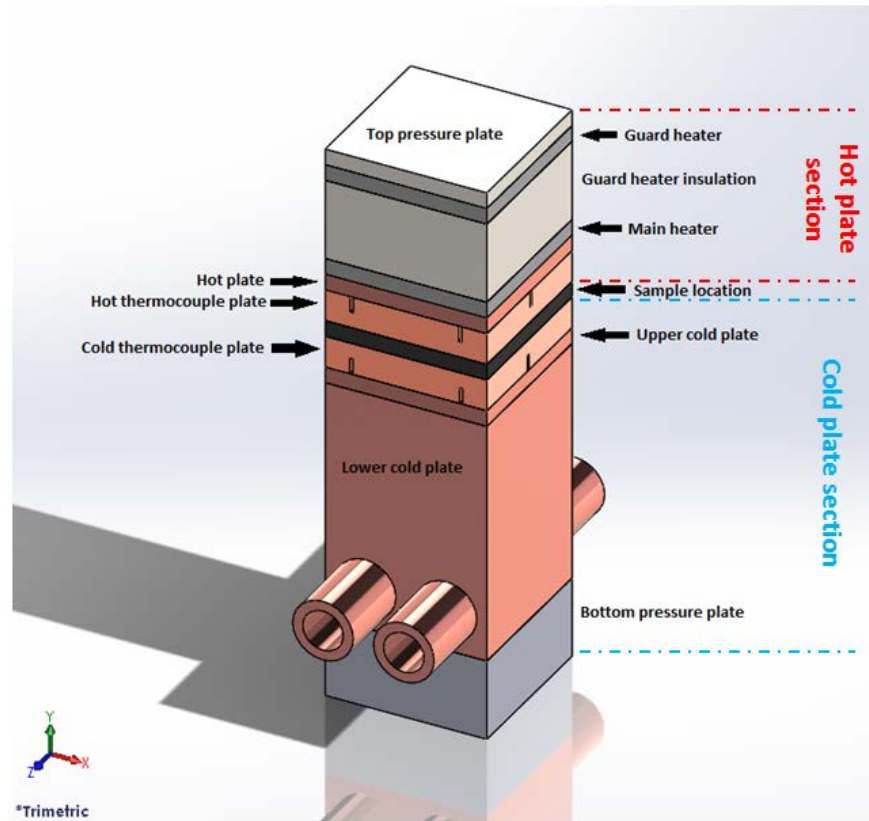
Figure displays central measurement device stack without added insulation
layers.

The design of each subcomponent in the measurement device was motivated by
the need to establish a 1-D heat flux, ensure a uniform temperature distribution at the
sample to device interface, and minimize heat losses. With the overall design of the
measurement device completed as shown in Figure 32, the next phase of the project
moved toward the construction of the overall system.

B.   CONSTRUCTION

The construction of the complete thermal contact resistance and thermal
conductivity measurement system brought together many different components and
subsystems. The overall system design consisted of a cooling system, electrical system,
and measurement device. The cooling and electrical systems in particular required the

purchase of specific COTS units to ensure accurate and replicable measurement results could be obtained while minimizing result uncertainties. Construction procedures used in the creation of each system had to be specific enough to ensure that the complete measurement system could be built at any DON/DOD facility. Furthermore, through the implementation of good engineering practice, a prototype model of the measurement device was machined and tested prior to the finalization and manufacturing of the proposed design. This led to important findings such as the need to separate the cold plate section into an upper and lower portion separated by a thin film of plastic. The final results of this construction phase would directly influence the ability of the measurement system to reliably produce accurate results.

1. Cooling System

To ensure that the thermal contact resistance and thermal conductivity measurement system could reach steady state conditions, a cooling system had to be designed that could maintain a constant heat sink temperature. For this reason a chiller, the primary component of the system, had to be selected that could operate at the low temperatures desired without any large temperature drift over time. Lower working fluid temperatures enabled the device to operate at higher powers without risk of damage due to overheating, thus enabling the creation of larger difference in temperatures across the sample. These two factors enabled the reduction of result uncertainties calculated using the Kline and McClintock Uncertainty analysis (see Equation 10) Using the chiller as a starting point, the rest of the system was constructed using various piping, metal connections, and insulation (see Appendix B, Figure 33).

Figure 33.   Parts required for cooling system construction

Unlabeled items: red and blue tubing used to connect flex piping to lower cold plate. Not shown: Optional but recommended hose clamps to be used on each hose connection.

Parts in Figure 33 were selected based on their ability to maximize cooling flow (i.e., flex pipe inner diameter), minimize the temperature increase of the coolant in the lines between the chiller and the measurement device, and to prevent any unwanted coolant leaks.

The selected chiller for the system was the Heidolph RotaChill large chiller based on its performance capability to maintain constant low temperature fluid temperatures (see Figure 34).

Figure 34.   Heidolph RotaChill large chiller unit

This particular chiller could operate using glycol making it capable of lowering the working fluid's temperature to below freezing (see Table 9).

Table 9.   Heidolph RotaChill large chiller specifications

Heidolph RotaChill Large Chiller Specifications	
Parameter	Specifications
Operating temperature*	-20°C to +60°C
Device thermocouple probe accuracy	±0.25°C
Temperature stability	±0.1°C
* Full temperature range for 50/50 ethylene glycol and water	

After *RotaChill Large Chiller Operating Manual*, Heidolph Instruments GmbH & Co., Germany.

As shown in Table 9, the ability to maintain a narrow band of constant outlet fluid temperatures ensured that the measurement system could be operated at steady state conditions. If the chosen chiller had been unable to accomplish this, additional cooling system components would need to be added (i.e., an insulated reservoir tank) to minimize fluid temperature fluctuations reaching the device. These added components would also include device inlet coolant temperature measurements to monitor for any temperature fluctuations. In addition to this purpose, when combined with device outlet temperature and individual channel fluid mass flowrate measurements, this data could have served to measure the amount of heat being withdrawn from the device. These added components, however, would introduce undesired complexities to the system and introduce additional

locations where leaks could occur. Furthermore, the number and type of measurements needed to calculate heat withdrawn from the device in this manner would add more uncertainty to calculated results than just measuring heater input from the power units. Therefore, to optimize the system performance and reliability, the Heidolph RotaChill large chiller unit was selected as the main unit comprised within the cooling system and the decision was made to not include additional inline coolant temperature measurements.

During the construction of the remainder of the cooling system, parts were assembled based on the desire to maintain the lowest working fluid temperatures reaching the measurement device cold plate. To accomplish this, the flex line lengths between the chiller and the device were minimized. Additionally, during construction these lines were wrapped in two layers of foam pipe insulation to prevent any heat transfer with the surrounding environment. This included any hose connections (i.e., U and tee connections) which were wrapped first in insulation tape. By reducing the inlet line lengths to the device and fully insulating them, the cold working fluid would spend less time between the chiller and measurement device and less heat transfer to the environment would occur.

The overall design and construction of the cooling system was based on the desire to ensure steady state conditions during the measurement of thermal contact resistance and thermal conductivity of samples. Without the capability of establishing these conditions, use of Fourier's Law of Conduction (see Equation 1) to calculate sample results could lead to large measurement inaccuracies. Furthermore, selection of a high performance chilling unit provided the capability to reduce working fluid temperatures to the device. This would be important for reducing uncertainty in results by allowing the device to operate at higher powers with a larger difference in temperature across the sample. Using the outlined construction procedures, the individual parts were assembled using the reasoning provided into a fully operational system (see Figure 35).

Figure 35.   Fully assembled cooling system

Shown with prototype lower cold plate installed

Following the completed assembly, shown in Figure 35, the first stage of the construction process for the measurement system was completed. With an operational cooling system built, the construction process could proceed to assembling and testing the electrical system used to power each of the measurement device's heaters.

2.   Electrical System

To be able to supply sufficient power to each of the measurement system's heaters, adequate power units had to be acquired. Additionally, these units would have to be able to produce accurate measurements of their own output current, voltage, and power to be used in measurement calculations. This was desired to reduce the overall complexity of the system. To be able to use these indications to produce accurate measurement results required any unwanted electrical losses, such as electrical line losses, to be minimized. The final completed setup allowed for each heater to be controlled separately and output values to be recorded directly from the power units.

It was necessary that the power to each measurement system heater be controlled separately. A setup where the main and guard heaters were connected directly in series or

parallel would prevent the guard heater power from being adjusted to minimize the temperatures between the two heaters. Furthermore, even if the power being sent to the guard heater could be controlled by an inline potentiometer, measurements for heater output power would add a large amount of complexity to the system. In this particular scenario, measurements of voltage and current would have to occur directly across each heater unit to obtain accurate results. It was therefore decided to use to separate power units to control the main heater and guard heater independently. The power units chosen for the project were the BK Precision XLN30052 (main heater supply) and XLN15010 (guard heater supply) (see Table 10).

Table 10.   BK Precision power supply specifications

BK Precision High Power Programmable DC Power Supply Specifications		
Power Unit	**Parameter**	**Specifications ***
XLN15010	Current	0.04 - 10.4 A
	Current measurement error	0.1% + 30 mA
	Voltage	5 - 150 V
	Voltage measurement error	0.05% + 75 mV
	Power	1560 W
XLN30052	Current	0.02 - 5.2 A
	Current measurement error	0.1% + 15.6 mA
	Voltage	5 - 300 V
	Voltage measurement error	0.05% + 150 mV
	Power	1560 W
* Specification values are after a 15 minute unit temperature stabilization time at an ambient temperature of 23°C ± 5°C.		

After *High Power Programmable DC Power Supply User Manual,* BK Precision Corp, Yorba Linda, CA, 2013.

As shown in Table 10, these units were capable of producing the power needed for each of the system's heaters and could provide accurate output current, voltage, and power indications. The XLN30052 power unit was specifically chosen to power the main heater since it had the lower current measurement error out of the two units purchased. The expected output current to the main heater for all of the measurements was less than

one amp; therefore minimizing this error would have a greater effect on reducing result uncertainties.

To ensure that the output indications for the power units could be used in calculations to determine a sample's thermal contact resistance and thermal conductivity, any unwanted power losses between the power unit and heater had to be minimized. To reduce these losses, any added wire length between the power unit and heater was minimized, used low gauge wire, and was connected using low resistance solder (see Appendix B). Once lengthened, the resistance of the wires was measured in comparison to the resistance across the main heater at various heater temperatures (see Figure 36, Appendix A).

Figure 36.   Measurement system setup to determine heater wire resistance
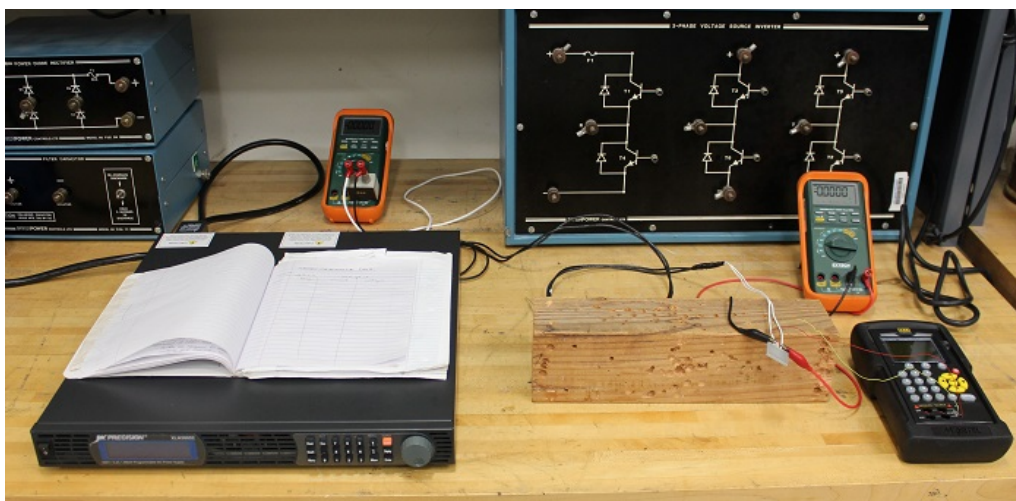
The goal of these measurements was to ensure that regardless of how the main heater resistance changed in respect to temperature, the resistance of the wire was much smaller in comparison. For each measurement, the resistance of the wire was less than 1.0% of the main heater's resistance. These results support the decision to neglect power loss due to the resistance of the wire, especially considering the low currents expected to be run throughout the experiments.

Through minimizing power losses between the heaters and the power units the output indications for current, voltage, and power could be used to calculate measured

thermal contact resistance and thermal conductivity. By carefully selecting the power units based on their measurement accuracies, result uncertainties was minimized for each measurement produced. With the electrical system constructed, work could be started on the assembly of an aluminum prototype to test fit design components of the final measurement device. Once these analyses were conducted successfully, the project could move to the final assembly of the copper measurement device.

3.   Prototype

With the cooling and electrical systems assembled the next phase of system construction moved to the measurement device. Before constructing the actual copper assembly, an aluminum prototype was machined to test fit the subcomponents and attempt to isolate any issues that could affect accurate measurement capabilities. Although the actual measurement device was to be constructed of C110 copper, the prototype was made of aluminum to minimize cost while performing these design validations. This prototype model consisted of the lower cold plate, hot and cold thermocouple plates, and hot plate (see Figure 37)

Figure 37.   Aluminum prototype model
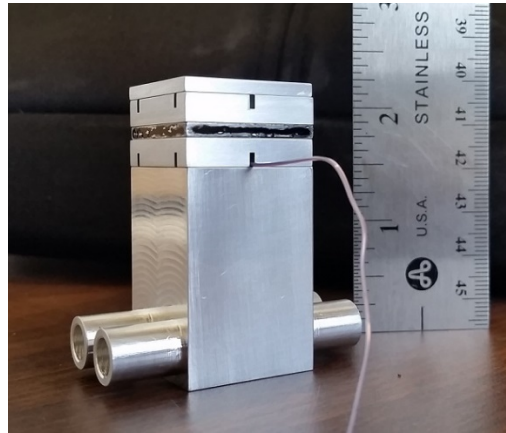
In addition to these sub-components, Figure 37 also displays the placement of one of the thermocouples in the cold thermocouple plate and representative sample location (black colored plate in the figure).

One of the main reasons that the prototype was constructed was to test fit the thermocouples and validate attachment techniques to each of the thermocouple plates. Using the model, the thermocouples were shown to be able to fit snuggly inside each of the grooves. This indicated that the width chosen for the grooves adequately accommodated the thermocouples while still minimizing the effect of disturbing the established 1-D heat flux from the upper heater assembly through the sample. In order to securely attach the thermocouples inside each of the grooves, an assembly technique was devised (see Appendix B). After securely fastening each of the thermocouples, the plates were tested to ensure that the thermocouples were operating as expected. This test involved installing the prototype cold plate and cold thermocouple plate into the cooling system (see Figure 38).

Figure 38.   Prototype testing with attached cooling system
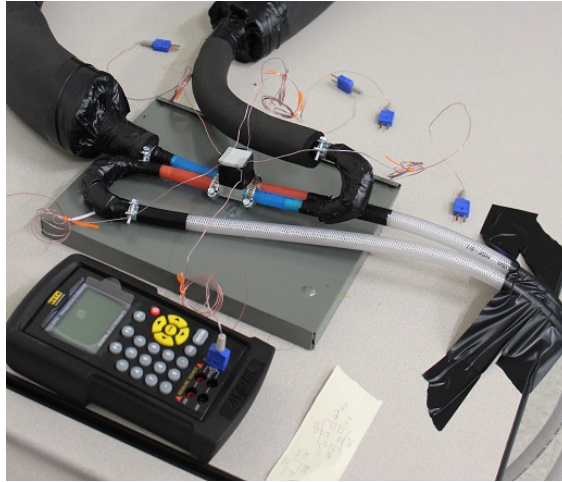
In Figure 38 the prototype is shown insulated using black tape along with a thermocouple measurement device (Martel Electronics PTC 8010 Thermocouple Calibrator). Using this device, temperatures were recorded to check for proper thermocouple operation (see Figure 39, Table 11).

Figure 39.   Prototype thermocouple numbering scheme
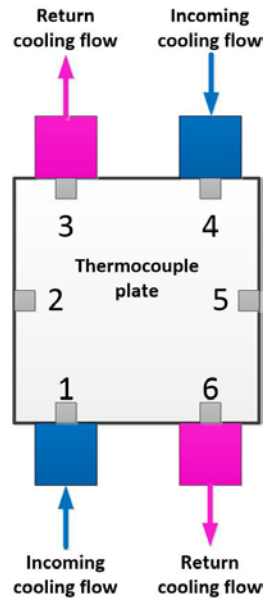
Figure shows prototype cold thermocouple plate numbering scheme
indicating the relative position of each thermocouple above the lower cold
plate incoming and return cooling channels.

Table 11.   Prototype cold thermocouple plate temperature distribution

Prototype Cold Plate Temperature						
Thermocouple	1	2	3	4	5	6
Temperature	22.2	22.4	23	22.9	22.4	22.6

Table 11 was produced by measuring each of the thermocouples while the cooling system was run at 20°C with an ambient room temperature of 25°C. From these initial measurements, the conclusion could be made that the proposed thermocouple attachment procedure was successful in firmly securing the thermocouple bead to the plate. In the case where a gap existed between the bead and plate, the measured temperature would have been expected to be significantly higher than the other thermocouples. These temperature measurements, however, indicated that the device would need to be fully insulated to ensure temperature uniformity when fully operational. The results of this analysis were not unexpected since the early ANSYS models created during the design phase required adequate insulation around the device to ensure temperature uniformity.

An unexpected result of the prototype testing which resulted in a major design alteration occurred when the thermocouples began to produce rapidly fluctuating temperature measurements. This occurred after the thermocouples were attached to a data acquisition unit and the system had been tested for a few days to verify proper overall system operation. Upon analysis, it was discovered that the thermocouples would produce these fluctuating results only when they were in direct contact to the lower cold plate through the thermocouple plate. Fluctuations were not observed once the thermocouple plate was lifted off the lower cold plate or when a piece of plastic was inserted between the two plates. After removing the lower cold plate from the system, it was determined that the temperature fluctuations were most likely due to an electrical potential established within the lower cold plate due to corrosion occurring within the cooling channels (see Figure 40).

Figure 40.   Corrosion product buildup in prototype cooling channels
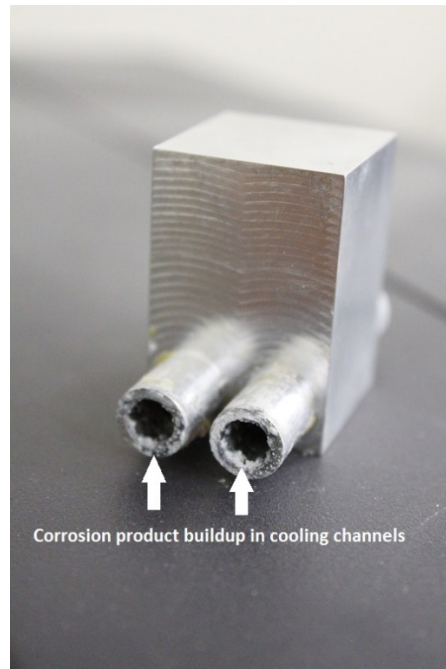
The capability of the corrosion occurring within the cooling channels to affect the accuracy of the temperature measurements necessitated a design change to the final

measurement device setup. This change was made in two areas, the device design and method of recording temperatures.

In order to remove the capability of any possible copper corrosion in the cooling channels from affecting the temperature measurements, a thin plastic sheet was inserted into the device design between the upper and lower cold plates. The thickness of the plastic sheet would isolate electrical disturbances from the lower cold plate while minimizing any temperature drop. Minimizing the plastic layer thickness was important since any temperature drop resulting from this added layer would in turn reduce the device's ability to establish a large difference in temperature across the sample. For this reason it was determined that 3 layers of COTS plastic-wrap would suffice.

In addition to the additional plastic layer incorporated into the device design, it was determined that the temperature measurements from each thermocouple plate would be made using a hand held thermocouple measurement tool. For the purposes of this project the Martel Electronics PTC8010 Thermocouple Calibrator was chosen due to its accuracy in measuring thermocouple temperatures in the expected operational temperature band (see Table 12)

Table 12.   Martel Electronics PTC8010 Thermocouple Measurement Accuracy

Martel Electronics PTC8010 Thermocouple Read Error			
TC Type	Range [°C]		Accuracy [°C]*
	Minimum	Maximum	CJC ON
T	-250	-200	1.7
	-200	0	0.7
	0	400	0.4
*Cold Junction Compensation (CJC) function error outside 23±5°C is 0.05°C/°C			

After *PTC8010 Reference Manual, 4th ed.,* Martel Electronics, Derry, NH, 2014.

During the determination of the cause for the temperature fluctuations discussed earlier, it was noted that the PTC8010 was less susceptible than the data acquisition unit

originally being used. Furthermore the PTC8010 was a stand-alone system that did not require an additional computational device. For these two reasons, the PTC8010 was chosen over the data acquisition unit to complete the temperature measurements for each of the experimental test runs.

Using the aluminum prototype to analyze the methods in which the final measurement device would be constructed was very beneficial. It allowed for subcomponent fitment testing as well as finalization of a process to firmly attach each of the thermocouples. Additionally, it was discovered that a modification to the original design setup would need to be made to ensure that corrosion occurring in the cooling channels between the metal and working fluid did not affect the accuracy of the temperature measurements. These changes were then carried out on the construction of the final measurement device, which would be used to measure thermal contact resistance and thermal conductivity.

4. Measurement Device

Applying the lessons learned with the prototype analysis, hot and cold plate sections of the device were assembled to form the final design. This process included performing device thickness measurements with each added layer and the application of insulation. The final product of this process was a complete thermal contact resistance and thermal conductivity measurement device that could be connected to the already constructed cooling and electrical subsystems.

Using a high thermally conductive adhesive, subcomponents of the hot and cold plate sections were assembled (see Appendix B). For the assembly of each section, this adhesive layer was kept as uniform and thin as possible. By ensuring that each adhesive layer was applied in this manner, the overall thickness variation of the hot and cold plate sections could be minimized (see Appendix A). Any large variation in thickness could impact the accuracy of thermal grease thickness measurements made during each experimental analysis. These measurements would be obtained from subtracting the sum of the measured device and sample thicknesses from the device and sample thickness with added grease layer at the end of each run. Smaller variances in thickness of the

67

measurement device would allow fewer thickness measurements to be taken from the experimental setup to get an accurate average grease thickness. These average grease thicknesses would then be used for thermal contact resistance and thermal conductivity calculations.

As discussed in the previous sections, for the measurement device to establish a 1-D heat flux, uniform temperature distribution at the sample interface, and minimize unwanted heat losses, insulation needed to be incorporated into the design. Following the assembly of the hot and cold plate sections, balsa wood was applied (see Appendix B). This insulation was attached using an adhesive that would tolerate high operating temperatures and water exposure. Insulation adhered to the hot plate section would be subjected to temperatures as high as 80°C, while insulation on the cold plate section could be exposed to water from condensation effects during normal operations. It was therefore necessary to choose an adhesive that would perform well under each scenario to ensure proper attachment of the insulation.

Through the careful assembly of the measurement device, the capability to measure thermal contact resistance and thermal conductivity could be improved. Thickness measurements taken throughout the assembly went into determining an average device thickness that could be used to determine grease layer thicknesses. This information would be required to produce accurate sample measurements following each experimental run. Application of insulation to hot and cold plate sections was needed to ensure 1-D heat flux, uniform sample interface temperature distributions, and minimized unwanted device heat loss. The benefits of these processes toward making an accurate and precise measurement system would be revealed during the design sensitivity analysis of this project.

5.   Construction Summation

Following the proposed methodology and construction procedures the thermal contact resistance and thermal conductivity measurement system was able to make the transition from paper to an actual physical device (see Figure 41).

Figure 41.   Completely assembled measurement system

Decisions made in this process involving the acquisition of COTS components were made to ensure the replicability of accurate results performed by any experimentalist regardless of his or her background. Minimizing the complexity of the device served not only to allow the system to be built at any DON/DOD facility and reduce measurement uncertainties, but also reduced overall system build costs (see Table 13).

Table 13.   Measurement system summary of build costs

Apparatus Assembly Cost					
Component	Quantity	Manufacturer	Description	Price/unit	Subtotal
Main Heater Power Supply	1	BK Precision	DC Power Supply - XLN30052-GL	$2,600.00	$2,600.00
Guard Heater Power Supply	1	BK Precision	DC Power Supply - XLN15010-GL	$2,600.00	$2,600.00
Chiller	1	Heidolph	Bench Top Rotary Chiller - 036306510	$5,733.68	$5,733.68
Thermocouple Calibrator	1	Martel Electronics	PTC8010	$1,308.00	$1,308.00
Heaters	2	WATLOW	ULTRAMIC - CER-1-01-00093	$500.00	$1,000.00
Thermocouples - Type T	3	Omega	5TC-TT-T-30-72	$67.00	$201.00
Copper Material	1	Online Metals	C110 1.25in x 1.25in x 12in	$64.18	$64.18
Copper Material	1	Online Metals	C110 1.5in X 1.5in X 12in	$92.44	$92.44
Pyrex Insulation	-	Netzsch	Area in² - 1/2in, 1/10in, and 1in thicknesses	-	$300.00
Part Machining	-	-	Subcomponent Machining	-	$500.00
Miscellaneous	-	-	Piping, Fittings, Adhesives, Insulation	$200.00	$200.00
				Total:	$14,599.30

With the acquisition, machining, and construction complete, a normal operating procedure was needed to ensure the replicability of measurement analysis. The proposed procedure and the thought processes that went into its creation are the subject of the next section of this report.

C.   OPERATION

Operation of the system focused on two main priorities, ensuring the safety of the operator and producing accurate results. From these priorities, operating procedures were produced for the overall system (see Appendix C). In addition to operator safety, the procedures for the system are written to prevent damage from occurring during operation at high and low powers. Special precaution should be taken to follow all steps including ones outlined with cautionary statements.

Use of the system can be performed at various power levels to vary the temperature in which a sample's thermal conductivity can be measured. This is especially important since most materials have thermal conductivities that vary with increasing or decreasing temperatures [11]. At higher power levels and temperatures it is especially important to allow sufficient time for the device to cool prior to handling the plates. During experimental runs performed for this project, it was not uncommon for the main heater to reach temperatures of 70°C (158°F). The designed balsa wood and foam insulation layer adequately reduces the temperature on the outside surface of the device to prevent injury during operation, however, they do not protect the operator from injury if the hot plate assembly is removed.

In order to allow rapid cooling of the assembly, thus minimizing down time, the written operating procedure enables the experimentalist to use the cooling system to force cool the device. This process should be performed up until the main heater temperature is below 25°C. Cooling below this temperature can lead to the formation of condensation on the device plates. Constant exposure to moisture can lead to device insulation degradation and plate surface corrosion and pitting. Both of these effects can result in the inability of the device to accurately measure thermal contact resistance and thermal conductivity of samples.

D.   SUMMARY

Using analytical and numerical results, as well as sound engineering judgement, a measurement system design, construction method, and operation procedure has been proposed in this section to produce replicable and accurate thermal contact resistance and

thermal conductivity results. Initially, various design considerations were investigated to ensure 1-D heat flux, the establishment of a uniform temperature distribution at the sample interface, and a minimized amount of heat loss from the device. This investigation indicated that a copper device with a square cross-section was the ideal choice. Using this information as a starting point, measurement system sub-components such as the hot and cold plate sections were designed to ensure accuracy of sample measurements. Using prototype analysis, design modifications were incorporated into the cold plate section due to observed thermocouple inaccuracies resulting from coolant channel corrosion. The design of the overall device was then tied to its construction and the construction of the supporting cooling and electrical systems to ensure reliable and accurate measurement capability. The accuracy and replicability of the measurement results was then solidified by creating a normal operation procedure that any experimentalist can use regardless of his or her background. From the system and procedural guidance outlined in this section, experimental methodology will be added in order to establish a means to test and evaluate the system. This methodology and the device capability results it generated are the topics of the next two sections of this report.

THIS PAGE INTENTIONALLY LEFT BLANK

IV.   EXPERIMENTAL METHODS

With the measurement system design and construction completed, and operation procedure outlined, the next phase of the project moved to analyzing measurement accuracy and replicability. For the purposes of assessing the accuracy of the system, measurements were performed on Pyroceram 9606 and 99.8% Alumina samples. Using the Kline and McClintock Uncertainty equation (see Equation 10), the uncertainties of these results were assessed using data gathered during each of the experimental runs. Follow-on analyses were designed to compare results from a fully assembled system to a system where parts such as sample insulation and thermal grease were removed. To ensure that the accuracies obtained could be replicated, measurement results were also taken from system operation by different experimentalists. By developing experimental methodology to verify system accuracy and data replicability, results generated could be used to prove the capability of the system to perform as designed.

A.   VERIFYING ACCURACY AND DESIGN SENSITIVITY

One of the critical performance metrics of the designed measurement system was the capability of accurately measuring thermal contact resistance and thermal conductivity within a range of 0.1 – 40 W/m-K. To assess the device's capability Pyroceram 9606 (k = 4.015 W/m-K @ 25°C) and 99.8% Alumina (k = 31.55 W/m-K @ 25°C) [45, 46] samples were used since they allowed for experimental validation of the system at either end of the proposed useful thermal conductivity range. Result certainty from measuring both the Pyroceram 9606 and 99.8% Alumina was then calculated based off the Kline and McClintock Uncertainty analysis. Following this initial analysis, the overall design sensitivity of the measurement system was tested. In this stage of the analysis, design factors such as insulation and thermal grease application were varied to determine their contribution to obtaining accurate measurement results.

1.   Pyroceram 9606 and 99.8% Alumina Reference Samples

To validate the thermal contact resistance and thermal conductivity measurement system's ability to measure accurately, samples of Pyroceram 9606 and 99.8% Alumina

were used. These materials were specifically chosen due to their room temperature thermal conductivities, which were at either end of the desired sample capability range (0.1-40 W/m-K). Using data gathered from outside institutions and published documents, reference data was generated for each of the samples that could be used to evaluate the data generated from each of the measurement runs.

Reference data for the thermal conductivity of Pyroceram 9606 indicated that the material's thermal conductivity was dependent on sample temperature as shown in Tleoubaev [45] (see Table 14).

Table 14.   Pyroceram 9606 Thermal Conductivity Data

Pyroceram 9606 Thermal Conductivity			
Temp [C]	k [W/m-K]	k Error ± 5%	
0	4.15	4.3575	3.9425
20	4.04	4.242	3.838
40	3.94	4.137	3.743
60	3.85	4.0425	3.6575
80	3.78	3.969	3.591
100	3.71	3.8955	3.5245

After A. Tleoubaev, A. Brzezinski and L. Braga, "Accurate simultaneous measurements of thermal conductivity and specific heat of rubber, elastomers, and other materials," in Proceedings of 12th Brazilian Rubber Technology Congress, Sao Paulo, Brazil, 2008, pp. 22–24.

As shown in Table 14, to properly analyze the accuracy of each measurement, the results would need to be compared to the expected thermal conductivity at the particular measured sample temperature. To accomplish this, a linear interpolation was used with the provided data at a temperature calculated by averaging the cold and hot thermocouple plate temperatures. Uncertainty in the reference data was set to 5% based off recommendations provided with the thermal conductivity measurements [45]. In addition to this data, manufacturer data was also provided with the sample on expected thermal conductivities for the sample (see Appendix D). This data was very similar to the thermal conductivity data discussed in Table 14 in the expected sample measurement temperature band (see Figure 42).

Figure 42.   Thermal Conductivity reference data for Pyroceram 9606
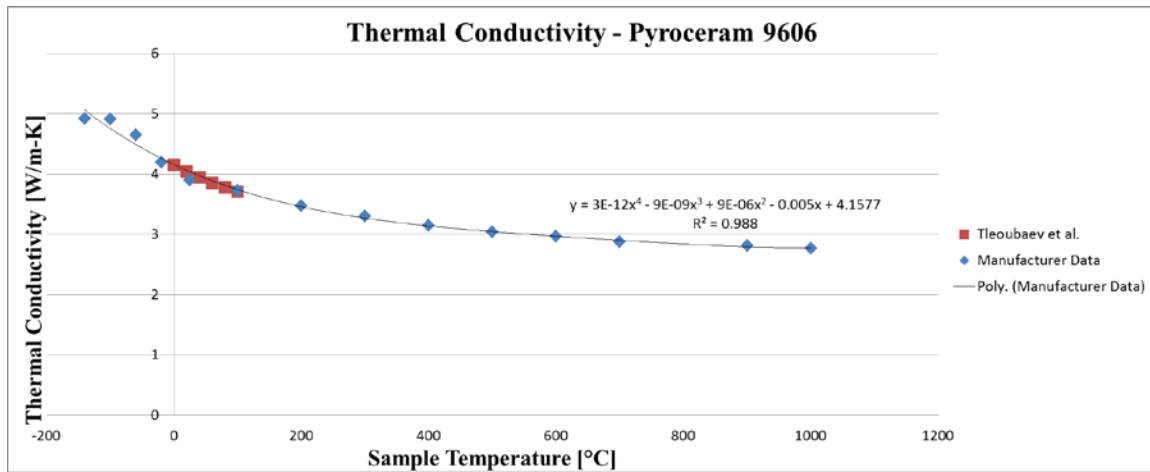
Thermal Conductivity - Pyroceram 9606

$y = 3E\text{-}12x^4 - 9E\text{-}09x^3 + 9E\text{-}06x^2 - 0.005x + 4.1577$
$R^2 = 0.988$

After A. Tleoubaev, A. Brzezinski and L. Braga, "Accurate simultaneous measurements of thermal conductivity and specific heat of rubber, elastomers, and other materials," in *Proceedings of 12th Brazilian Rubber Technology Congress,* Sao Paulo*,* Brazil*,* 2008, pp. 22–24, and M. Manuelian, private communication, Sept. 2015.

Although this data was very similar, the higher uncertainty in the results calculated using the manufacturer's data (10%) made using the data in Table 14 preferred.

Similar to the Pyroceram 9606, thermal conductivity for 99.8% Alumina is temperature dependent. For this reason, reference data for the thermal conductivity of 99.8% Alumina was calculated based off information provided by the manufacturer (see Appendix D). Using the data provided for the material, a curve fit was performed in order to obtain a regression equation to estimate expected thermal conductivities at particular sample temperatures (see Figure 43).

Figure 43.   Thermal Conductivity reference data for 99.8% Alumina
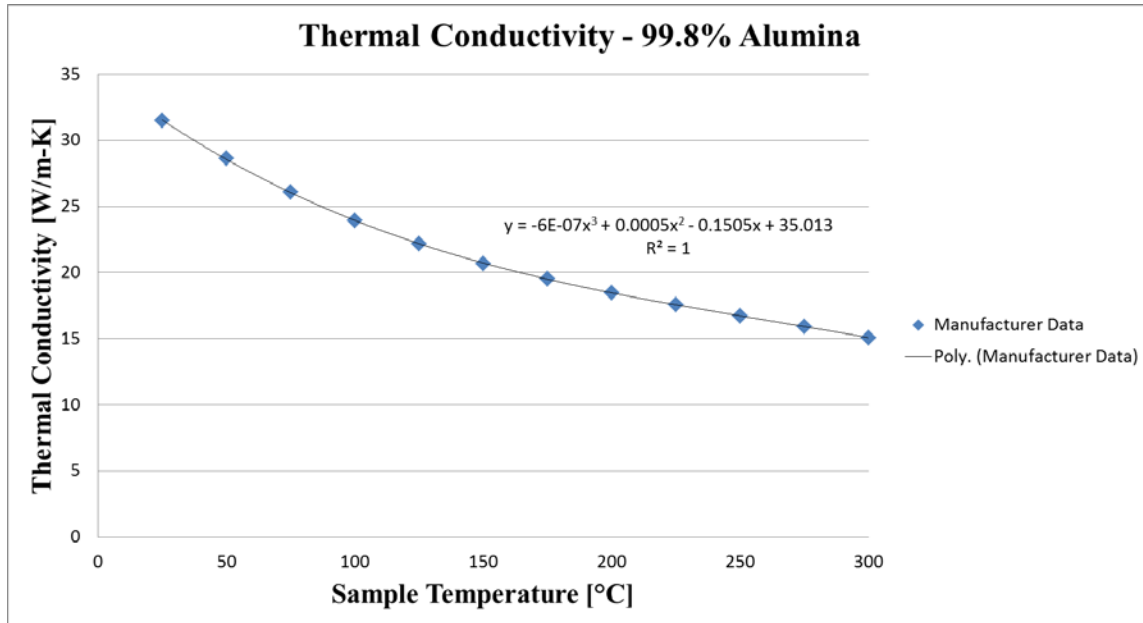
After M. Manuelian, private communication, Sept. 2015.

Using the same process as for the Pyroceram 9606 comparison, 99.8% Alumina expected values would be determined using the sample temperature calculated using an average of the hot and cold thermocouple plates. Uncertainty in the expected results was established at 10% due to the curve fitting that needed to take place to establish the baseline regression equation.

2.   Measurement Accuracy and Uncertainty Determination

Using Pyroceram 9606 and 99.8% Alumina samples, the accuracy of the thermal contact resistance and thermal conductivity measurement system was assessed. Multiple experimental runs for each sample were completed over the course of multiple days at various times. Thermal contact resistance between the sample and device was mitigated using Dow Corning 340 Heat Sink Compound. This type of thermal grease was used due to its ease of applicability and availability. Experimental runs were conducted at both low power and high power output voltages to the main heater (see Table 15).

76

Table 15.   Experimental run power level definitions

Power Level Definition		
	Main Heater Power Unit Output Voltage	
Sample	Low Power	High Power
	[V]	[V]
Pyroceram 9606	35	50
99.8% Alumina	35	48

For each of the runs these voltages were kept fixed using a constant voltage setting on the power unit. The data produced by these runs were then used to calculate the measured thermal conductivity of each sample as well as measurement uncertainty.

In order to accurately calculate the sample thermal conductivity, the thermal grease and copper layers between the temperature measurement locations needed to be taken into account (see Equation 12).

$$k_{sample} = \frac{\left[\left(\dfrac{\Delta x}{A}\right)_{sample}\right]}{\left[\dfrac{T_H - T_C}{q_x} - \left[\left(\dfrac{\Delta x}{kA}\right)_{copper} + \left(\dfrac{\Delta x}{kA}\right)_{grease}\right]\right]} \tag{12}$$

Equation 12 is a rearranged from of Equation 2 solving for the sample's thermal conductivity in a multiple layered composite comprised of the sample layer and copper and grease layers (see Figure 44).

77

Figure 44.   Composite layers included in sample thermal conductivity
calculations
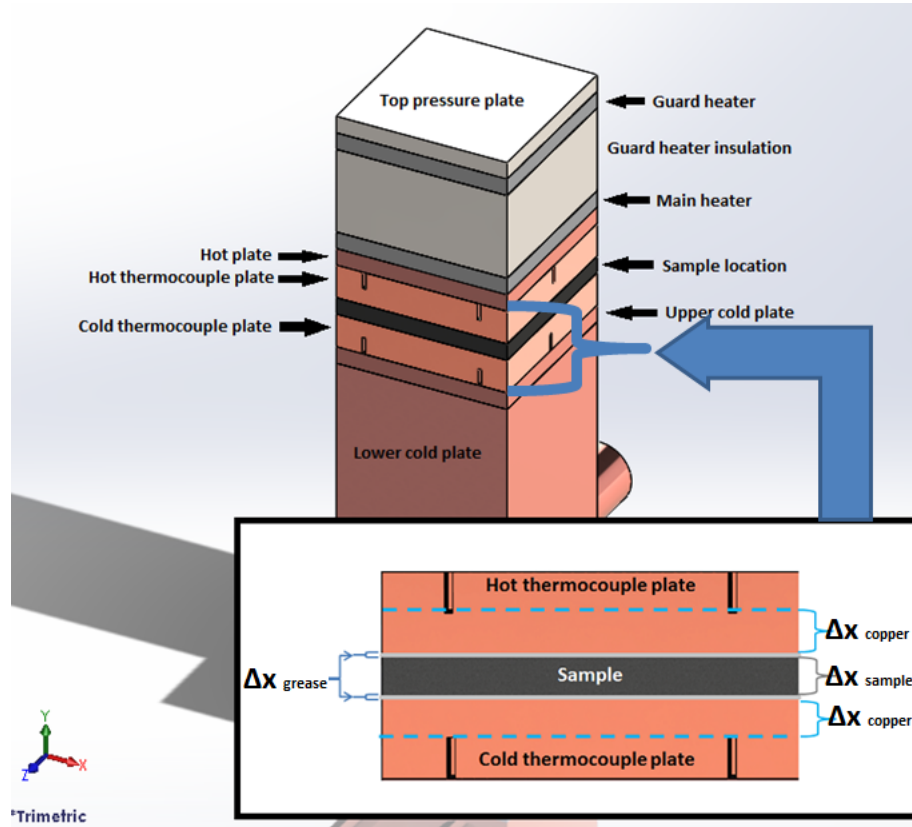
Copper, thermal grease, and sample composite layers used in thermal
conductivity calculation (see Equation 12) shown between blue dotted
lines.

Values for thicknesses (Δx) and area (A) for the copper and sample were directly
measured using a precision micrometer (accuracy: ± 2.54E-5m, ± 0.001in). The area of
the grease was set equal to the area of the sample that it was applied to. For the grease
thickness, the summation of all the average thicknesses of the components in the hot
plate, sample, and upper cold plate was subtracted from the measured overall average
apparatus thickness taken at the end of each measurement. This method provided the
thickness of the grease layer that was unique to each experimental run. The thermal
conductivity for the copper was based off the data provided in Table 5 for C110 copper.
Thermal conductivity for the grease layer was based off measured data conducted at the
onset of the experimental runs. Hot (T_H) and cold (T_C) plate temperatures were

determined using an average temperature of all six thermocouple readings taken per plate. Heat transfer through the sample was based off the product of the output voltage and current coming from the main heater power unit.

Once the thermal conductivity was calculated for each measurement run, the values were assessed for accuracy. Using the expected thermal conductivity generated for Pyroceram 9606 and 99.8% Alumina, the error in the measured result was calculated (see Equation 13).

$$\text{Error } (\%) = \frac{\left| k_{\text{exp}ected} - k_{measured} \right|}{k_{\text{exp}ected}} (100\%) \tag{13}$$

The percent error calculated in Equation 13 then was used for comparison purposes and to calculate overall average measurement system accuracy.

In addition to result accuracy, the uncertainty in the results was calculated applying the Kline and McClintock Uncertainty analysis method (see Equation 10) to the data gathered for each experimental run. Uncertainty in the measured thermal conductivity results was based off uncertainty contributions due to measured current, voltage, thickness, area, and difference in temperatures (see Equation 14).

$$w_k = \sqrt{\left(\left(\frac{\partial k}{\partial I} \Delta I \right)^2 + \left(\frac{\partial k}{\partial V} \Delta V \right)^2 + \left(\frac{\partial k}{\partial (\Delta x)} \Delta (\Delta x) \right)^2 + \left(\frac{\partial k}{\partial A} \Delta A \right)^2 + \left(\frac{\partial k}{\partial (dT_{avg})} \Delta (dT_{avg}) \right)^2 \right)} \tag{14}$$

In Equation 14, variable uncertainties were used calculated off the data discussed throughout this report (see Appendix D, Table 16).

Table 16.   Summarized uncertainty values for various measurements

Variable Uncertainty Calculation Equations
ΔV = 0.0005*V + 0.150V
ΔI = 0.001*I + 0.0156A
Δ(Δx) = 0.0000254m
ΔA = SQRT((ΔL1/L1)^2 + (ΔL2/L2)^2)*A
ΔdT_avg = SQRT((ΔT_hot)^2 + (ΔT_cold)^2)

Using the Fourier-Biot heat-conduction equation (see Equation 8), the partial differential equations required for the uncertainty analysis were determined (see Table 17).

Table 17.   Partial differential equations of the Fourier-Biot heat-conduction equation

Measurement Uncertainty Calculation Equations
(∂k/∂I)*ΔI = (V*Δx*A^-1*dT_avg^-1)*ΔI
(∂k/∂V)*ΔV = (I*Δx*A^-1*dT_avg^-1)*ΔV
(∂k/∂(Δx))*Δ(Δx) = (I*V*A^-1*dT_avg^-1)*Δ(Δx)
(∂k/∂A)*ΔA = (-I*V*Δx*A^-2*dT_avg^-1)*ΔA
(∂k/∂(dT_avg))*ΔdT_avg = (-I*V*Δx*A^-1*dT_avg^-2)*ΔdT_avg

Data from each of the experimental runs were entered into the equations in Table 17 to obtain the uncertainty in the overall measured thermal conductivity (w_k). This value was then used to calculate a percent uncertainty for each run (see Equation 15).

$$\text{Uncertainty } (\%) = \frac{w_k}{k_{measured}}\left(100\%\right) \qquad (15)$$

Once the percent uncertainty was calculated for all experimental runs, an average was determined based on what type of power was used during the measurement: low or high power. Using this averaged value, uncertainty in the measured results would be provided during overall data analysis.

3.   Design Sensitivity Determination

Using the results generated while measuring the Pyroceram 9606 as a baseline, design sensitivity analysis was performed on the measurement system. The first portion of this sensitivity analysis specifically looked into the effects on sample measurements due to using various types of insulation on the device. The second portion of the

sensitivity analysis investigated how the thermal contact resistance mitigation layer between the sample and device (i.e., thermal grease) effected measurements and whether it could be neglected during calculations. Both of these analyses were devised in order to test the device design, construction, and calculation methods for determining accurate sample thermal conductivity results.

To assess the need to fully insulate the device and sample, several experimental runs were completed with various insulation setups. For each set of runs, the low power output setting to the main heater was used. Measured thermal conductivity and result accuracy was calculated using the same method as for the fully insulated runs. For the first set of runs, all insulation was removed from the upper portion of the device and sample to include the balsa wood and foam layers (see Figure 45).

Figure 45. Insulation layout for full and no device insulation runs
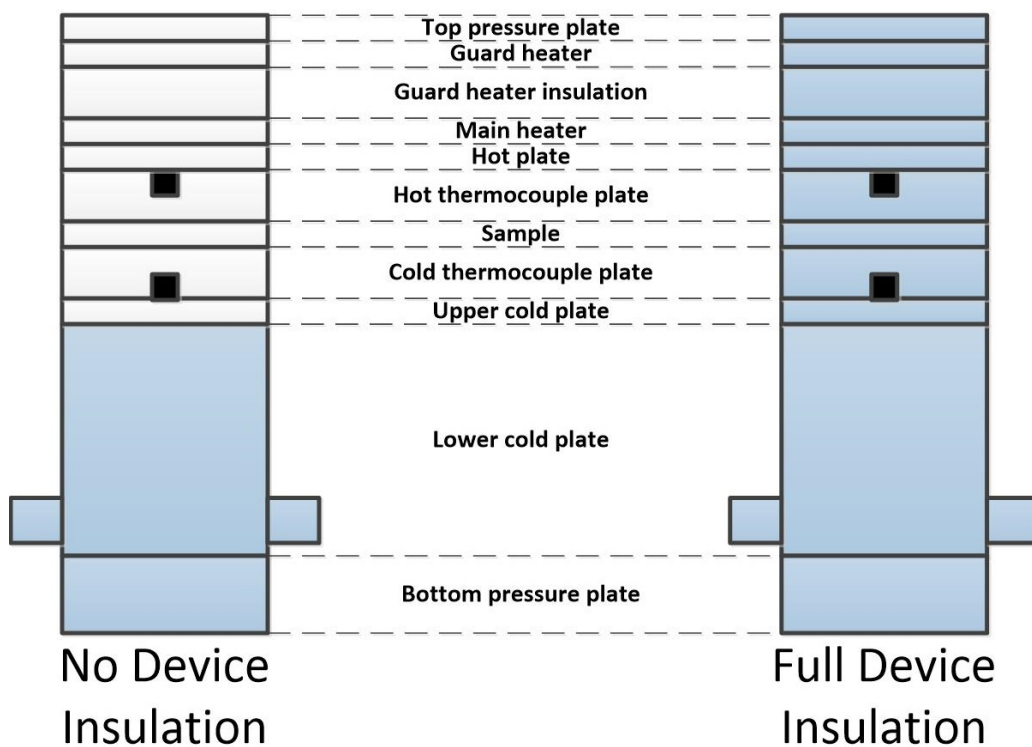
Bler areas indicate locations where the device was insulated. Lower cold plate and upper portion of bottom pressure plate insulated with balsa wood. Top pressure plate, guard heater, guard heater insulation, main

heater, and hot plate insulated with balsa wood. Hot thermocouple plate, sample, cold thermocouple plate, and upper cold plate insulated with foam.

For the second set of analyses, only the insulation around the sample was varied from the original foam layer used. These variations involved completing runs using no sample insulation or applying a thin tape layer to insulate the sample in place of the foam (see Figure 46).

Figure 46.   Insulation layout for various sample insulation runs
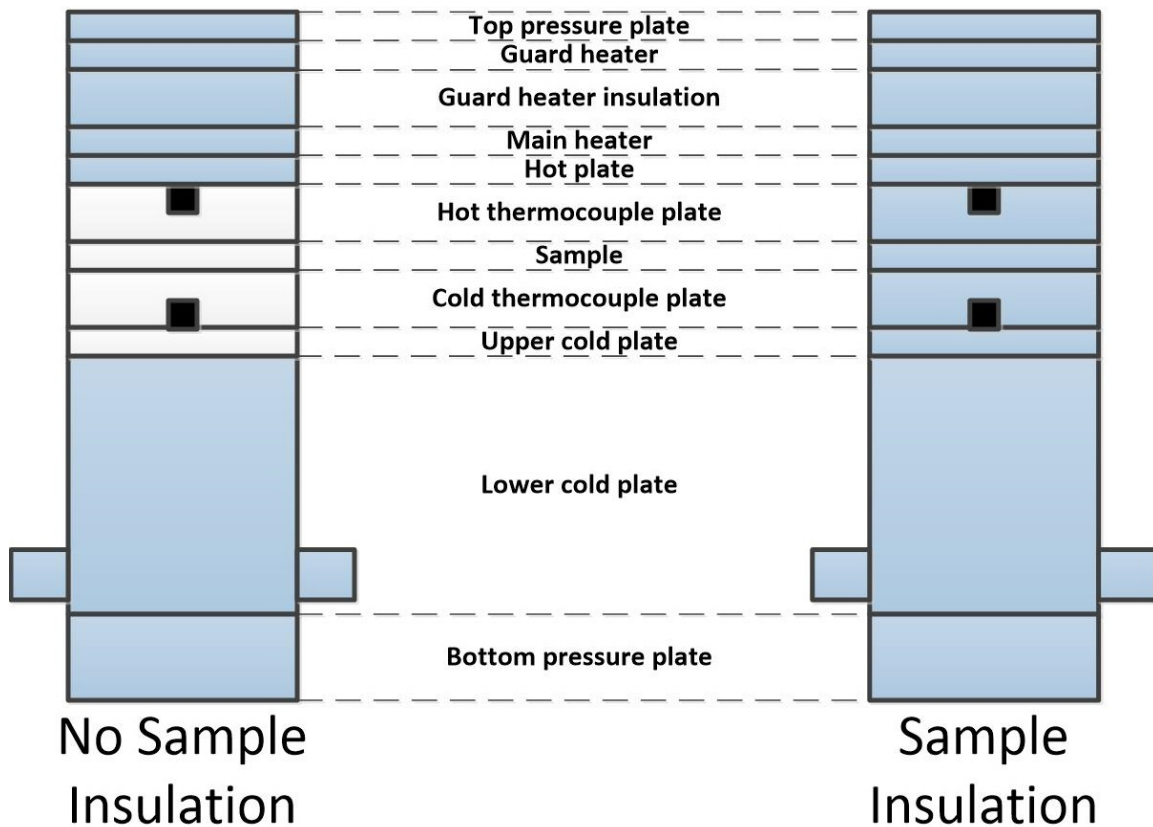
Blue areas indicate locations where the device was insulated. Lower cold plate and upper portion of bottom pressure plate insulated with balsa wood. Top pressure plate, guard heater, guard heater insulation, main heater, and hot plate insulated with balsa wood. Hot thermocouple plate, sample, cold thermocouple plate, and upper cold plate insulated with tape layer.

Figures 45 and 46 show the central measurement device with subcomponents indicating where each type of insulation was applied for the design analysis runs.

To assess the application of thermal grease, experimental analysis looked into completing a measurement run without grease as well as neglecting grease calculations in Equation 12. These evaluations were completed using a fully insulated device at low power output to the main heater. Results for each of the runs were calculated for accuracy using the same method as described for the normal experimental runs to determine measurement system accuracy.

4.   Summation

From the methods discussed to measure the measurement system's accuracy and design sensitivity, conclusions will be made determining the performance of the system. In order to assess system accuracy to measure thermal conductivity between 0.1 – 40 W/m-K, Pyroceram 9606 and 99.8% Alumina were chosen for experimental runs. To determine device accuracy and measurement uncertainties, data such as power unit output will be used. Follow-on runs using Pyroceram 9606 were devised in order to assess design sensitivity and validate the conclusions drawn from early design analysis. Using this outlined methodology, the accuracy and design of the system can be assessed. This assessment will then be combined with results from replicability analysis to determine if the measurement system is of use to the DON/DOD.

B.   VERIFYING REPLICABILITY OF RESULTS

In addition to the analyses performed to verify measurement accuracy, experimental methods were established to assess the replicability of the produced results. To validate this capability the measurement system was operated by different experimentalists as well as run at different times throughout the day. The purpose of this evaluation was to ensure that this device design produced similar results regardless of when it was used and which operator was using it.

One of the main contributors to any experimental result inaccuracy is from operator error [35, 36]. To ensure that the thermal contact resistance and thermal

conductivity measurement system could repeatedly produce accurate results regardless of who operated it, different experimentalists were used to perform measurements. During these runs, experimentalists ran four separate runs using the normal operating procedure for the measurement system (see Appendix C). Each of these runs were conducted at low power output with full device insulation. Each individual ran each of their runs individually without the other experimenter present to minimize any outside interference. Measurements completed during each of these runs were assessed for accuracy to determine the replicability of the results produced by the author of this report (Experimentalist 1) (see Equation 16).

$$\text{Result Replicability (\%)} = \frac{\left| k_{\text{experimentalist 1}} - k_{\text{comparison experimentalist}} \right|}{k_{\text{experimentalist 1}}} (100\%) \qquad (16)$$

Using the results from Equation 16, average result replicability could be calculated using measurement data taken at approximately the same sample temperature.

In addition to operator influence, to ensure the device produced similar results regardless of laboratory environment, the device was run at different times on varying days. This approach was taken to ensure that the measurement capability remained the same regardless of other routine experimental operations occurring in the room. Measurement analysis was scheduled throughout the week (Sunday through Saturday) from the morning to late evening. No set schedule for measurements was used to minimize the chance that results were being affected by any one set of external variables such as room temperature or occupation/inoccupation by other experimentalists.

Assessing the capability of the measurement system to produce accurate measurements regardless of operator or environmental conditions will be used to verify its ability to replicate results. This assessment is important to conduct to ensure the thermal contact resistance and thermal measurement system can produce accurate results regardless of the DON/DOD installation it resides in and the researcher who uses it.

C. SUMMARY

From the outlined experimental methodology to assess the accuracy and replicability of measurement results, the goal is to establish the usefulness of the

proposed system to measure thermal contact resistance and thermal conductivity at any DON/DOD facility by any researcher regardless of his/her background. Experimental methods outlined to measure result accuracy assess the ability of the system to perform as designed throughout the proposed thermal conductivity range of 0.1 – 40 W/m-K. To accomplish this, the project will measure materials at either end of this range: Pyroceram 9606 and 99.8% Alumina. Results provided from these measurements will be then analyzed for uncertainty. In addition to these analyses, design sensitivity will be assessed to validate the processes discussed in the design and construction phase. Finally, replicability analysis will be performed to ensure that the device can be operated as desired regardless of environment or operator. From the results gathered using this methodology, an answer can be provided to whether or not the designed system will be of value to the DON/DOD and their energy program.

THIS PAGE INTENTIONALLY LEFT BLANK

V. RESULTS AND DISCUSSION

Using the experimental methods established in the previous section, results were generated to validate the thermal contact resistance and thermal conductivity measurement system's accuracy and performance replicability. In most of the analyses performed, the measurement design was able to meet or exceed expectations established for measuring accuracy. Further analysis indicated the ability to reduce result uncertainties based on the power levels used during each analysis. The results from the design sensitivity analysis lead to the conclusion that the proposed design and calculation methods produced the most accurate results. Finally, replicability analysis indicated the device's capability to repeatedly produce these accurate results regardless of the operator.

A. ACCURACY

For the measurement system to be of use to the DON/DOD it would have to be capable of producing accurate results. Using the methodology discussed in the experimental section for thermal conductivity analysis, results were produced that indicated that the chosen design successfully met expectations set forth for the project. Furthermore, result uncertainties were shown to be controllable by changing the power levels at which the system was operated. Finally, design sensitivity analysis indicated that the proposed design and method of construction was the best at obtaining these results.

1. Pyroceram 9606

The average measurement error for all of the Pyroceram 9606 measurements completed with a fully insulated device was 2.303%. The results generated by the measurement system closely matched the expected decrease in thermal conductivity for Pyroceram 9606 as temperature was increased (see Figure 47).

Figure 47.   Pyroceram 9606 measurement data and result uncertainties
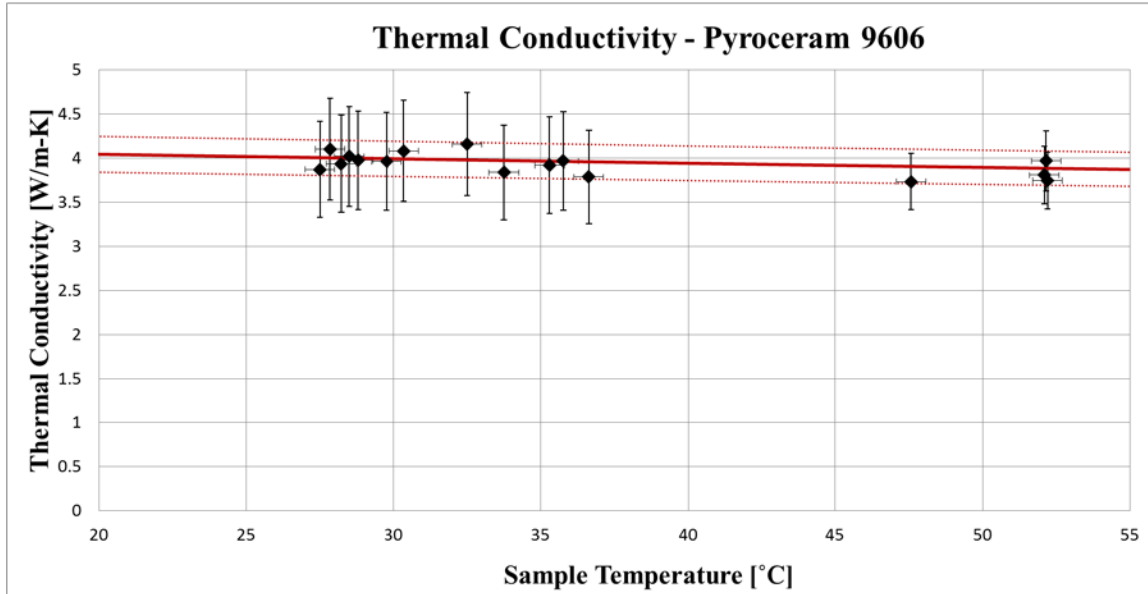
In Figure 47, thermal conductivity results for Pyroceram 9606 are plotted corresponding to the sample temperature calculated at the time of data collection. The solid red line in Figure 47 corresponds to the data provided from the literature discussed previously in the experimental methods section. Dotted red lines represent the ±5% uncertainty in the expected thermal conductivity values that was expressed in the literature from which they were gathered [45]. Horizontal error bars in Figure 47 represent the uncertainty associated with the calculated sample temperature due to thermocouple errors (±0.4°C). Vertical error bars reflect the average result uncertainty calculated for low power (below 40°C in figure) and high power runs (above 40°C in figure). These averages were calculated as 12.38% for low power runs and 7.93% for high power runs (see Table 18).

Table 18.   Average result uncertainty for Pyroceram 9606

Average Result Uncertainty	
Run Type	[%]
Low Power	12.38
High Power	7.93

As shown in Table 18, analysis performed at high powers indicated the ability to reduce measurement uncertainty to below 10%. Calculation review indicated that the two most dominant factors in the uncertainty analysis were the output current and difference in temperature across the sample (see Appendix E). Operating the measurement system at higher powers significantly reduced each of these measurement uncertainties, therefore causing the overall measurement uncertainty to decrease. The power levels to which the system could be run to further reduce these uncertainties was limited based on the working fluid used in the cooling system; water. The observed trend however indicates that with a different working fluid such as glycol, which would allow the cooling system to be run at much lower temperatures, much lower average result uncertainties can be obtained.

Overall, results from the experimental runs for the Pyroceram 9606 consistently fell within the 5% error threshold values set as a goal for the project (see Figure 48).

Figure 48.   Thermal conductivity measurement error for Pyroceram 9606

89
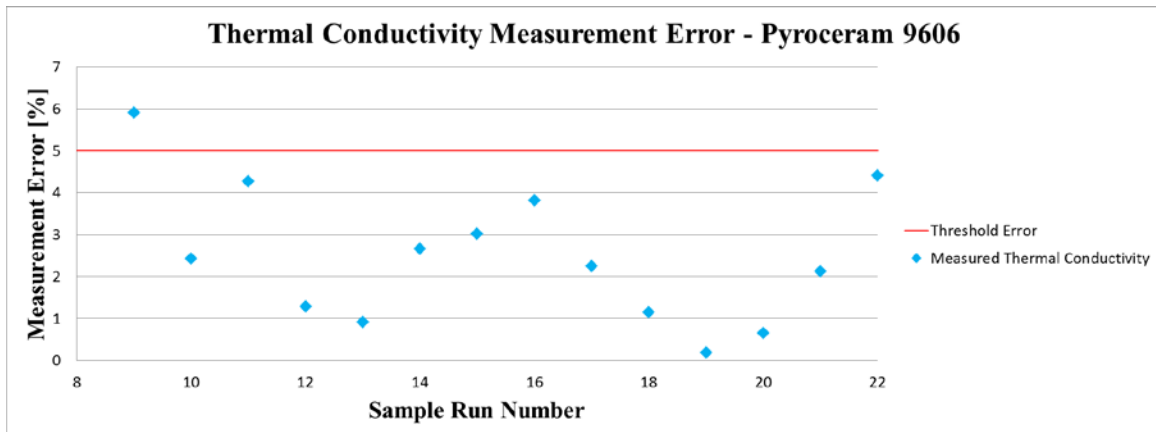
The only exception to these results was one measurement that had an error of ~5.92%, which corresponded to the first measurement conducted using the fully insulated measuring system (see Appendix E). Compared to this run, the next highest measurement error that occurred during analysis was over 1% less.

From the results gathered during this project, the thermal contact resistance and thermal conductivity measurement system was shown to operate well within expectations at the lower end of the proposed thermal conductivity range. Average result error for all runs completed using a fully insulated device were less than half the threshold error of 5%. Uncertainty analysis indicated that the result uncertainty could be reduced below 10% by operating at high power. Review into the main contributing factors of result uncertainty indicated that with a change of the working fluid used in the cooling system these values could be reduced even further.

2.   99.8% Alumina

The results from the 99.8% Alumina runs indicated the difficulty of obtaining accurate results from materials with thermal conductivities closer to the 40 W/m-K upper limit of the desired measurement range. The average measurement error for all of the 99.8% Alumina measurements completed with a fully insulated device was 6.382%. This average includes three runs with an error above 10% in which loose thermocouples were expected to be the cause (see Appendix E). Based on this belief, following the third run resulting in a high measurement error, the thermocouples were removed and reinstalled onto the measurement device. After the reattachment of the thermocouples, 7 follow-on runs were completed all with errors less than 9%. Each of these three runs (3.1, 4.1, and 5.1) occurred during high power runs, while all the remaining runs occurred at low power (see Figure 49).

Figure 49.   99.8% Alumina measurement data and result uncertainties
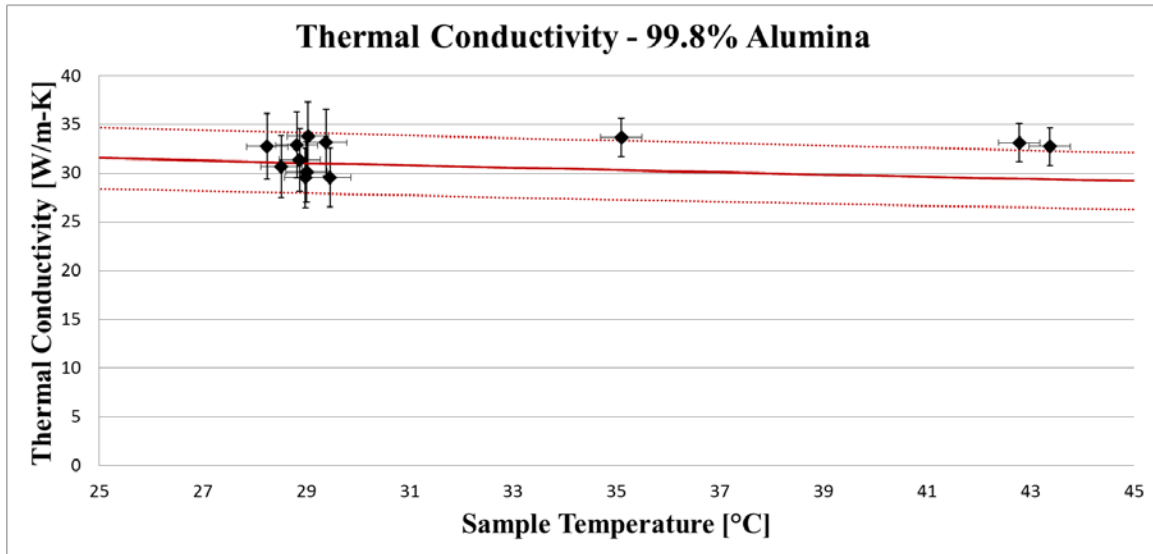
Figure 49 reveals that all the low power runs fell within the 10% uncertainty limits (dotted red lines) of the expected data (solid red line). When an average measurement error was calculated for these runs in particular the result was 4.67%. At this juncture, it is believed that the loose thermocouples affected the runs at higher powers leading to the higher errors. In spite of this belief, the average measurement error recorded for 99.8% Alumina still took into account these results since it could not be determined whether the loose thermocouples or the high powers lead to the errors.

Similarly to the results from Pyroceram 9606, 99.8% Alumina result uncertainties were shown to decrease with higher power runs and were mostly influenced by output current and difference in temperature across the sample (see Table 19, Appendix E).

Table 19.   Average result uncertainty for 99.8% Alumina

Average Result Uncertainty	
Run Type	[%]
Low Power	10.28
High Power	5.92

Table 19 indicates that with higher power runs, the average result uncertainty dropped from just above 10% to below 6%. The average result uncertainties (vertical

error bars) are plotted along with the data displayed in Figure 48 for high (above 30°C in figure) and low power runs (below 30°C in figure). Horizontal error bars indicate the uncertainty within the calculated sample temperature due to thermocouples used in the experiment (±0.4°C).

Compared to the results from the Pyroceram 9606 analysis, the 99.8% Alumina results varied in accuracy from less than 1% to over 12% (see Figure 50).

Figure 50.   Thermal conductivity measurement error for 99.8% Alumina
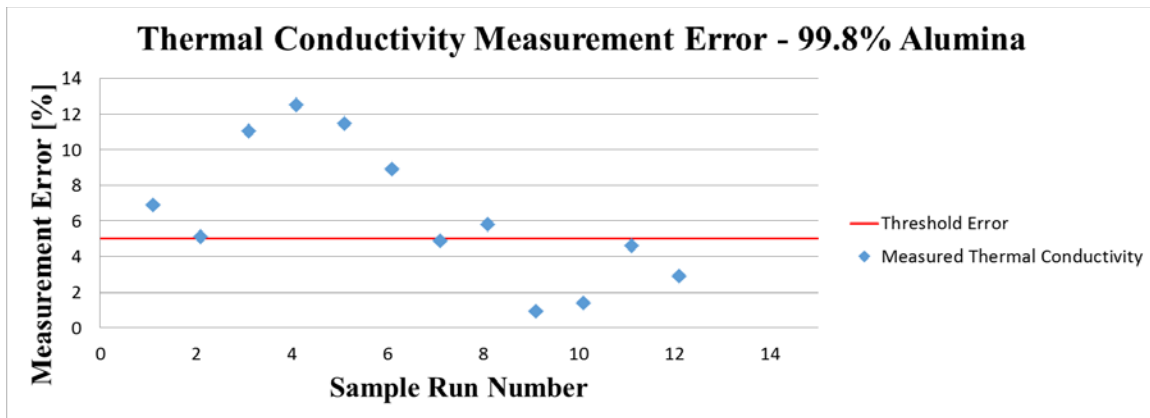
The thermal conductivity measurement errors shown in Figure 50 indicate that a larger number of measurements on expected higher thermal conductivity samples would need to be run with the device. In contrast to the Pyroceram 9606 sample results where almost all fell below 5% measurement error, the results for 99.8% Alumina were less precise. Measurement accuracies fell equally below and above the threshold of 5%. Due to these results, it is recommended that more runs are performed at a given sample temperature for higher thermal conductivity samples to statistically reduce measurement error when analyzing unknown samples.

B.   DESIGN SENSITIVITY

Design sensitivity analysis indicated that all proposed design components for the thermal contact resistance and thermal conductivity device were necessary to ensure accurate results. Investigation into the removal of insulation indicated that a fully insulated device was required to produce data with low measurement errors.

Additionally, the inclusion of a thermal grease layer to reduce thermal contact resistance was important both in the physical device and while conducting the calculations to determine a sample's thermal conductivity.

1. Effects of Device Side Heat Losses

Applying the methodology discussed in the Experimental Methods section of this report, results were generated indicting that insulation was required for all portions of the measurement system. These portions included the hot plate, sample, and cold plate. Results indicated an increasing trend in accuracy as more efficient insulation was used. In addition to accuracy, added insulation was shown to improve the precision of the measurement system.

a. Device Insulation

Full device insulation was shown to produce accurate and precise measurement results when analyzing Pyroceram 9606 at low powers. In contrast, when the device was not insulated, results produced, while accurate, were not precise (see Figure 51).

Figure 51.   Pyroceram 9606 measurement data for full verse no device insulation
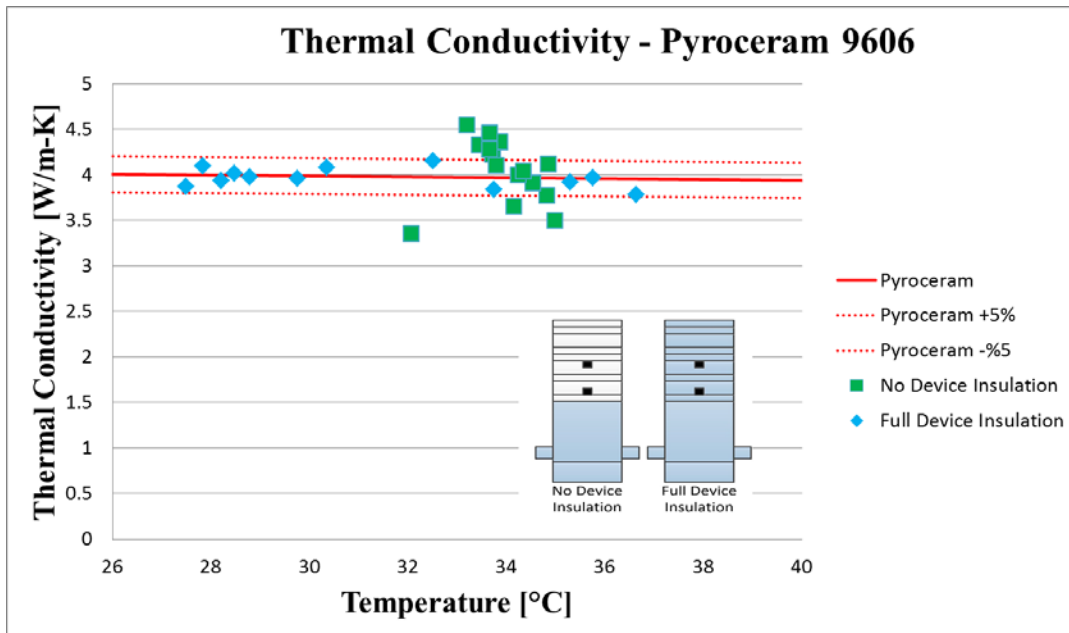
Figure 51 displays a much larger variance in thermal conductivity measurements conducted with no device insulation despite similar sample temperatures. Measurement errors while sampling without insulation were as high at 16% with a majority of the measurements having errors above 6% (see Figure 52).

Figure 52.   Thermal conductivity measurement error for full verse no device insulation
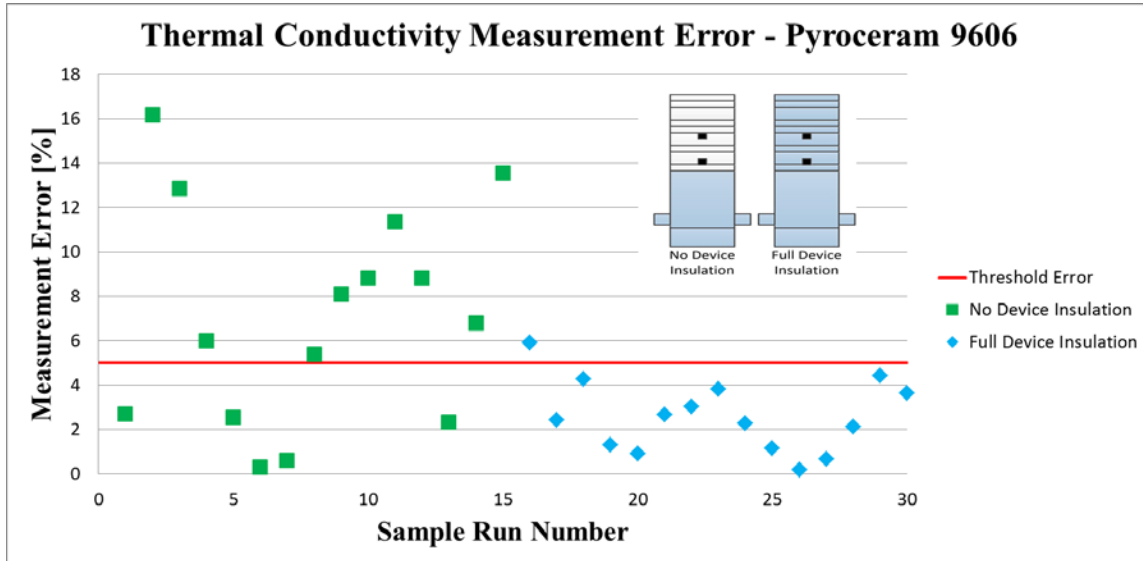
The overall average measurement error for all the runs shown in Figure 52 performed without insulation was 7.348% (see Table 20).

Table 20.   Effect on average measurement error due to device insulation

Average Measurement Error	
Device Insulation Type	[%]
No Insulation	7.090
Full Insulation	2.303

As displayed in Table 20, the incorporation of full insulation around the measurement device reduced this average error almost 5%. This large reduction in average error is a direct result from the gained measurement precision displayed in Figure 51 due to the added insulating device layers.

b. *Sample Insulation*

Analysis on results generated from runs where sample insulation varied indicated similar trends as discussed for full verses no device insulation. Overall results calculated for thermal conductivity measurements of Pyroceram 9606 at low power indicated accurate results (see Figure 53).

Figure 53.   Pyroceram 9606 measurement data for various sample insulation
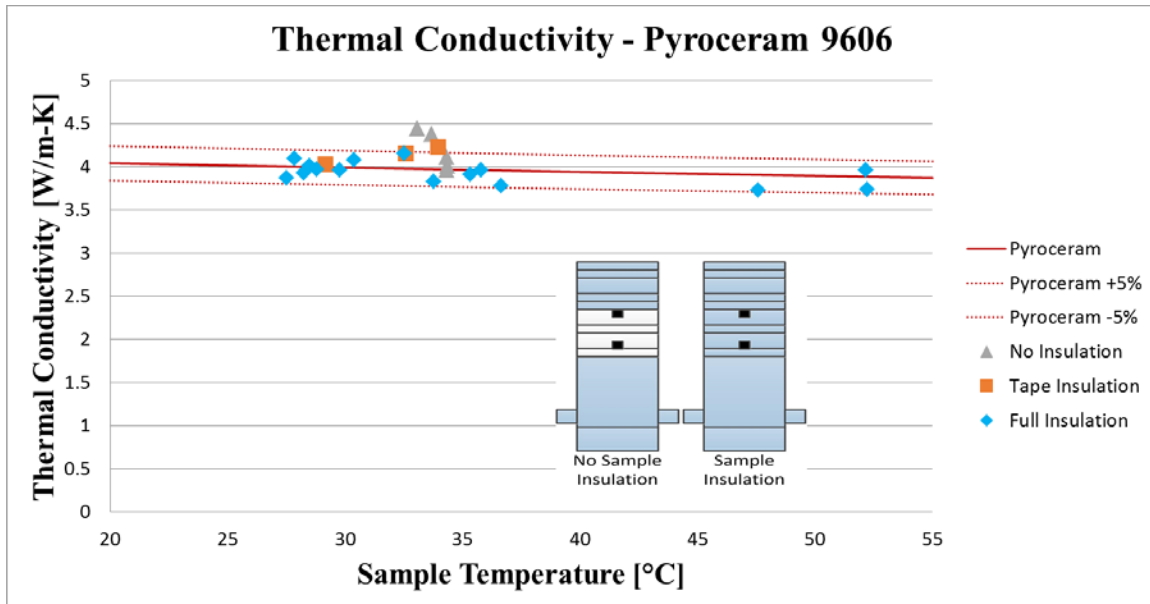
Although all the different sample insulation types produced accurate results, as the insulation layer was improved (i.e., full foam insulation vice a thin tape layer), the results became more precise (see Figures 53 and 54).

Figure 54.   Thermal conductivity measurement error for various sample
insulation
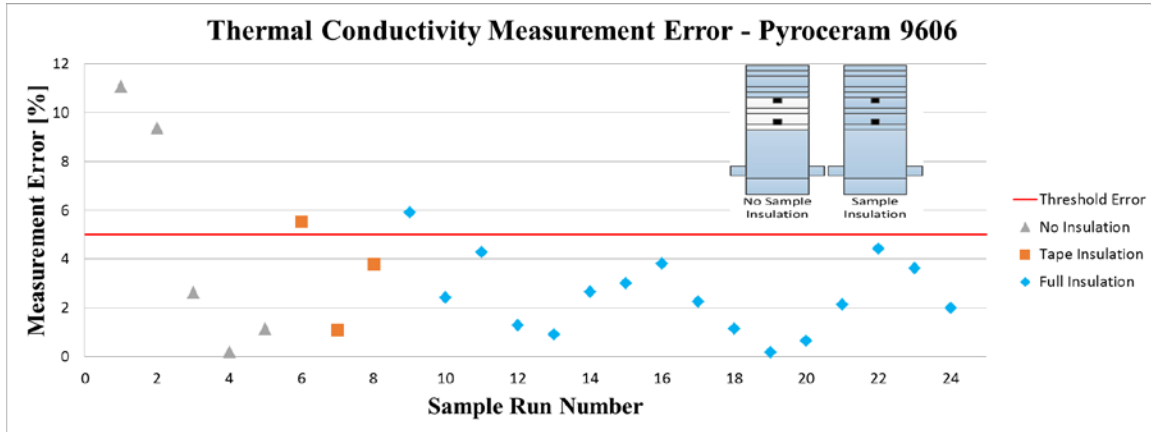
The lack of precision in results generated by analyzing the Pyroceram 9606 sample not insulated or insulated with tape contributed to higher average measurement errors (see Table 21).

Table 21.   Average measurement error for different sample insulation types

Average Measurement Error	
Sample Insulation	[%]
No insulation	4.889
Tape insulation	3.477
Foam insulation	2.303

Each successive improvement to the sample insulation layer led to a greater than 1% decrease in average measurement error. Although over twice as high as using foam insulation, the average measurement error for runs conducted with the device fully insulated with the exception of the sample was significantly less than runs performed with no device insulation at all (see Table 20). These results indicate the benefit of simply insulating the cold and hot plates of the device over no insulation at all.

c.   Summation

Design sensitivity analysis performed on insulation methods indicated that by adding insulation to the device, more accurate results could be produced. Measurement precision successively improved as the design moved from having no insulation to full

insulation. This improved precision directly contributed to the reduction in average measurement error. Improving the precision of the device leads to a reduction of runs required during routine sample analysis to statistically remove any experimental errors. The overall results indicate that the proposed insulation design and construction produced the most accurate and precise sample measurements.

2.   Mitigation of Thermal Contact Resistance

While insulation was shown to improve measurement precision, the application of a thermal contact resistance mitigation layer (i.e., Dow Corning 340 Heat Sink Compound thermal grease) significantly improved result accuracy of the measurement system. System measurements conducted without grease resulted in an average measurement error of almost 9 times greater than with grease (see Table 22).

Table 22.   Effect on average measurement error due to thermal grease application

Average Measurement Error	
Grease Application	[%]
No Grease	63.547
Grease	7.090

The significant increase in measurement accuracy indicates the importance of applying a thermal grease layer between the sample and the device's hot and cold plates. In addition, it underscores the drastic effect contact resistance can have on the thermal conductivity of a composite system. This result reinforces the importance of thermal contact resistance mitigation discussed in the background section of this report.

3.   Neglected Thermal Grease Calculations for Thermal Conductivity

Similar to the impact on results that the use of no thermal grease had, neglecting the impact of the thermal grease layer in thermal conductivity calculations resulted in very high average measurement errors. The calculated thermal conductivities for all insulation cases discussed previous decreased when the grease layer was neglected (see Figure 55).

Figure 55.   Pyroceram 9606 measurement data calculated with grease layer
neglected
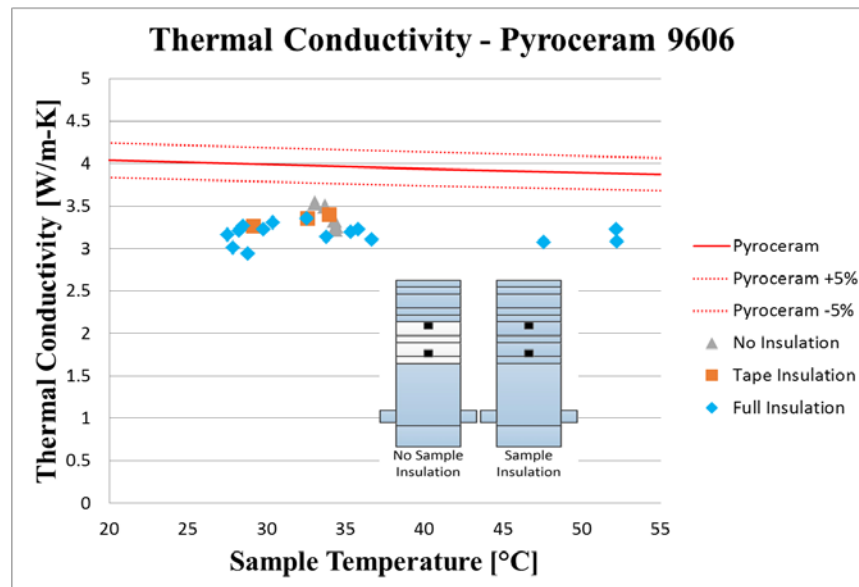
As shown in Figure 55, even though the accuracy of the results decreased, the
precision of the results remained constant to what was shown in Figure 53. While the
average measurement error increased for all sample insulation type runs, the runs whose
accuracy was most affected by neglecting the grease layer were the fully insulated ones
(see Figure 56).

Figure 56.   Thermal conductivity measurement error calculated with grease
layer neglected
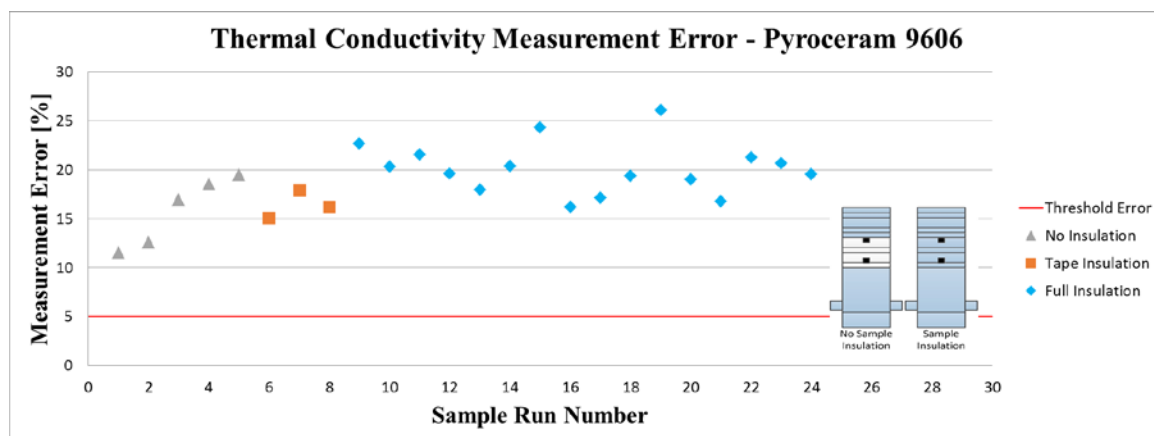
In most cases, measurement errors shown in Figure 56 are shown to increase over 4 times their value when the grease layer calculation was included. This change in accuracy is echoed in the recalculated average measurement error neglecting grease for each type of sample insulation (see Table 23).

Table 23.   Effect on average measurement error due to neglecting grease layer contribution

Average Measurement Error	
Sample Insulation	[%]
No insulation	15.836
Tape insulation	16.390
Foam insulation	20.198

Table R6 indicates the importance of including each layer's contribution into calculating the measured sample thermal conductivity. Neglecting the grease layer in the calculations would indicate that the designed system was ineffective at accurately measuring thermal properties. This would be a misleading conclusion based on the previously discussed accuracies obtained when all layers are accounted for.

4.   Summation

Measurement runs performed on Pyroceram 9606 and 99.8% Alumina indicated the thermal contact resistance and thermal conductivity measurement system's capability to produce accurate results. Average measurement error for Pyroceram 9606 was 2.303%, less than one half of the desired threshold for the system. Average measurement results for 99.8% Alumina were calculated to be 6.382% as a result of three data measurements that had higher measurement error as a result of possible faulty thermocouple attachment. When this data was neglected, overall average measurement error for 99.8% Alumina dropped to 4.67%. During both sets of runs, higher power device operations indicated the ability to reduce measurement uncertainty to below 10%.

Results provided during the design sensitivity analysis provided two main takeaways to be considered for future measurement system designs. First, the method used to insulate the measurement system directly affects the precision of the results

produced. Second, the accuracy in which all layers are measured and accounted for between the hot and cold thermocouple plates directly impacts the accuracy of the sample thermal conductivity results. Using these takeaways, device improvements can be made in order to adjust the performance of the measurement system to meet the needs of the DON and DOD.

C.   REPLICABILITY

In addition to measurement accuracy throughout the proposed thermal conductivity range, the results must be able to be replicated by any experimentalist to be of value to the DON/DOD. Results created by different experimentalists indicated the ability to fulfill this requirement (see Figure 57).

Figure 57.   Pyroceram 9606 measurement data for different experimentalists
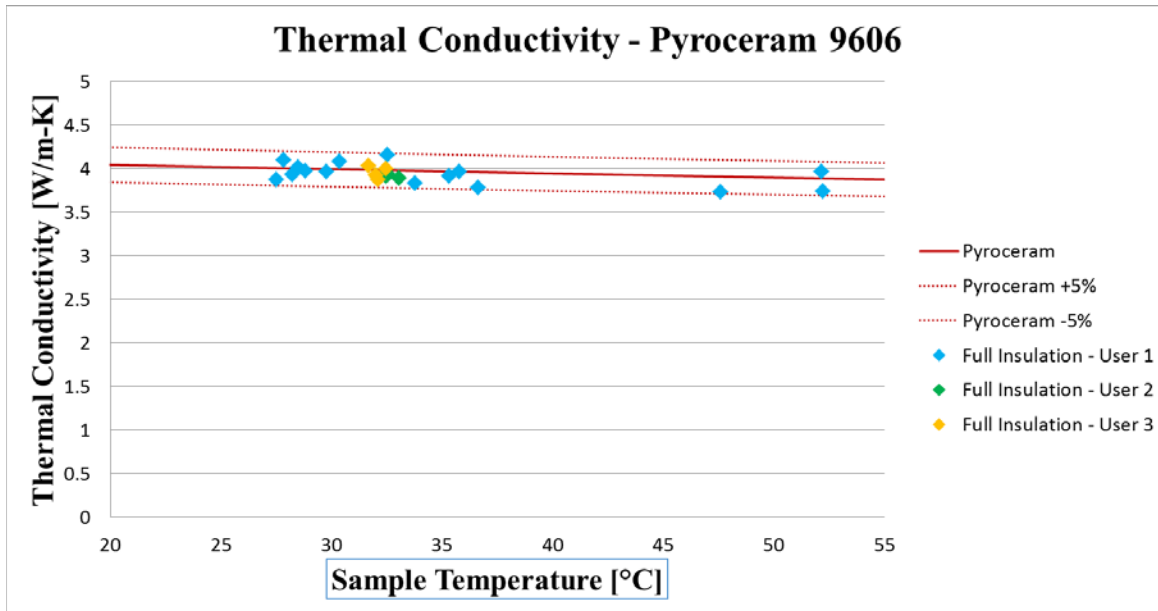
Figure 57 indicates the ability of experimentalists other than the author to achieve similar measurement accuracies. The thermal conductivity measurement errors associated to runs conducted by the second and third experimentalists all fell below 4% (see Figure 58).

Figure 58.   Thermal conductivity measurement error for different
experimentalists
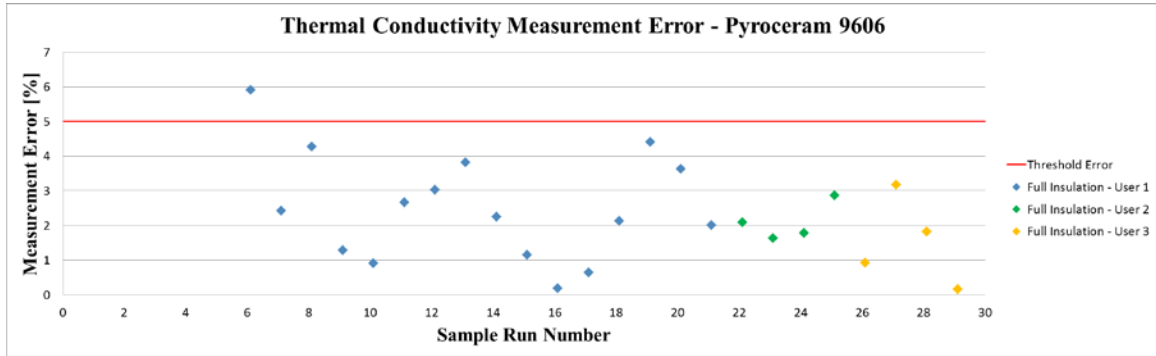
In fact, the average measurement results from the runs conducted by the second and third operator were both less than the author's results; 2.096% and 1.524% respectively (see Appendix E). Furthermore, result replicability analysis for measurements conducted at a sample temperature of approximately 32.5ºC indicated that measurement results from the second and third operator fell within 6% to the author's results (see Table 24).

Table 24.   Result replicability analysis

Result Replicability Analysis			
Experimentalist	Tavg Plate [C]	k_ΔTavg [W/m-K]	Replicability [%]
1	32.51	4.155	-
2	32.44	3.919	5.69
	32.54	3.937	5.24
	32.45	3.930	5.41
3	32.10	3.873	6.78
	32.46	3.996	3.83
Average Replicability [%]			5.39

These results of the replicability analysis indicate that the thermal contact resistance and thermal conductivity measurement system can achieve accurate results regardless of the operator using it.

101

D. SUMMARY

The overall outcome of the result analysis reveals a measurement system that can replicate very accurate results regardless of the operator. This is an important finding that upholds the usefulness of the system at any DON/DOD facility to measure proprietary materials with expected thermal conductivities between 0.1 – 40 W/m-K. Results for the thermal conductivity measurements of Pyroceram 9606 and 99.8% Alumina produced an average measurement error of 2.303% and 6.382%, respectively. High power runs proved to be an effective method to reduce result uncertainties to within 10%. Through design sensitivity analysis, the capability to control measurement precision and accuracy was tied to device insulation and thermal grease application methods. Replicability analysis indicated that experimentalists unfamiliar with the design could produce the same accurate results to within 6% of each other without any needed revisions to the proposed normal operating procedure. The outcome of these testing and evaluation indicates that the thermal contact resistance and thermal conductivity system can be used without any needed modifications to the proposed design or operation procedures. Any added modifications to the design would only serve to increase its usefulness to DON and DOD applications for selecting the best materials to use in WHR and CPV systems.

VI.   RECOMMENDATIONS

Without requiring any modifications to the proposed thermal contact resistance and thermal conductivity design, two recommendations are made toward future experiments studying the thermal properties of materials. The first recommendation is to perform follow-on measurements to analyze the effects on the contact resistance between selected composites due to varying pressure. The second recommendation is to look into how the thermal conductivity of coatings is affected as a function of temperature and pressure. Both of these investigations can be used to look into how pressure and temperature affect non-homogeneous materials employed in DON/DOD energy systems.

Measuring thermal contact resistance of composites as a function of pressure is important since many energy systems within the DON and DOD undergo cyclic pressure stresses. The affect that this changing pressure has on the thermal contact resistance within composite materials can lead to changes in heat distribution characteristics and temperature measurement accuracies. Cyclic pressure stress can contribute to the failure of adhesives holding a given composite together exposing micro-voids that result in a decrease of that component's effective thermal conductivity. This could cause major system issues if the component is designed to serve at an interface where high heat transfer is desired such as in heat exchanger components such as gaskets. As designed with the top and bottom Pyrex pressure plates, the proposed measurement system can measure the thermal contact resistance and effective thermal conductivity of these components. The results of this study would aim at establishing which type of composite adhesives work the best at maintaining overall integrity of the component during its service lifetime.

A second study of use to the DON and DOD involves investigating the effective thermal conductivity of coatings such as HVOF and cold spray as a function of temperature and pressure changes. With new advances in coating technology, including the use of antifouling coatings on ship hulls [47-49], it is only a matter of time before these advanced coatings find their way into energy systems such as engines [50]. The ability to measure the affects these coatings have on the efficiency of the energy system

will be extremely invaluable to the DOD. Studies can be performed using the proposed system on various coating techniques to determine which methods properly adhere a desired substrate to a component while obtaining the required effective thermal conductivity necessary for proper system operation.

Both of the proposed studies on composites and spray coatings can be completed with no necessary modifications to the proposed thermal contact resistance and thermal conductivity device within this report. Measurements of the thermal contact resistance of composites as a function of pressure can be used to indicate which adhesives perform best to minimize composite corrosion affecting a component's thermal properties over its designed lifetime. Research into the effects of pressure and temperature on spray technology could lead to important discoveries in how this rapidly developing technology can be integrated into energy systems such as WHR and CPV. The possibilities of studies such as these, which can be performed by the designed thermal contact resistance and thermal conductivity device, indicate the usefulness that this project has toward advances in energy efficiency within the DON and DOD.

VII. CONCLUSION

This project has shown from the results produced that a thermal contact resistance and thermal conductivity measurement system can be built based using a simplistic design and construction, yet produce accurate and reliable results. Using analytical and numerical analysis, a proposed design was derived off the *Plate Method* to analyze the thermal conductivity of materials within a range of 0.1 to 40 W/m-K using Fourier's Law of Conduction. This *Plate Method* approach was selected based on its simplistic design compared to transient methods and other steady state methods such as the *Rod Method*. In-depth design considerations included the type and dimensions of the sample cross sectional area, material to be used for the device construction, and the subcomponents comprised within the measurement device. These decisions had to be made to ensure that a 1-D heat flux was maintained throughout the device, a uniform temperature distribution existed at the sample interface, and any unwanted heat losses were minimized to ensure device accuracy.

In addition to device accuracy, replicability of results was important to consider in order to make the measurement system of value to the DON/DOD. Replicability of results, along with continuing to ensure measurement accuracy, influenced the construction of the electrical and cooling subsystems. Accuracy and replicability concerns also directly impacted the proposed normal thermal contact resistance and thermal conductivity measurement system operating procedure. The focus of both the detailed construction and operation procedures was to enable the device to be built at any DON/DOD facility and operated by any researcher regardless of experience.

The measurement system was successfully tested using Pyroceram 9606 and 99.8% Alumina. Results indicated the ability of the system to measure the thermal conductivity of Pyroceram 9606 to within 2.5% from published literature values and manufacturer's data. Results for the measurement of 99.8% Alumina indicated an average measurement error less than 6.5% with manufacturer's data. For either material, uncertainty calculations using the Kline and McClintock Uncertainty analysis indicated that result uncertainties could be reduced to within 10%. Design sensitivity analysis

revealed that full insulation was necessary for the device to produce precision measurements. These analyses also indicated that the accuracy in which the contact resistance mitigation layers between the device and sample were accounted for directly affected the accuracy of the thermal contact resistance and thermal conductivity results. Finally, replicability assessments indicated that the same measurement accuracies could be obtained by three different users. All of these results were an important indicator of the benefits and potential that this device has in measuring thermal contact resistance and thermal conductivity of proprietary materials currently under research by the DON/DOD.

The suggested design and construction for a thermal contact resistance and thermal conductivity measurement system provided within this report is driven toward improving energy efficiency within the DOD. The discussed design successfully establishes the capability of measuring thermal properties of advanced materials at the Naval Postgraduate School. Additionally, this work establishes the infrastructure for the measurement of thermal contact resistance outlined in the Waste Heat Recovery Systems roadmap developed for the U.S. Navy. By accomplishing these tasks, this project enables the pursuit of follow-on research into areas such as material composites and the value of incorporating spray coatings such as High Velocity Oxygen Fuel and cold spray into current military energy systems. Developments into these areas can directly contribute to advancements in overall DOD energy efficiency, meeting the objectives outlined by the Secretary of the Navy and President of the United States.

APPENDIX A. DESIGN DATA AND ANALYSIS

A.   SQUARE VERSES ROUND ANSYS MODEL DESIGN PARAMETERS

Table A.A.1.   Square vs. circular ANSYS model design parameters (q" = 100750 W/m²)

Sample Cross-Section Type	ANSYS Model Parameters					
	$T_{AMBIENT}$	T_{BASE}	h	k_{sample}	$k_{insulation}$	q"
	[˚C]	[˚C]	W/m²-K	W/m-K	W/m-K	W/m²
Square	25	15	10	400	4.5	100750
Square	25	15	50	400	4.5	100750
Square	25	15	100	400	4.5	100750
Circular	25	15	10	400	4.5	100750
Circular	25	15	50	400	4.5	100750
Circular	25	15	100	400	4.5	100750

Table A.A.2.   Square versus circular ANSYS model design parameters
(q" = 232500.5 W/m²)

Sample Cross-Section Type	ANSYS Model Parameters					
	$T_{AMBIENT}$	T_{BASE}	h	k_{sample}	$k_{insulation}$	q"
	[˚C]	[˚C]	W/m²-K	W/m-K	W/m-K	W/m²
Square	25	15	10	400	4.5	232500.5
Square	25	15	50	400	4.5	232500.5
Square	25	15	100	400	4.5	232500.5
Circular	25	15	10	400	4.5	232500.5
Circular	25	15	50	400	4.5	232500.5
Circular	25	15	100	400	4.5	232500.5

B.   MAIN AND GUARD HEATER DESIGN PARAMETERS

Figure A.B.1. Main and guard heater design layout

From WATLOW, "ULTRAMIC Advanced Ceramic Heaters," 2015. [Online]. Available: http://www.watlow.com/products/heaters/ultramic-ceramic-heaters.cfm?famid=10. [Accessed 21 June 2015].

C.   WIRE VERSES MAIN HEATER RESISTANCE ANALYSIS

Table A.C.1.   Difference between resistance in wire verses main heater for various heater temperatures

Main Heater				Wire		Calculations			
Heater Temperature	Current	Voltage	Resistance	Resistance	Wire Voltage Drop	Power_HTR	Power_Wire	Percent Difference
[C]	[A]	[VDC]	[Ω]	[Ω]	[VDC]	[W]	[W]	-
35.3	0.05	5.257	105.14	0.8	0.04	0.26285	0.002	0.761%
56.8	0.08	9.866	123.325	0.8	0.064	0.78928	0.00512	0.649%
64.2	0.09	11.031	122.5666	0.8	0.072	0.99279	0.00648	0.653%
74.8	0.11	12.658	115	0.8	0.088	1.39238	0.00968	0.695%
84	0.12	14.161	113.288	0.8	0.096	1.69932	0.01152	0.678%
95.5	0.14	15.721	112.292	0.8	0.112	2.20094	0.01568	0.712%
104.7	0.15	17.125	114.1666	0.8	0.12	2.56875	0.018	0.701%

108

D. ASSEMBLY AND INDIVIDUAL SUBCOMPONENT THICKNESS MEASUREMENTS

Table A.D.1. Measurement device and individual subcomponent assembly thicknesses

	Component	Thickness (in)					Thickness (m)					Largest Δ	(Largest Δ / Avg)*100%
Individual Heater Elements	Copper Plate Hot	0.1012	0.1013	0.10091	0.1007	-	0.00257	0.002573	0.002563	0.002558	-	1.524E-05	**0.594%**
	Thin Pyrex	0.09985	0.0999	0.0999	0.0999	-	0.002536	0.002537	0.002537	0.002537	-	1.27E-06	**0.050%**
	1/2" Pyrex	0.49975	0.49975	0.5	0.4997	0.49925	0.012694	0.012694	0.0127	0.012692	0.012681	1.905E-05	**0.150%**
	Main Heater (MH)	0.09655	0.09625	0.09635	0.09645	0.0963	0.002452	0.002445	0.002447	0.00245	0.002446	7.62E-06	**0.311%**
	Guard Heater (GH)	0.0959	0.0959	0.09565	0.09545	0.09595	0.002436	0.002436	0.00243	0.002424	0.002437	0.0000127	**0.522%**
Heater Assembly	Thin Pyrex + GH	0.1988	0.1987	0.1993	0.1986	0.1979	0.00505	0.005047	0.005062	0.005044	0.005027	3.556E-05	**0.705%**
	Thin Pyrex + GH + 1/2" Pyrex	0.7003	0.7007	0.70095	0.6996	0.6995	0.017788	0.017798	0.017804	0.01777	0.017767	3.683E-05	**0.207%**
	Copper Plate Hot + MH	0.2009	0.2007	0.2008	0.2007	0.2007	0.005103	0.005098	0.0051	0.005098	0.005098	5.08E-06	**0.100%**
	Total Heater Assembly	0.912	0.916	0.913	0.9075	0.9098	0.023165	0.023266	0.02319	0.023051	0.023109	0.0002159	**0.932%**
Individual Thermocouple Elements	Thermocouple Depth	0.1001	0.1	0.0999	0.1	0.1	0.002543	0.00254	0.002537	0.00254	0.00254	5.08E-06	**0.200%**
	Cold Thermocouple Plate	0.2012	0.2013	0.201	0.201	0.2013	0.00511	0.005113	0.005105	0.005105	0.005113	7.62E-06	**0.149%**
	Hot Thermocouple Plate	0.201	0.201	0.201	0.2015	0.2015	0.005105	0.005105	0.005105	0.005118	0.005118	0.0000127	**0.249%**
	Copper Plate Cold	0.101	0.1008	0.1011	0.1013	0.1008	0.002565	0.00256	0.002568	0.002573	0.00256	0.0000127	**0.495%**
Total Assembly	Upper Hot Assembly	1.1151	1.1112	1.1175	1.209	1.1148	0.028324	0.028224	0.028385	0.030709	0.028316	0.00248412	**8.628%**
	Cold Upper Assembly	0.3037	0.3044	0.3041	0.304	0.3039	0.007714	0.007732	0.007724	0.007722	0.007719	1.778E-05	**0.230%**

THIS PAGE INTENTIONALLY LEFT BLANK

APPENDIX B. MEASUREMENT SYSTEM CONSTRUCTION PROCEDURES

A. COOLING SYSTEM ASSEMBLY

1. Parts/Tools Needed

Figure B.A.1. Cooling system parts needed

Additional/Optional parts and tools (not shown): hose clamps, scissors, knife

2.   Procedure

Figure B.A.2. Cooling system layout diagram
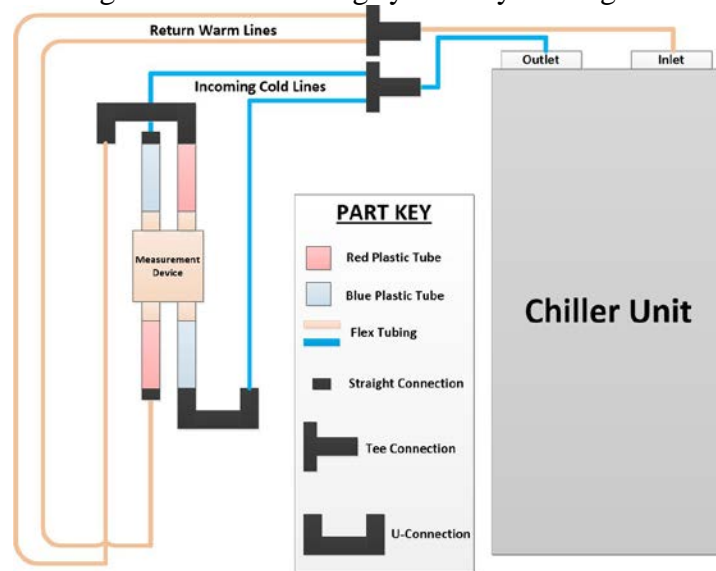
1.   Using the diagram of the cooling system (see Figure B.A.2), layout the system to verify the lengths of tubing required to connect the measurement device to the chiller.

2.   Cut 76.3mm (3 inch) hose lengths from the red (hot) and blue (cold) solid plastic tubes. These tubes will be directly connected to the measurement device cooling channels.

3.   Cut adequate hose lengths from the flex piping for the incoming (cold) and return (warm) lines. Pay particular attention to minimize overall hose lengths to reduce the amount of insulation needed. Incoming lines should be minimized to ensure the coldest fluid temperatures are delivered to the measuring device. Additionally, ensure that the total lengths of piping for each coolant channel (total incoming and return sections) are similar in length. This will minimize the chance that the temperature of coolant in one line will be different than the other.

4.   Using the sealant, coat the following hose connections liberally and insert into the appropriate sections of flex and plastic piping as shown in Figure B.A.2.

     i.   U-connections (x2)
    ii.   Straight connections (x2)
   iii.   Tee connections (x2)

Optional: For additional leak protection, tighten hose clamps around each connection.

5.   Allow sufficient time for the sealant to cure according to the manufacturer's directions for use.

6.   Test fit the red and blue plastic piping to the measurement device (see Figure B.A.3). Some minor sanding may be required to reduce the outer diameter of the piping so that hose clamps can be fit between the coolant channels on the lower cold plate.

Figure B.A.3.   Test fit of plastic tubing to measurement device
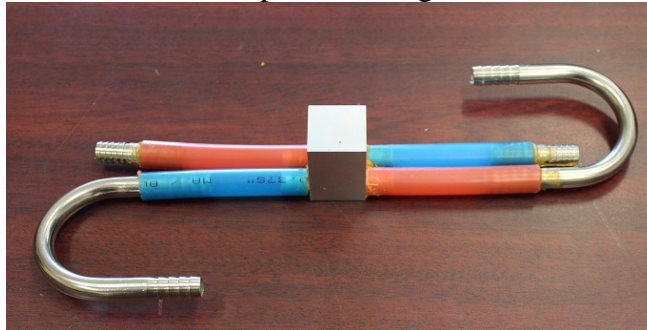
Prototype lower cold plate shown in this figure.

7.   Secure the plastic piping to the measurement device using the hose clamps. A sealant may be used to serve as additional protection against leaks.

8.   Using the hose clamps and sealant attach the remaining portions of the flex tubing to the chiller and measurement device.

9.   Allow sufficient time for the sealant to cure according to the manufacturer's directions for use.

10.   Following the *CHILLER UNIT OPERATION* procedure in Appendix C, run the cooling system for an hour at 25°C using water to ensure no system leaks.

11.   After verifying no temperature leaks and flow in each of the cooling channels, insulate the incoming lines using the hose insulation.

NOTE: To verify flow in each of the cooling channels reduce the chiller operating temperature to the minimum specified by the manufacturer for water. Check that each of the incoming line surface temperatures drops accordingly. If the temperature of one line

does not drop, secure and empty the cooling system. Upon refilling the system, ensure no air voids are present in either of the lines.

12. If flow cannot be established in both of the lines resize the piping using one of the following methods:

   i. Reduce the length of the return piping of the channel with the no flow going through it.
   ii. Increase the length of the return piping of the channel with flow going through it.
   iii. Insert a throttle valve into the return piping section of the channel with flow going through it. Throttle this valve until flow goes through the other channel.

NOTE: In either method described above, the outcome will be to reduce the head loss in the piping without flow going through it when compared to the other channel. By reducing the head loss compared to the other channel, the coolant will flow more freely through the problematic line.

13. Using the insulation tape, cover all metal joints such as the metal U-connections. Figure B.A.4 shows the final cooling system layout with installed prototype.

Figure B.A.4. Completed cooling system

B.   ELECTRICAL SYSTEM ASSEMBLY

1.   Parts/Tools Needed

Note: Number of pieces identified in parentheses
Extra lengths of braided wire
Shrink wrap
Solder
Wire stripper
Solder gun
Heat gun
Multimeter

2.   Procedure

If necessary, follow the following procedure for extending heater wires to the upper heater assembly.

1.   Measure and cut needed lengths of wire. Ensure to use wire that is at least the same gauge or less as the original heater wire. Using thicker wire will minimize any added resistance in the lines to and from the heater unit.

2.   Using the wire stripper, remove some of the insulation off the ends of the extension wire and heater wire.

3.   Using the multimeter, measure the resistance across the heater.

4.   Un-twist the one end of the extension wire and the free end of the heater wire.

5.   Place the two ends together and twist the stands together tightly.

6.   Using the solder and solder gun, solder the connection together ensuring uniform coverage.

7.   Allow the connection time to cool.

8.   Slip shrink wrap over the free end of the extension wire and cover the soldered connection.

9.   Using the heat gun, heat the shrink wrap in place covering the exposed wire connection.

10.   Repeat for all heater wires that require an extension.

11.   Using the multimeter measure the resistance across the heater with the newly attached extension wires.

12.   Note the change in wire resistance due to the added extensions.

C.   THERMOCOUPLE PLATE ASSEMBLY

1.   Parts/Tools Needed

Note: Number of pieces identified in parentheses
Thermocouple plates (2)
Type T thermocouples (12)
Punch tool (1)
Hammer (1)
Sonic washer (1)
Compressed air source (1)
Rubber gloves (1)
Tape
Adhesive

2.   Procedure

1.   Using the hammer and punch tool, tap small indents in the thermocouple channel on each thermocouple plate. The best technique for accomplishing this is to direct the punch tool through the side of the plate (see Figure

B.C.1). This technique avoids damaging the thermocouple-to-sample surface located on the opposite side of the plate.

Figure B.C.1.   Thermocouple groove indentation method
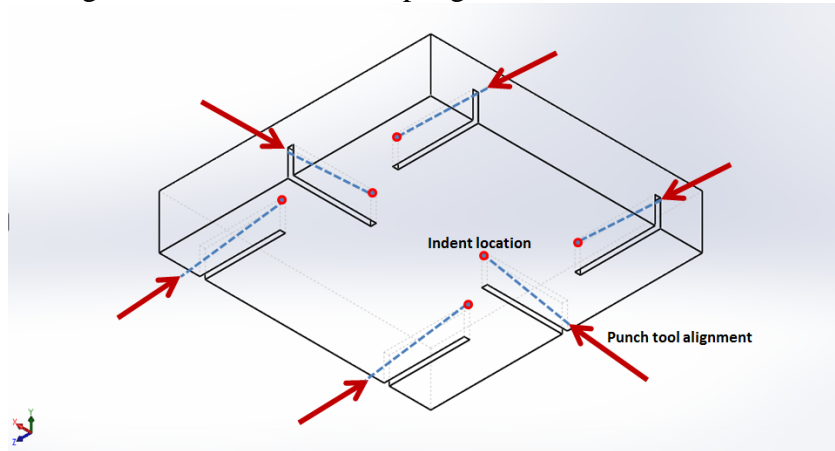
These indents will be for the thermocouple bead placement

2.   Using the compressed air source remove any debris that may remain in the channels from the machining process.

3.   Using the sonic washer clean each of the thermocouple plates. This needs to be performed to ensure no oils or chemicals remain within the grooves from the machining process. Any residue oils or chemicals may prevent proper adhesion of the thermocouple to the groove surface, subsequently reducing the contact between the thermocouple bead and indent.

Important: Use gloves for the remainder of this procedure to ensure no oils are introduced to component surfaces

4.   Remove each of the plates and thoroughly dry using the compressed air source. Compressed air is highly recommended since other techniques will not be able to ensure each of the channels and indents are dried completely.

5.   Securely fasten each of the thermocouple plates to a rigid surface with tape.

6.   Straighten the last 50.8mm (2 inches) of thermocouple wire prior to the thermocouple bead.

7.   Carefully cover the last 12.7 mm (0.5 inches) of thermocouple wire prior to the thermocouple bead with adhesive. This should also include any exposed thermocouple wire prior to the bead location. Ensure that the thermocouple bead does not get covered by any adhesive (see Figure B.C.2)

Figure B.C.2. Thermocouple adhesive application location
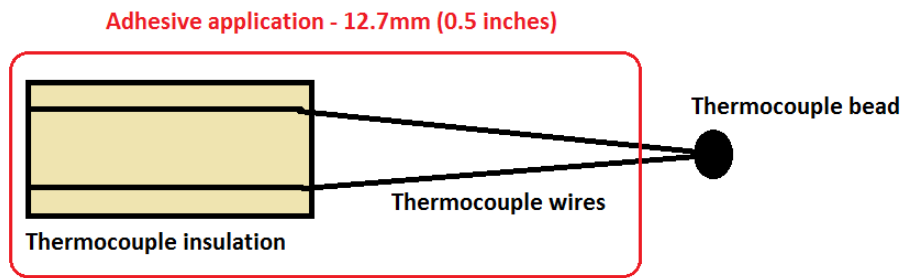
8.   Insert the thermocouple into the groove from the side of the plate. This will be the same direction that was used in Step 1 for the punch tool. Ensure that the thermocouple bead enters the indent created (see Figure B3).

Figure B.C.3. Thermocouple placement inside thermocouple channel
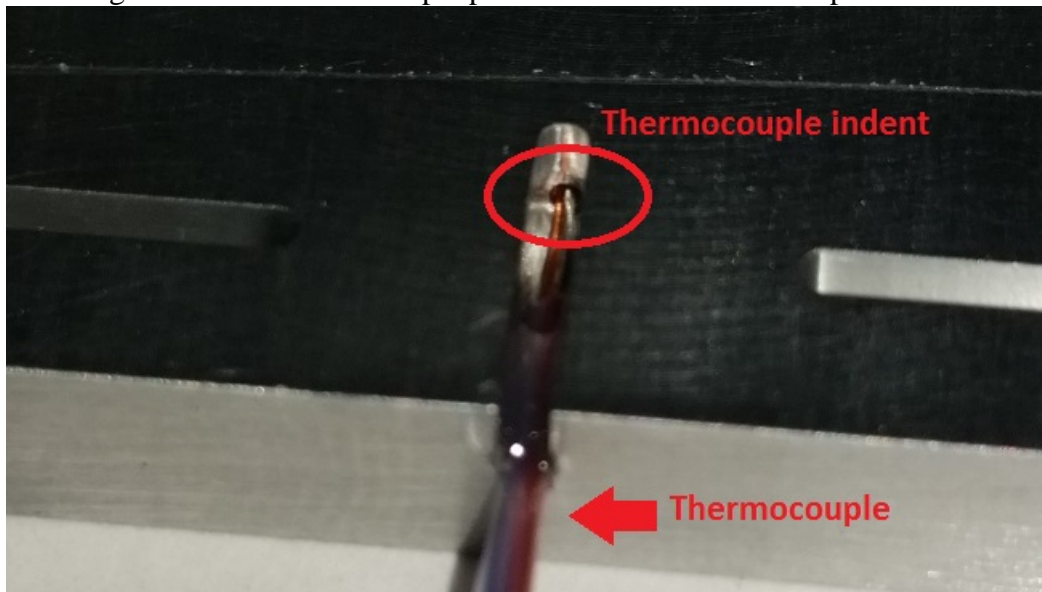
9.   Firmly secure the thermocouple to the same rigid surface the thermocouple plate was secured to in Step 5.

10.   Repeat for each thermocouple and thermocouple channel (see Figure B.C.4).

Figure B.C.4. Attachment of thermocouples to thermocouple plate
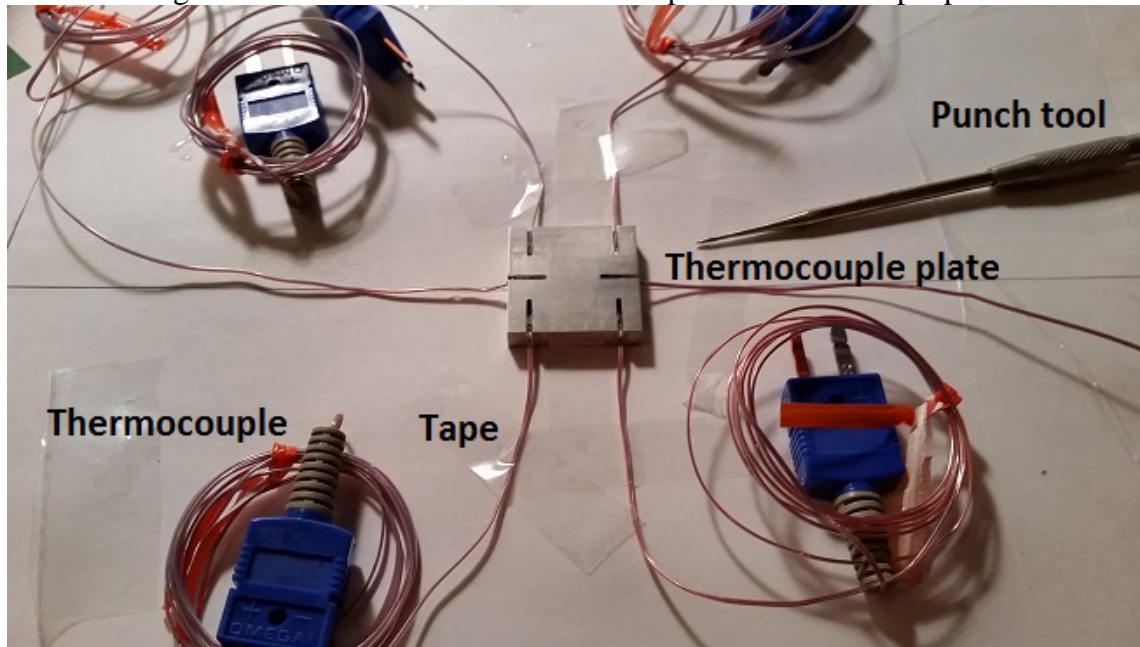
11. Using the punch tool, cover the insulated end of each thermocouple with a small amount of adhesive to secure. Guide this adhesive into the thermocouple channel working from the outside-in direction. Ensure no excess adhesive gets onto surface of the thermocouple plate.

12. Test all thermocouples to ensure they are operating normally and that the thermocouple bead is not broken

13. Allow the adhesive to set according to manufacturer's guidelines.

14. Clean tool punch thoroughly before reusing it on any thermocouple plates to prevent any remaining adhesive from entering the created indents.

D. MEASUREMENT DEVICE ASSEMBLY

1. Parts/Tools Needed

Figure B.D.1. Measurement device parts needed
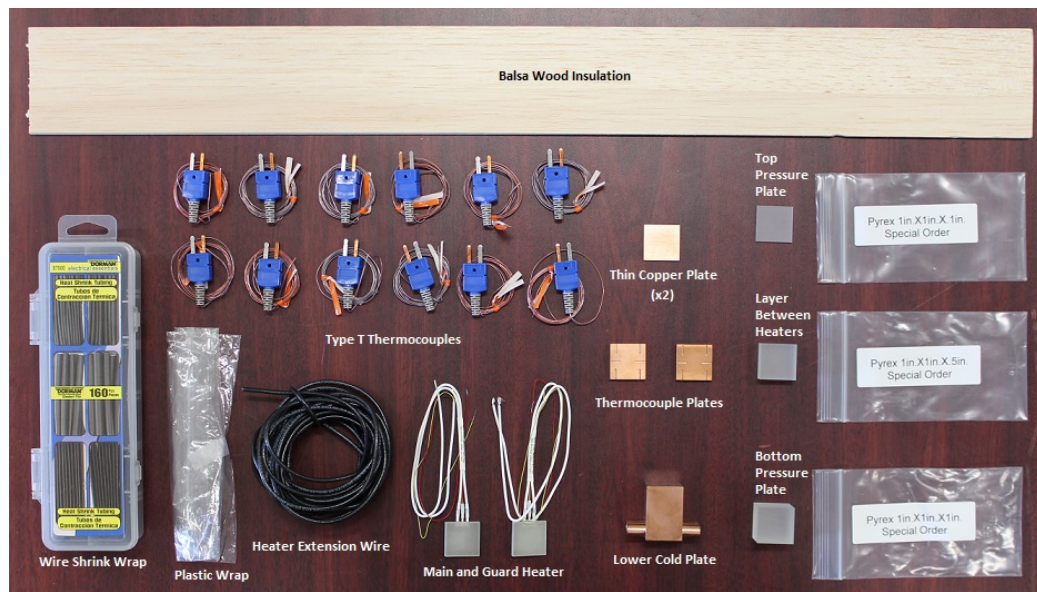
Additional/Optional parts and tools (not shown): scissors, knife, 1kg weight, precision micrometer, foam insulation, high temperature adhesive, thermally conductive adhesive paste

2.   Procedure

Figure B.D.2. Measurement device subcomponent assembly placement
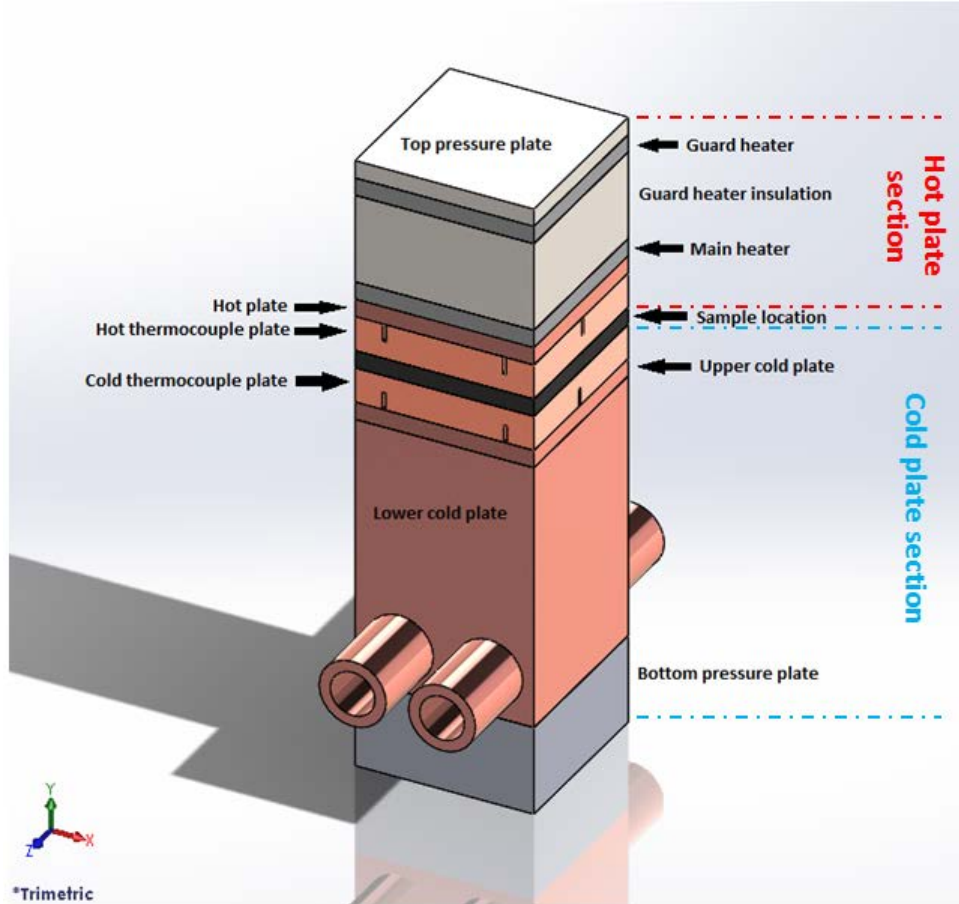
1.   Measure all subcomponents of the overall measurement device using a precision micrometer. Each subcomponent should be measured in five locations; the four corners and the center. Measure: Thin copper plate (x2), top pressure plate(x1), guard heater insulation (layer between heaters, x1), bottom pressure plate (x1), main heater (x1), guard heater (x1), thermocouple plates (assembled, x2), and lower cold plate (x1).

For all following steps, use Figure B.D.2 as a guide to subcomponent placement while constructing the measurement device sections.

2.   For the **UPPER HOT PLATE SECTION**, begin to assemble the subcomponents using the thermally conductive adhesive paste. After each new layer is created, re-measure and record the subcomponent thickness using the same process as step 1.

3.   Once the **HOT PLATE SECTION** is complete, insulate all portions of this section with the exception of the hot thermocouple plate and upper

surface of top pressure plate using three layers of balsa wood. For the purposes of insulation and structural rigidity, align the balsa wood so that the grains in each layer are 90º to the preceding layer attached to the device. Use the high temperature adhesive for this process.

4.   The **COLD PLATE SECTION** will need to be built in two separate layers: the **LOWER COLD PLATE SECTION** and **UPPER COLD PLATE SECTION**. These sections will not be adhered to each other to allow for ease of sample removal during normal operations.

5.   The **LOWER COLD PLATE SECTION** is comprised of the bottom pressure plate and lower cold plate. Adhere these two subcomponents together using the high temperature adhesive (Note: To minimize heat loss, do not use thermally conductivity adhesive).

6.   The **LOWER COLD PLATE SECTION** will be insulated using three layers of balsa wood. Similarly to step 3 attach the balsa wood to this subsection.

7.   The **LOWER COLD PLATE SECTION** will be separated from the **UPPER COLD PLATE SECTION** by a thin layer of plastic. Cut a piece of plastic and adhere to the top of the **LOWER COLD PLATE SECTION** using a very thin layer of adhesive (see Figure B.D.3).

Figure B.D.3. Plastic layer on top of lower cold plate section.
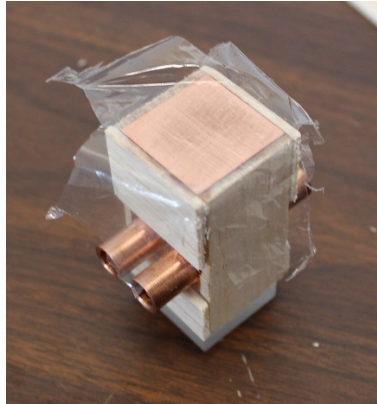
8.   Once the **LOWER COLD PLATE SECTION** is completed (Figure B.D.4), the **UPPER COLD PLATE SECTION** should be assembled using the thermally conductive adhesive paste and measured. The **UPPER COLD PLATE SECTION** is comprised of the upper cold plate and cold thermocouple plate.

Figure B.D.4. Fully assembled lower cold plate section with insulation and plastic layer.
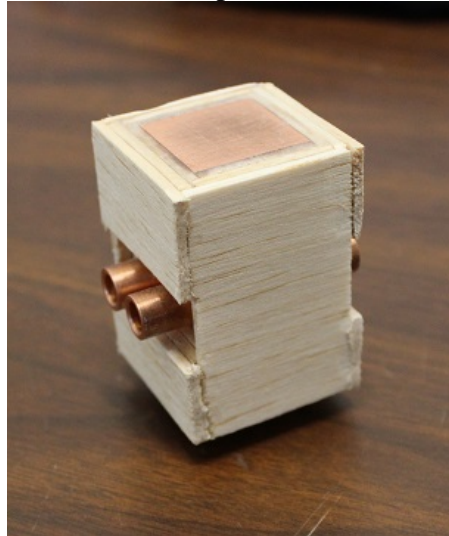
9.   Once all sections are completed, arrange the measurement device stack so that the foam insulation around the sample portion can be sized and cut.

10.   To ensure the device remains fixed during measurements, a 1kg weight can be placed on top of the top pressure plate to hold the stack in place. This weight is only necessary when no pressure analyses are conducted.

THIS PAGE INTENTIONALLY LEFT BLANK

APPENDIX C. NORMAL MEASUREMENT SYSTEM AND SUBSYSTEM OPERATIONS

A.   NORMAL SYSTEM OPERATIONS

1.   Tools

Note: Number of pieces identified in parentheses
Sonic washer (1)
Rubber gloves (1)
Precision micrometer (1)
Lint-free chemwipes
Thermal grease
Spatula

2.   Procedure

Important: Use rubber gloves for **Steps 1–18** of this procedure where either the sample or device is handled to ensure no oils are introduced to sample surfaces that can affect measurement accuracies.

1. Ensure either side of the hot and cold plates on the device are cleaned thoroughly

2. Ensure both sides of the sample are cleaned and dried thoroughly. This can be completed with a sonic washer and lint-free chemwipes. Any oils or chemicals on the sample surface can affect measurement accuracies.

3. Apply a small amount of thermal grease on either side of the sample. For adequate thickness and coverage, a pea-sized amount of grease should be sufficient.

4. Spread the thermal grease across either side of the sample with a small spatula ensuring uniform thickness and coverage.

5. Wipe any excess grease off the sides of the sample with the lint-free chemwipes paying particular attention to not disturb the grease layer on either face of the sample.

6. Place the sample on the top portion of the upper cold plate.

7. FOR THERMAL CONDUCTIVITY MEASUREMENTS ONLY. PERFORMING THIS STEP FOR THERMAL CONTACT RESISTANCE WILL LEAD TO MEASUREMENT ERRORS.

Move the sample back and forth to ensure grease uniformly covers both sides of the plates.

8. Place the insulation foam around the sample and upper cold plate.

9. Place the hot plate on top of the sample. Make sure no foam material gets between the plates as you perform this step.

10. FOR THERMAL CONDUCTIVITY MEASUREMENTS ONLY. PERFORMING THIS STEP FOR THERMAL CONTACT RESISTANCE WILL LEAD TO MEASUREMENT ERRORS.

   Move the hot plate back and forth to ensure grease uniformly covers both sides of the plates.

11. Place a weight on top of the device. The weight placed on top of the device can be varied to assess pressure effects on thermal contact resistance.

12. Ensure plate sides are aligned correctly including:

   -Hot plate to sample
   -Sample to upper cold plate
   -Upper cold plate to lower cold plate

13. Following the *CHILLER UNIT OPERATION* procedure, startup the cooling system at the desired working fluid temperature.

14. Using the *MEASURING TEMPERATURE* procedure, measure the main heater temperature.

15. When the main heater temperature begins to decrease, indicating proper cooling system operation, power on the main and guard heaters using the *POWER UNIT OPERATION* procedure.

16. Continue monitoring main heater temperature until temperature rate of increase decreases to less than 1°C/minute.

CAUTION: If heater exceeds 80°C at any point secure power to the heaters using the *POWER UNIT OPERATION* procedure. Failure to do so may result in a fire and/or severe damage to the measurement unit.

17. Adjust the guard heater power unit output voltage to minimize the difference in temperature between the guard heater and the main heater thermocouples.

18. Record ambient room temperature, date, and time.

19. Repeat **Step 12** to verify measurement device plates have not shifted. Realign plates if necessary.

20. Wait one hour for steady-state conditions to be established.

21. Record ambient room temperature. Verify that the ambient temperature has not changed greater than 5°C. If ambient temperature has changed greater than this amount, return to **Step 18** to verify that steady-state conditions have been established prior to measurements being taken.

22. Verify sample alignment. If sample has shifted, return to **Step 18**.

23. Record the following values:

    Main heater power supply output: voltage, current, power
    Guard heater power supply output: voltage, current

    Temperatures: ambient, main heater, guard heater, hot thermocouple plate temperatures, cold thermocouple plate temperatures

    This data will be used for the calculation of results and uncertainties for the measured sample.

24. After values have been recorded, secure power to the heaters using the *POWER UNIT OPERATION* procedure.

25. Monitor main heater temperatures using the *MEASURING TEMPERATURE* procedure.

CAUTION: At this point the device plates have the potential to be extremely hot and can cause injury to an operator if handled. DO NOT proceed with separating the device until the plates have been allowed to cool to at least 25°C.

26. When main heater temperature falls below 25°C secure the cooling system using the *CHILLER UNIT OPERATION* procedure.

CAUTION: This step is especially important at high power operations where the temperature of the plates can easily burn the operator. Leaving the cooling system running allows the plates to cool off rapidly and to be safe to handle.

27. Secure monitoring main heater temperature.

28. Remove the weight placed on top of the device during **Step 11**.

29. Carefully measure and record the average thickness of the hot plate, sample, and upper cold plate assembly using the precision micrometer. Thickness measurements should be taken in at least in three locations.

30. Carefully separate the hot plate assembly from the sample and upper cold plate making sure not to loosen the thermocouples.

31. Remove foam insulation layer.

32. Carefully separate the sample from the upper cold plate making sure not to loosen the thermocouples

33. Clean the thermal grease off the sample, hot plate, and upper cold plate surfaces.

34. Using the recorded values calculate the thermal conductivity of the sample analyzed.

B. MEASURING TEMPERATURE – MARTEL ELECTRONICS PTC-8010

Material discussed in this section (Appendix C.B) from *PTC8010 Reference Manual, 4th ed.,* Martel Electronics, Derry, NH, 2014.

IMPORTANT NOTE:
This is not an all-inclusive operating procedure for this device. This procedure is written to serve as a basic guide to operating the PTC-8010 as specified for the purposes outlined in this study. Consult the PTC-8010 reference manual for any operation not outlined or for device troubleshooting.

Figure C.B.1. Martel Electronics PTC-8010

Figure C.B.2. PTC-8010 Terminal Locations and Description
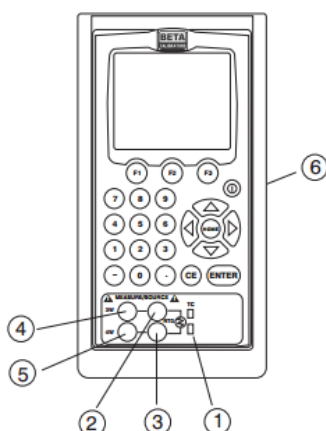
No.	Name	Description
1	TC input/output	Terminal for measuring, or simulating thermocouples. Accepts miniature polarized thermocouple plugs with flat in-line blades spaced 7.9 mm (0.312 in) center to center.
2,3	Source/Measure	Terminals for sourcing and measuring RTDs
4,5	Measure RTD, 3W 4W	Terminals for performing RTD measurements with 3-wire or 4-wire setups.
6	Serial port	Connects calibrator to a PC for remote control.

From *PTC8010 Reference Manual, 4th ed.,* Martel Electronics, Derry, NH, 2014.

Figure C.B.3.PTC-8010 Key Pad Functions
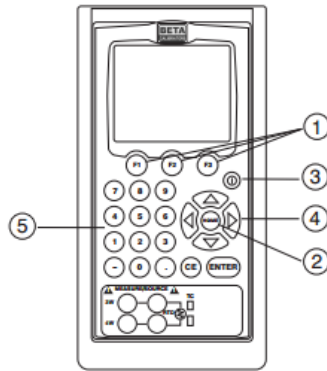
No.	Name	Function
1	Function Keys F1, F2, F3	Used to operate the menu bar at the bottom of the calibrator display. F1 is used for selecting options in the left box, F2 for the center box, and F3 for the right box.
2	Home	Returns to home menu on the menu bar.
3	Power	Turns calibrator on and off.
4	Cursor Control Key	Left and right arrow keys are used to select which decade to be changed in output value. Up and down arrow keys are used to increase, decrease, or ramp output value.
5	Numeric Keypad	Allows user to enter Numeric values.

From *PTC8010 Reference Manual, 4th ed.,* Martel Electronics, Derry, NH, 2014.

1.   Using Thermocouples

The PTC8010 calibrator supports the following thermocouple types: B, C, E, J, K, L, N, R, S, T, U, BP, and XK. The characteristics for type T thermocouples used in this project are provided (see Table C.B.1). For additional thermocouples reference the PTC8010 calibrator user manual. The calibrator also has a Cold Junction Compensation (CJC) function. For this procedure, this function should be ON so that the actual temperature of the thermocouple will be measured.

Table C.B.1.   Thermocouple Read and Source (errors in °C)

Martel Electronics PTC8010 Thermocouple Read Error			
TC Type	**Range [°C]**		**Accuracy [°C]***
	Minimum	**Maximum**	**CJC ON**
T	-250	-200	1.7
	-200	0	0.7
	0	400	0.4
*CJC error outside 23±5°C is 0.05°C/°C			

After *PTC8010 Reference Manual, 4th ed.,* Martel Electronics, Derry, NH, 2014.

To use the thermocouple to measure temperature, follow these steps:

1.   Attach the thermocouple leads to the TC miniplug, and insert the plug into the input/output of the calibrator, as in Figure C.B.2.

NOTE: For best accuracy wait 2 to 5 minutes for the temperature between the miniplug and the calibrator to stabilize before are measurements are taken.

2.   Select the [CONFIG] option from the main menu using Function Keys (see Figure C.B.3).

3.   Select TC from the primary parameters. Choose [IN] in the input/output control, and then 'TYPE T' thermocouple from the sensor types. The temperature unit may also be changed from Celsius to Fahrenheit or Kelvin.

C.   POWER UNIT OPERATION – BK PRECISION MODELS XLN30052 AND XLN15010

Material discussed in this section (Appendix C.C) from *High Power Programmable DC Power Supply User Manual,* BK Precision Corp, Yorba Linda, CA, 2013.

IMPORTANT NOTE:
This is not an all-inclusive operating procedure for this device. This procedure is written to serve as a basic guide to operating the XLN30052 and XLN15010 as specified for the purposes outlined in this study. Consult the XLN30052 and XLN15010 reference manual for any operation not outlined or for device troubleshooting.

Figure C.C.1. BK Precision High Power Programmable DC Power Supply (Model XLN30052 and XLN15010 shown)

Figure C.C.2. Front Panel Overview
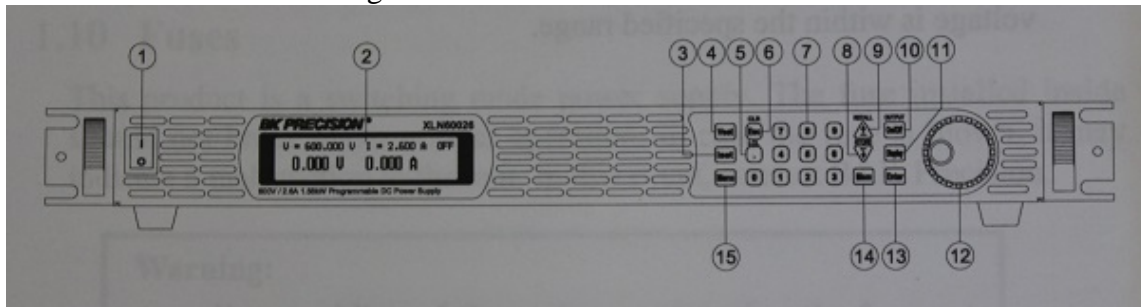
From High Power Programmable DC Power Supply User Manual, BK Precision Corp, Yorba Linda, CA, 2013.

1.   Front Panel Overview (Figure A2-2)

- (1) Power Switch – Turns on main unit power.

- (2) Display

- (3) Current Setting – Sets up current limit

- (4) Voltage Setting – Sets up voltage limit

- (5) Dot/Local – Applied as decimal point. See reference for additional uses in REMOTE/LOCAL mode.

- (6) ESC/CLR – Clears numerical settings or exit main menu or go to previous menu

- (7) Numerical Keys – Used to directly input current or voltage. Also used to select setting options in menu.

- (8) Down/Right/Store – See reference for use.

- (9) Up/Left/Recall – See reference for use.

- (10) Output – Allows user to turn ON and OFF main DC output from power unit's rear panel

- (11) Display – Allows user to toggle between showing voltage and current to power and load resistance.

- (12) Rotary Knob – Allows user to adjust current or voltage when output is ON.

- (13) Enter – Confirms changes to voltage, current, or menu options.

- (14) Mem – Accesses instrument settings memory location. See reference for more information.

- (15) Menu – Allows access to change key parameters within power unit. See reference for more information.

2. Operation

a. *Startup*

1. Ensure all rear panel connections including power cord are secure and set screws are tightened.

2. Turn on main power to the unit using the power switch located on the front panel

3. Select voltage/current setting

   i. Press Vset/ISet and set the desired output value using the numerical keys.
   ii. Press Enter to confirm the setting.

4. Confirm Overvoltage Protection, Overcurrent Protection, and Overpower Protection are established per the operating reference manual.

5. Press On/Off Output button. LCD screen will display actual output values.

6. If necessary to change voltage/current values during operation, repeat step 3.

7. Cycle through displays using Display button to monitor power, voltage, and current values.

b. *Shutdown*

1. Press On/Off Output button. Ensure LCD screen displays no output voltage, current, and power.

2. Turn off main power to the unit using the power switch located on the front panel

D. CHILLER UNIT OPERATION – HEIDOLPH ROTACHILL LARGE CHILLER

Material discussed in this section (Appendix C.D) from *RotaChill Large Chiller Operating Manual*, Heidolph Instruments GmbH & Co., Germany.

IMPORTANT NOTE:
This is not an all-inclusive operating procedure for this device. This procedure is written to serve as a basic guide to operating the RotaChill as specified for the purposes outlined in this study. Consult the RotaChill reference manual for any operation not outlined or for device troubleshooting.

Figure C.D.1. Heidolph RotaChiller large chiller unit front panel

Figure C.D.2. Rear panel unit main power switch

1. **Operation**

   a. *Startup*

1. Ensure all rear panel connections including power cord and hoses are secure.

2. Ensure proper fluid level in machine by verifying through front fill level display.

3. If necessary add additional working fluid to the reservoir by opening the reservoir cap located on the top of the unit.

4. Turn on main power to the unit using the power switch located at the rear of the unit (See Figure C.D.2).

5. Verify front display will turns on.

6. Press On/Off button on the front of the chiller located under the down directional button.

7. Set desired operating temperature:

   i. Press the SET button on the front of the unit. Observe that the display decimal will flash.
   ii. Using the Up/Down directional buttons select desired temperature. Make sure to observe manufacturer's recommendations on temperature set point based on working fluid.
   iii. Press the SET button. Observe that the display decimal will stop flashing.

8. While machine is operating verify no cooling system leaks or sudden drop in fill level occurs.

   b. *Shutdown*

1. Press On/Off Output button on front of Chiller.

2.   Turn off main power to the unit using the power switch located at the rear of the unit.

APPENDIX D. EXPERIMENTAL METHODS

A. MANUFACTURER EXPERIMENTAL DATA FOR PYROCERAM 9606

Table D.A.1.   Data provided by manufacturer for Pyroceram 9606

Pyroceram 9606 Experimental Data from Netzsch Laboratories						
Temperature [°C]	Diffusivity		Cp		ρ	Conductivity
[°C]	[mm^2/s]	[m^2/s]	[J/(g*K)]	[J/(kg*K)]	[kg/m^3]	[W/m*K]
-140	5.24	0.00000524	0.361	361	2600	4.918264
-100	3.88	0.00000388	0.487	487	2600	4.912856
-60	2.99	0.00000299	0.598	598	2600	4.648852
-20	2.36	0.00000236	0.684	684	2600	4.197024
25	1.926	0.000001926	0.779	779	2600	3.9009204
50	1.771	0.000001771	No Data	-	2600	
100	1.596	0.000001596	0.898	898	2600	3.7263408
200	1.365	0.000001365	0.9796	979.6	2600	3.4766004
300	1.233	0.000001233	1.03	1030	2600	3.301974
400	1.136	0.000001136	1.0665	1066.5	2600	3.1500144
500	1.069	0.000001069	1.094	1094	2600	3.0406636
600	1.017	0.000001017	1.121	1121	2600	2.9641482
700	0.972	0.000000972	1.1395	1139.5	2600	2.8797444
800	0.938	0.000000938	No Data	-	2600	
900	0.906	0.000000906	1.194	1194	2600	2.8125864
1000	0.877	0.000000877	1.214	1214	2600	2.7681628

After M. Manuelian, private communication, Sept. 2015.

Data highlighted for diffusivity and specific heat (Cp) were provided by the manufacturer for calculating thermal conductivity of reference sample.

B. MANUFACTURER EXPERIMENTAL DATA FOR 99.8% ALUMINA

Table D.B.1.   Data provided by manufacturer for 99.8% Alumina

99.8% Alumina Experimental Data from Netzsch Laboratories								
Temperature [°C]	Diffusivity		Cp		ρ	Conductivity		
[°C]	[mm^2/s]	[m^2/s]	[J/(g*K)]	[J/(kg*K)]	[kg/m^3]	[W/m*K]	[+10%]	[-10%]
25	10.23	1.02E-05	0.7752	775.1531	3970	31.481	34.630	28.333
50	8.74	8.74E-06	0.8248	824.7800	3970	28.618	31.480	25.756
75	7.57	7.57E-06	0.8672	867.1844	3970	26.061	28.668	23.455
100	6.65	6.65E-06	0.9065	906.5200	3970	23.933	26.326	21.539
125	5.94	5.94E-06	0.9398	939.8406	3970	22.163	24.379	19.947
150	5.37	5.37E-06	0.9696	969.5800	3970	20.670	22.737	18.603
175	4.93	4.93E-06	0.9969	996.8719	3970	19.511	21.462	17.560
200	4.56	4.56E-06	1.0188	1018.444	3970	18.444	20.289	16.600
225	4.25	4.25E-06	1.0420	1042.0281	3970	17.582	19.340	15.823
250	3.97	3.97E-06	1.0613	1061.3250	3970	16.727	18.400	15.055
275	3.72	3.72E-06	1.0791	1079.0594	3970	15.936	17.530	14.342
300	3.48	3.48E-06	1.0894	1089.3600	3970	15.050	16.555	13.545

After M. Manuelian, private communication, Sept. 2015.

Data highlighted for diffusivity and specific heat (Cp) were provided by the manufacturer for calculating thermal conductivity of reference sample.

C. EQUATIONS USED FOR UNCERTAINTY ANALYSIS

Table D.C.1.   Variable uncertainty calculation equations

Variable Uncertainty Calculation Equations
$\Delta V = 0.0005*V + 0.150V$
$\Delta I = 0.001*I + 0.0156A$
$\Delta(\Delta x) = 0.0000254m$
$\Delta A = SQRT((\Delta L1/L1)\char`\^2 + (\Delta L2/L2)\char`\^2)*A$
$\Delta dT\_avg = SQRT((\Delta T\_hot)\char`\^2 + (\Delta T\_cold)\char`\^2)$

After H. Castrup, "Estimating and combining uncertainties," in *8th Annual International Test and Evaluation Association Instrumentation Workshop*, Lancaster, CA, 2004, pp. 1–7.

Table D.C.2.   Measurement uncertainty calculation equations

Measurement Uncertainty Calculation Equations
$(\partial k/\partial I)*\Delta I = (V*\Delta x*A\char`\^-1*dT\_avg\char`\^-1)*\Delta I$
$(\partial k/\partial V)*\Delta V = (I*\Delta x*A\char`\^-1*dT\_avg\char`\^-1)*\Delta V$
$(\partial k/\partial(\Delta x))*\Delta(\Delta x) = (I*V*A\char`\^-1*dT\_avg\char`\^-1)*\Delta(\Delta x)$
$(\partial k/\partial A)*\Delta A = (-I*V*\Delta x*A\char`\^-2*dT\_avg\char`\^-1)*\Delta A$
$(\partial k/\partial(dT\_avg))*\Delta dT\_avg = (-I*V*\Delta x*A\char`\^-1*dT\_avg\char`\^-2)*\Delta dT\_avg$
$\Delta k = SQRT(((\partial k/\partial I)*\Delta I)\char`\^2 + ((\partial k/\partial V)*\Delta V)\char`\^2 + ((\partial k/\partial(\Delta x))*\Delta(\Delta x))\char`\^2 + ((\partial k/\partial A)*\Delta A)\char`\^2 + ((\partial k/\partial(dT\_avg))*\Delta dT\_avg)\char`\^2)$
Uncertainty $= (\Delta k/k\_measured)*100$

APPENDIX E. RESULTS

A. PYROCERAM 9606

Table E.A.1. Corrected thermal conductivity results for insulated runs
of Pyroceram 9606

USER	Graph Run #	Run	Insulation Type	Tavg Plate [C]	k_ΔTavg [W/m-K]	% error
			Result Summary for Temperature Corrected k Values			
EXPERIMENTALIST - 1	1	4.5	Heater Balsa Insulation - no sample insulation	33.04	4.449	11.070
	2	4.6	Heater Balsa Insulation - no sample insulation	33.68	4.384	9.375
	3	5.1.1	Heater Balsa Insulation - no sample insulation	34.29	4.117	2.627
	4	5.1.2	Heater Balsa Insulation - no sample insulation	34.35	4.021	0.218
	5	5.1.3	Heater Balsa Insulation - no sample insulation	34.32	3.965	1.157
	6	5.2.1	Heater Balsa Insulation - sample insulation: tape	33.93	4.232	5.545
	7	5.2.2	Heater Balsa Insulation - sample insulation: tape	29.13	4.030	1.101
	8	5.3	Heater Balsa Insulation - sample insulation: tape	32.57	4.154	3.786
	9	6.1	Full Insulation - sample insulation: Foam	36.63	3.785	5.915
	10	7.1	Full Insulation - sample insulation: Foam	35.30	3.919	2.428
	11	8.1	Full Insulation - sample insulation: Foam	33.75	3.837	4.282
	12	9.1	Full Insulation - sample insulation: Foam	35.77	3.967	1.290
	13	10.1	Full Insulation - sample insulation: Foam	28.48	4.019	0.915
	14	11.1	Full Insulation - sample insulation: Foam	27.49	3.872	2.663
	15	12.1	Full Insulation - sample insulation: Foam	27.83	4.100	3.026
	16	13.1	Full Insulation - sample insulation: Foam	32.51	4.155	3.819
	17	14.1	Full Insulation - sample insulation: Foam	30.35	4.082	2.259
	18	15.1	Full Insulation - sample insulation: Foam	28.22	3.935	1.155
	19	16.1	Full Insulation - sample insulation: Foam	28.79	3.976	0.189
	20	17.1	Full Insulation - sample insulation: Foam	29.76	3.963	0.652
	21	18.1	Full Insulation - sample insulation: Foam - High Pwr	52.15	3.968	2.133
	22	19.1	Full Insulation - sample insulation: Foam - High Pwr	47.58	3.733	4.418
	23	20.1	Full Insulation - sample insulation: Foam - High Pwr	52.20	3.744	3.634
	24	21.1	Full Insulation - sample insulation: Foam - High Pwr	52.09	3.807	2.012
EXPERIMENTALIST - 2	25	22.1	Full Insulation - sample insulation: Foam	32.44	3.919	2.089
	26	23.1	Full Insulation - sample insulation: Foam	32.54	3.937	1.635
	27	24.1	Full Insulation - sample insulation: Foam	32.45	3.930	1.787
	28	25.1	Full Insulation - sample insulation: Foam	33.04	3.891	2.874
EXPERIMENTALIST - 3	29	26.1	Full Insulation - sample insulation: Foam	31.66	4.036	0.932
	30	27.1	Full Insulation - sample insulation: Foam	32.10	3.873	3.183
	31	28.1	Full Insulation - sample insulation: Foam	31.99	3.927	1.822
	32	29.1	Full Insulation - sample insulation: Foam	32.46	3.996	0.157

B. 99.8% ALUMINA

Table E.B.1.   Corrected thermal conductivity results for insulated runs
of 99.8% Alumina

Run	Insulation Type	Tavg Plate [C]	k_ΔTavg [W/m-K]	% error
Result Summary for Temperature Corrected k Values				
1.1	Full Insulation - sample insulation: Foam	29.38333333	33.15386188	6.922842006
2.1	Full Insulation - sample insulation: Foam	28.24166667	32.74059059	5.113282896
3.1	Full Insulation - sample insulation: Foam	35.09166667	33.66947494	11.04162757
4.1	Full Insulation - sample insulation: Foam	42.78333333	33.12885312	12.5211724
5.1	Full Insulation - sample insulation: Foam	43.375	32.74721033	11.47305469
6.1	Full Insulation - sample insulation: Foam	29.03333333	33.81459802	8.902762126
7.1	Full Insulation - sample insulation: Foam	28.98333333	29.53983707	4.883306054
8.1	Full Insulation - sample insulation: Foam	28.81666667	32.89182659	5.839998215
9.1	Full Insulation - sample insulation: Foam	28.875	31.36628657	0.95442107
10.1	Full Insulation - sample insulation: Foam	28.51666667	30.67794801	1.401237217
11.1	Full Insulation - sample insulation: Foam	29.45833333	29.56425931	4.625512327
12.1	Full Insulation - sample insulation: Foam	29.00833333	30.14992418	2.90924355

C. UNCERTAINTY CALCULATIONS

1. Pyroceram 9606 Result Uncertainty Calculations

Table E.C.1.1. Variability uncertainty results

Run #	V [V]	ΔV [V]	I [A]	ΔI [A]	Δx [m]	Δ(Δx) [m]	L1 [m]	ΔL1 [m]	L2 [m]	ΔL2 [m]	A [m²]	ΔA [m²]	ΔT_hot [°C]	ΔT_cold [°C]	dT_avg [°C]	ΔdT_avg [°C]	
6.1	34.87	0.167435	0.3304	0.0159304	0.00452679	0.0000254	0.0254	0.0000254	0.0254	0.0000254	0.00064516	9.1239E-07	0.4	0.4	11.63	0.56568542	Low Power Runs
7.1	34.87	0.167435	0.3309	0.0159309	0.00452679	0.0000254	0.0254	0.0000254	0.0254	0.0000254	0.00064516	9.1239E-07	0.4	0.4	11.33	0.56568542	
8.1	34.87	0.167435	0.3318	0.0159318	0.00452679	0.0000254	0.0254	0.0000254	0.0254	0.0000254	0.00064516	9.1239E-07	0.4	0.4	11.57	0.56568542	
9.1	34.87	0.167435	0.3309	0.0159309	0.00452679	0.0000254	0.0254	0.0000254	0.0254	0.0000254	0.00064516	9.1239E-07	0.4	0.4	11.23	0.56568542	
10.1	34.87	0.167435	0.3343	0.0159343	0.00452679	0.0000254	0.0254	0.0000254	0.0254	0.0000254	0.00064516	9.1239E-07	0.4	0.4	11.23	0.56568542	
11.1	34.87	0.167435	0.3347	0.0159347	0.00452679	0.0000254	0.0254	0.0000254	0.0254	0.0000254	0.00064516	9.1239E-07	0.4	0.4	11.58	0.56568542	
12.1	34.87	0.167435	0.3344	0.0159344	0.00452679	0.0000254	0.0254	0.0000254	0.0254	0.0000254	0.00064516	9.1239E-07	0.4	0.4	12.17	0.56568542	
13.1	34.87	0.167435	0.3327	0.0159327	0.00452679	0.0000254	0.0254	0.0000254	0.0254	0.0000254	0.00064516	9.1239E-07	0.4	0.4	10.88	0.56568542	
14.1	34.87	0.167435	0.3337	0.0159337	0.00452679	0.0000254	0.0254	0.0000254	0.0254	0.0000254	0.00064516	9.1239E-07	0.4	0.4	11.07	0.56568542	
15.1	34.87	0.167435	0.3347	0.0159347	0.00452679	0.0000254	0.0254	0.0000254	0.0254	0.0000254	0.00064516	9.1239E-07	0.4	0.4	11.43	0.56568542	
16.1	34.87	0.167435	0.334	0.015934	0.00452679	0.0000254	0.0254	0.0000254	0.0254	0.0000254	0.00064516	9.1239E-07	0.4	0.4	12.42	0.56568542	
17.1	34.87	0.167435	0.334	0.015934	0.00452679	0.0000254	0.0254	0.0000254	0.0254	0.0000254	0.00064516	9.1239E-07	0.4	0.4	11.35	0.56568542	
18.1	49.98	0.17499	0.4579	0.0160579	0.00452679	0.0000254	0.0254	0.0000254	0.0254	0.0000254	0.00064516	9.1239E-07	0.4	0.4	22.27	0.56568542	High Power Runs
19.1	49.98	0.17499	0.46	0.01606	0.00452679	0.0000254	0.0254	0.0000254	0.0254	0.0000254	0.00064516	9.1239E-07	0.4	0.4	23.52	0.56568542	
20.1	49.97	0.174985	0.4573	0.0160573	0.00452679	0.0000254	0.0254	0.0000254	0.0254	0.0000254	0.00064516	9.1239E-07	0.4	0.4	23.30	0.56568542	
21.1	49.97	0.174985	0.4576	0.0160576	0.00452679	0.0000254	0.0254	0.0000254	0.0254	0.0000254	0.00064516	9.1239E-07	0.4	0.4	23.02	0.56568542	

141

Table E.C.1.2.　　　　　Measurement uncertainty result

	Measurement Uncertainty Analysis								
Run #	$(\partial k/\partial I)*\Delta I$	$(\partial k/\partial V)*\Delta V$	$(\partial k/\partial(\Delta x))*\Delta(\Delta x)$	$(\partial k/\partial A)*\Delta A$	$(\partial k/\partial(dT\_avg))*\Delta dT\_avg$	w_k	k_measured	Uncertainty [%]	
6.1	0.3350404	0.033366053	0.038990077	-0.009827104	-0.33789468	0.478701343	3.785	12.65	LOW POWER RUNS
7.1	0.343919911	0.034301102	0.040082734	-0.010102498	-0.356558753	0.498297402	3.919	12.72	
8.1	0.337001082	0.033700561	0.039380968	-0.009925624	-0.343249253	0.483916197	3.837	12.61	
9.1	0.346981512	0.034606453	0.040439554	-0.010192431	-0.362935236	0.505029707	3.967	12.73	
10.1	0.347055566	0.034962035	0.04085507	-0.010297159	-0.366664398	0.507826603	4.019	12.64	
11.1	0.336577444	0.033946197	0.039668008	-0.00999797	-0.345253638	0.485087935	3.872	12.53	
12.1	0.320434136	0.032289672	0.037732266	-0.009510083	-0.312660277	0.450545528	4.100	10.99	
13.1	0.358180648	0.035913674	0.041967114	-0.010577439	-0.388757337	0.531590591	4.155	12.79	
14.1	0.352269041	0.035424877	0.041395927	-0.010433477	-0.377113611	0.519023655	4.082	12.72	
15.1	0.340993183	0.034391555	0.040188433	-0.010129139	-0.354372197	0.494728707	3.935	12.57	
16.1	0.31397456	0.031601698	0.036928331	-0.009307459	-0.299837592	0.43695721	3.976	10.99	
17.1	0.343481714	0.034571608	0.040398835	-0.010182168	-0.358842937	0.499678777	3.963	12.61	
18.1	0.252902147	0.025249419	0.040464853	-0.010198808	-0.183212116	0.316077726	3.968	7.97	HIGH POWER RUNS
19.1	0.239490754	0.024016959	0.038489707	-0.00970099	-0.165006202	0.294508488	3.733	7.89	
20.1	0.241628786	0.024097324	0.038611877	-0.009731782	-0.167069211	0.297427062	3.744	7.94	
21.1	0.244607787	0.024409964	0.039112828	-0.009858042	-0.171320061	0.30233487	3.807	7.94	

2.   99.8% Alumina Result Uncertainty Calculations

Table E.C.2.1.   Variability uncertainty results

Run #	V [V]	ΔV [V]	I [A]	ΔI [A]	Δx [m]	Δ(Δx) [m]	L1 [m]	ΔL1 [m]	L2 [m]	ΔL2 [m]	A [m²]	ΔA [m²]	ΔT_hot [°C]	ΔT_cold [°C]	dT_avg [°C]	ΔdT_avg [°C]	Run Type
1.1	34.87	0.167435	0.3361	0.0159361	0.00452679	0.0000254	0.0254	0.0000254	0.0254	0.0000254	0.00064516	9.1239E-07	0.4	0.4	3.40	0.56568542	Low Power
2.1	34.87	0.167435	0.3369	0.0159369	0.00452679	0.0000254	0.0254	0.0000254	0.0254	0.0000254	0.00064516	9.1239E-07	0.4	0.4	3.42	0.56568542	Low Power
3.1	47.98	0.17399	0.4565	0.0160565	0.00452679	0.0000254	0.0254	0.0000254	0.0254	0.0000254	0.00064516	9.1239E-07	0.4	0.4	6.32	0.56568542	Low Power
4.1	47.98	0.17399	0.4512	0.0160512	0.00452679	0.0000254	0.0254	0.0000254	0.0254	0.0000254	0.00064516	9.1239E-07	0.4	0.4	7.30	0.56568542	High Power
5.1	47.98	0.17399	0.4503	0.0160503	0.00452679	0.0000254	0.0254	0.0000254	0.0254	0.0000254	0.00064516	9.1239E-07	0.4	0.4	7.32	0.56568542	High Power
6.1	34.86	0.16743	0.3363	0.0159363	0.00452679	0.0000254	0.0254	0.0000254	0.0254	0.0000254	0.00064516	9.1239E-07	0.4	0.4	3.93	0.56568542	Low Power
7.1	34.87	0.167435	0.3365	0.0159365	0.00452679	0.0000254	0.0254	0.0000254	0.0254	0.0000254	0.00064516	9.1239E-07	0.4	0.4	3.53	0.56568542	Low Power
8.1	34.87	0.167435	0.3363	0.0159363	0.00452679	0.0000254	0.0254	0.0000254	0.0254	0.0000254	0.00064516	9.1239E-07	0.4	0.4	3.97	0.56568542	Low Power
9.1	34.86	0.16743	0.3362	0.0159362	0.00452679	0.0000254	0.0254	0.0000254	0.0254	0.0000254	0.00064516	9.1239E-07	0.4	0.4	4.02	0.56568542	Low Power
10.1	34.87	0.167435	0.3362	0.0159362	0.00452679	0.0000254	0.0254	0.0000254	0.0254	0.0000254	0.00064516	9.1239E-07	0.4	0.4	4.60	0.56568542	Low Power
11.1	34.87	0.167435	0.3359	0.0159359	0.00452679	0.0000254	0.0254	0.0000254	0.0254	0.0000254	0.00064516	9.1239E-07	0.4	0.4	4.08	0.56568542	Low Power
12.1	34.87	0.167435	0.336	0.015936	0.00452679	0.0000254	0.0254	0.0000254	0.0254	0.0000254	0.00064516	9.1239E-07	0.4	0.4	4.62	0.56568542	Low Power

Table E.C.2.2.   Measurement uncertainty results

Run #	(∂k/∂I)*ΔI	(∂k/∂V)*ΔV	(∂k/∂(Δx))*Δ(Δx)	(∂k/∂A)*ΔA	(∂k/∂(dT_avg))*ΔdT_avg	w_k	k_measured	Uncertainty [%]	Run Type
1.1	1.146773898	0.116133781	0.135708742	-0.034204186	-4.024021919	4.188187749	33.154	12.63	Low Power
2.1	1.141237167	0.115842353	0.135368193	-0.034118354	-3.994343857	4.158138187	32.741	12.70	Low Power
3.1	0.855747995	0.088226659	0.136514678	-0.034407315	-2.17882735	2.346741851	33.669	6.97	High Power
4.1	0.740231585	0.075455907	0.116754266	-0.029426878	-1.612431695	1.779907263	33.129	5.37	High Power
5.1	0.738503998	0.075133858	0.116255954	-0.029301283	-1.60189248	1.76959509	32.747	5.40	High Power
6.1	0.991007291	0.100443564	0.117343701	-0.02957544	-3.00767189	3.170633818	33.815	9.38	Low Power
7.1	1.10352711	0.111884372	0.130743073	-0.032952633	-3.730486793	3.894226693	29.540	13.18	Low Power
8.1	0.982961392	0.099602475	0.116390998	-0.02933532	-2.958183519	3.121120137	32.892	9.49	Low Power
9.1	0.970440884	0.098330425	0.114875016	-0.02895323	-2.883309211	3.04613377	31.366	9.71	Low Power
10.1	0.847620809	0.085863551	0.100336306	-0.025288877	-2.199032789	2.360568934	30.678	7.69	Low Power
11.1	0.954852813	0.096641606	0.112931059	-0.028463273	-2.788238985	2.951088564	29.564	9.98	Low Power
12.1	0.844550207	0.08550268	0.099914608	-0.025182592	-2.181885214	2.343462383	30.150	7.77	Low Power

D. DEVICE SENSITIVITY ANALYSIS FOR INSULATION

Table E.D.1. Results for Pyroceram 9606 runs using no device insulation

Graph Run #	Run	Insulation Type	Tavg Plate [C]	k_ΔTavg [W/m-K]	% error
		Result Summary for Temperature Corrected k Values			
0	0.1	No Insulation with No Grease	38.45	1.470	63.549
1	1.1	No Insulation with Grease	34.86	4.122	2.689
2	1.2	No Insulation with Grease	32.07	3.353	16.193
3	2.1	No Insulation with Grease	34.98	3.499	12.847
4	2.2	No Insulation with Grease	34.83	3.773	6.011
5	2.3	No Insulation with Grease	34.54	3.911	2.536
6	2.4	No Insulation with Grease	34.24	3.999	0.309
7	2.5	No Insulation with Grease	34.35	4.037	0.619
8	3.1	No Insulation with Grease	33.73	4.225	5.387
9	3.2	No Insulation with Grease	33.46	4.332	8.102
10	3.3	No Insulation with Grease	33.88	4.362	8.807
11	3.4	No Insulation with Grease	33.66	4.463	11.350
12	4.1	No Insulation with Grease	34.16	3.657	8.831
13	4.2	No Insulation with Grease	33.80	4.103	2.345
14	4.3	No Insulation with Grease	33.66	4.280	6.778
15	4.4	No Insulation with Grease	33.20	4.549	13.543

E.   DEVICE SENSITIVITY ANALYSIS FOR NEGLECTED GREASE

Table E.E.1.   Results for Pyroceram 9606 full insulated runs neglecting grease calculations

USER	Graph Run #	Run	Insulation Type	Tavg Plate [C]	k_ΔTavg [W/m-K]	% error
			Result Summary for Temperature Corrected k Values			
EXPERIMENTALIST - 1	1	4.5	Heater Balsa Insulation - no sample insulation	33.04	3.544	11.522
	2	4.6	Heater Balsa Insulation - no sample insulation	33.68	3.503	12.615
	3	5.1.1	Heater Balsa Insulation - no sample insulation	34.29	3.330	16.989
	4	5.1.2	Heater Balsa Insulation - no sample insulation	34.35	3.267	18.573
	5	5.1.3	Heater Balsa Insulation - no sample insulation	34.32	3.230	19.482
	6	5.2.1	Heater Balsa Insulation - sample insulation: tape	33.93	3.405	15.082
	7	5.2.2	Heater Balsa Insulation - sample insulation: tape	29.13	3.273	17.890
	8	5.3	Heater Balsa Insulation - sample insulation: tape	32.57	3.355	16.197
	9	6.1	Full Insulation - sample insulation: Foam	36.63	3.110	22.707
	10	7.1	Full Insulation - sample insulation: Foam	35.30	3.199	20.346
	11	8.1	Full Insulation - sample insulation: Foam	33.75	3.145	21.558
	12	9.1	Full Insulation - sample insulation: Foam	35.77	3.231	19.597
	13	10.1	Full Insulation - sample insulation: Foam	28.48	3.266	18.000
	14	11.1	Full Insulation - sample insulation: Foam	27.49	3.168	20.361
	15	12.1	Full Insulation - sample insulation: Foam	27.83	3.010	24.353
	16	13.1	Full Insulation - sample insulation: Foam	32.51	3.355	16.174
	17	14.1	Full Insulation - sample insulation: Foam	30.35	3.307	17.152
	18	15.1	Full Insulation - sample insulation: Foam	28.22	3.210	19.367
	19	16.1	Full Insulation - sample insulation: Foam	28.79	2.943	26.124
	20	17.1	Full Insulation - sample insulation: Foam	29.76	3.228	19.062
	21	18.1	Full Insulation - sample insulation: Foam - High Pwr	52.15	3.232	16.814
	22	19.1	Full Insulation - sample insulation: Foam - High Pwr	47.58	3.075	21.285
	23	20.1	Full Insulation - sample insulation: Foam - High Pwr	52.20	3.082	20.680
	24	21.1	Full Insulation - sample insulation: Foam - High Pwr	52.09	3.125	19.586
EXPERIMENTALIST - 2	25	22.1	Full Insulation - sample insulation: Foam	32.44	3.199	20.068
	26	23.1	Full Insulation - sample insulation: Foam	32.54	3.211	19.767
	27	24.1	Full Insulation - sample insulation: Foam	32.45	3.207	19.878
	28	25.1	Full Insulation - sample insulation: Foam	33.04	3.180	20.602
EXPERIMENTALIST - 3	29	26.1	Full Insulation - sample insulation: Foam	31.66	3.276	18.063
	30	27.1	Full Insulation - sample insulation: Foam	32.10	3.169	20.792
	31	28.1	Full Insulation - sample insulation: Foam	31.99	3.205	19.882
	32	29.1	Full Insulation - sample insulation: Foam	32.46	3.250	18.785

THIS PAGE INTENTIONALLY LEFT BLANK

LIST OF REFERENCES

[1]   United States. Office of the Under Secretary of Defense for Acquisition, Technology, and Logistics, "Report of the Defense Science Board task force on DOD energy strategy; more fight less fuel," Feb. 2008.

[2]   R. Mabus, *Department of the Navy's Energy Program for Security and Independence,* Darby, PA: DIANE Publishing, 2010.

[3]   Talking with Rear Adm. Philip Hart Cullom. (2010, Jul-Sept.). CHIPS. [Online]. Available: http://www.doncio.navy.mil/CHIPS/ArticleDetails.aspx?ID=2365

[4]   S. Sathe and K. Millsaps, *WHRS Program Roadmap 2014–2020,* Monterey, NPS, 2014.

[5]   R. S. Bohning, "Optimal placement of non-intrusive waste heat recovery devices in exhaust ducts," M.S. Thesis, Mech. Eng. Dept., Naval Postgraduate School, Monterey, CA, 2015.

[6]   C. H. E. Koh, "Performance and reliability of exhaust gas waste heat recovery units," M.S. Thesis, Mech. Eng. Dept., Naval Postgraduate School, Monterey, CA, 2014.

[7]   M. Beale, "Turning vanes in exhaust duct flow: study for energy efficiency, optimization and pressure drop mitigation," M.S. Thesis, Mech. Eng. Dept., Naval Postgraduate School, Monterey, 2014.

[8]   T. P. Mastronarde, "Energy conservation utilizing waste heat boilers—the challenge, problems, and solutions," *Nav. Eng. J.,* vol. 94, pp. 277–285, 1982.

[9]   United States Marine Corps, "Marine Corps Expeditionary Energy Office," 2015. [Online]. Available: http://www.hqmc.marines.mil/e2o/E2OHome.aspx. [Accessed 20 June 2015].

[10]   L. M. Jiji, *Heat Conduction*, 3rd ed. Berlin, Germany: Springer-Verlag, 2009, pp. 1–17.

[11]   T. L. Bergman and F. P. Incropera, *Introduction to Heat Transfer*, 6th ed. Hoboken, NJ: John Wiley & Sons, 2011.

[12]   E. Fried, "Interface thermal contact resistance problem in space vehicles," *ARS Journal,* vol. 32, no. 2, pp. 237–243, 1962.

[13]   J. R. Wilson, (2006, May 1) The great cooling dilemma: conduction, convection, or liquid. [Online]. Available: http://www.militaryaerospace.com/articles/print/volume-17/issue-5/features/technology-focus/the-great-cooling-dilemma-conduction-convection-or-liquid.html

[14]   D. D. L. Chung, "Thermal interface materials," *Journal of Materials Engineering and Performance,* vol. 10, no. 1, pp. 56–59, Feb. 2001.

[15]   G. K. Reddy, N. Chikkanna and B. U. M. Gowd, "A novel method to reduce the thermal contact resistance," *International Journal of Recent Technology and Engineering*, vol. 1, no. 2, pp. 11–15, Jun. 2012.

[16]   Y. S. Touloukian, R. W. Powell, C. Y. Ho, P. G. Klemens, *Thermophysical Properties of Matter; The TPRC Data Series; A Comprehensive Compilation of Data by the Thermophysical Properties Research Center (TPRC), Purdue University,* New York, NY: IFI/Plenum, 1970.

[17]   M. M. Yovanovich, "Four decades of research on thermal contact, gap, and joint resistance in microelectronics," *IEEE Transactions on Components and Packaging Technologies,* vol. 28, no. 2, pp. 182–206, May 2005.

[18]   L. S. Fletcher, "Recent developments in contact conductance heat transfer," *Journal of Heat Transfer,* vol. 110, no. 4b, pp. 1059–1070, Nov. 1988.

[19]   M. G. Cooper, B. B. Mikic and M. M. Yovanovich, "Thermal contact conductance," *Int. Journal Heat Mass Transfer,* vol. 12, pp. 279–300, 1969.

[20]   C. V. Madhusudana and L. S. Fletcher, "Contact heat transfer-the last decade," *AIAA Journal,* vol. 24, no. 3, pp. 510–523, Mar. 1986.

[21]   M. M. Yovanovich, "Thermal contact correlations," *AIAA Paper,* vol. 81, pp. 83–95, 1982.

[22]   C. Fieberg and R. Kneer, "Determination of thermal contact resistance from transient temperature measurements," *Int. Journal of Heat and Mass Transfer,* vol. 51, no. 5–6, pp. 1017–1023, Mar. 2008.

[23]   J. Kestin and W. A. Wakeham, "A contribution to the theory of the transient hot-wire technique for thermal conductivity measurements," *Physica A: Statistical Mechanics and its Applications,* vol. 92, no. 1–2, pp. 102–116, Jun. 1978.

[24]   H. M. Roder, "A transient hot wire thermal conductivity apparatus for fluids," *Journal of Research of the National Bureau of Standards,* vol. 86, no. 5, pp. 457–493, May 1981.

[25] C. J. M. Lasance. (2000, Sept. 1). High accuracy thermal interface resistance measurement using a transient method. *Electronics Cooling* [Online]. Available: http://www.electronics-cooling.com/2000/09/high-accuracy-thermal-interface-resistance-measurement-using-a-transient-method/

[26] H. Fukushima, L. T. Drzal, B. P. Rook and M. J. Rich, "Thermal conductivity of exfoliated graphite nanocomposites," *Journal of Thermal Analysis and Calorimetry,* vol. 85, pp. 235–238, 2006.

[27] H. Mehling, G. Hautzinger, O. Nilsson, J. Fricke, R. Hofmann and O. Hahn, "Thermal diffusivity of semitransparent materials determined by the laser-flash method applying a new analytical model," *Int. Journal of Thermophysics,* vol. 19, no. 3, pp. 941–949, May 1998.

[28] Y. Sato and T. Taira, "The studies of thermal conductivity in GdVO(4), YVO(4), and Y(3)Al(5)O(12) measured by quasi-one-dimensional flash method," *Optics Express,* vol. 14, no. 22, pp. 10528-10536, Oct. 2006.

[29] Y. Tada, M. Harada, M. Tanigaki and W. Eguchi, "Laser flash method for measuring thermal conductivity of liquids-application to low thermal conductivity liquids," *Rev. Sci. Instrum.,* vol. 49, no. 9, pp. 1305–1314, Sept. 1978.

[30] J. B. J. Fourier, *The Analytical Theory of Heat*, Cambridge, London: The University Press, 1878.

[31] P. Teertstra, "Thermal conductivity and contact resistance measurements for adhesives," in *ASME 2007 InterPACK Conference Collocated with the ASME/JSME 2007 Thermal Engineering Heat Transfer Summer Conf.,* Vancouver, Canada, 2007, pp. 381–388.

[32] J. R. Culham, P. Teertstra, I. Savija and M. M. Yovanovich, "Design, assembly and commissioning of a test apparatus for characterizing thermal interface materials," in *2002 Inter Society Conference on Thermal Phenomena*, San Diego, CA, 2002, pp. 128–135.

[33] S. B. Sathe, T. W. Tong and M. A. Faruque, "Experimental study of natural convection in a partially porous enclosure," *Journal of Thermophysics,* vol. 1, no. 3, pp. 260–267, Jul. 1987.

[34] A. W. Pratt, "Heat transmission in low conductivity materials," *Thermal Conductivity,* vol. 1, pp. 301–405, 1969.

[35] J. P. Holman and W. J. Gajda, *Experimental Methods for Engineers.* New York, NY: McGraw-Hill, 1989.

[36] T. G. Beckwith, R. D. Marangoni and J. H. Lienhard, *Mechanical Measurements*, 6th ed. Upper Saddle River, NJ: Pearson Prentice Hall, 2007.

[37]   D. R. Flynn, "Thermal conductivity of ceramics," *Mechanical and Thermal Properties of Ceramics (Wachtman, JB, Jr., Ed), NBS Spec. Publ,* vol. 303, pp. 63–123, 1969.

[38]   InvestmentMine, "Commodity and Metal Prices," 2015. [Online]. Available: http://www.infomine.com/investment/metal-prices/. [Accessed 28 August 2015].

[39]   L. S. Marks, E. A. Avallone and T. Baumeister, *Marks' Standard Handbook for Mechanical Engineers.* 11th ed. New York, NY: McGraw-Hill, 1996.

[40]   W. D. Callister and D. G. Rethwisch, *Materials Science and Engineering: An Introduction*, 8th ed. Hoboken, NJ: Wiley & Sons, 2010.

[41]   A. C. Ugural and S. K. Fenster, *Advanced Mechanics of Materials and Applied Elasticity,* 5th ed. Upper Saddle River, NJ: Pearson Education, 2012.

[42]   *RotaChill Large Chiller Operating Manual*, Heidolph Instruments GmbH & Co., Germany.

[43]   *High Power Programmable DC Power Supply User Manual,* BK Precision Corp, Yorba Linda, CA, 2013.

[44]   *PTC8010 Reference Manual, 4th ed.,* Martel Electronics, Derry, NH, 2014.

[45]   A. Tleoubaev, A. Brzezinski and L. Braga, "Accurate simultaneous measurements of thermal conductivity and specific heat of rubber, elastomers, and other materials," in *Proceedings of 12th Brazilian Rubber Technology Congress,* Sao Paulo, Brazil, 2008, pp. 22–24.

[46]   M. Manuelian, private communication, Sept. 2015.

[47]   L. D. Chambers, K. R. Stokes, F. C. Walsh and R. J. Wood, "Modern approaches to marine antifouling coatings," *Surface and Coatings Technology,* vol. 201, no. 6, pp. 3642–3652, Dec. 2006.

[48]   M. P. Schultz, J. A. Bendick, E. R. Holm and W. M. Hertel, "Economic impact of biofouling on a naval surface ship," *Biofouling,* vol. 27, no. 1, pp. 87–98, Jan. 2011.

[49]   D. M. Yebra, S. Kiil and K. Dam-Johansen, "Antifouling technology - past, present and future steps towards efficient and environmentally friendly antifouling coatings," *Progress in Organic Coatings,* vol. 50, no. 2, pp. 75–104, Jul. 2004.

[50]   T. M. Yonushonis, "Overview of thermal barrier coatings in diesel engines," *Journal of Thermal Spray Technology,* vol. 6, no. 1, pp. 50–56, Mar. 1997.

[51]   WATLOW, "ULTRAMIC Advanced Ceramic Heaters," 2015. [Online]. Available: http://www.watlow.com/products/heaters/ultramic-ceramic-heaters.cfm?famid=10. [Accessed 21 June 2015].

[52]   H. Castrup, "Estimating and combining uncertainties," in *8th Annual International Test and Evaluation Association Instrumentation Workshop*, Lancaster, CA, 2004, pp. 1–7.

THIS PAGE INTENTIONALLY LEFT BLANK

INITIAL DISTRIBUTION LIST

1.   Defense Technical Information Center
        Ft. Belvoir, Virginia

2.   Dudley Knox Library
        Naval Postgraduate School
        Monterey, California